RADAR EXPLORATION OF VENUS

Thesis By

Richard M. Goldstein

In Partial Fulfillment of the Requirements

For the Degree of

Doctor of Philosophy

California Institute of Technology

Pasadena, California

1962

ABSTRACT

The feasibility of studying Venus by radar was demonstrated on the tenth of March, 1961, when an echo from Venus was first detected in real time.

The spectrum of the echo may be expected to be broadened by the doppler shifts produced by any rotation Venus might have. In order to measure this broadening, a novel technique for accurate spectral estimation of this extremely weak signal was devised, analyzed and implemented. The results of the measurements indicate that Venus rotates only once for each of its years, so that one hemisphere always faces the sun. In addition, the spectral measurements together with some polarization measurements enable one to infer some scattering properties of the surface.

Time of flight measurements were also made, using a cross-correlation technique. These, compared with standard astronomical tables, provide a new value for the Astronomical Unit. The standard deviation of these measurements is only a few parts in 10^7.

ACKNOWLEDGMENTS

The Venus experiment could not have been performed without the dedicated and competent work of many people.

I wish to acknowledge the work of D. Schuster and G. S. Levy, who built the antenna feeds; T. Sato, who built the maser amplifier; L. R. Malling, who constructed the the programmable local oscillator; D. B. Holdridge, who calculated the required ephemerides; and many others.

I am also indebted to my advisor, Professor H. C. Martel, for his help and for many stimulating discussions.

TABLE OF CONTENTS

Chapter I

Venus

The study of Venus by radar holds the best hope (at present) of clearing up some of the mysteries that surround that planet. Although Venus is our nearest planetary neighbor, coming at times to within 25 million miles of earth, we know far less about her than we know about any of the other major planets except, of course, the earth. The reason for our lack of knowledge is the dense mantle of clouds that perpetually covers Venus. No one has ever seen through that atmosphere to the surface below.

The lack of precise knowledge of Venus becomes evident when one consults the literature to find information on the surface or atmosphere or rotation of Venus. There, one finds tremendous disagreement even among astronomers of recognized stature. The early estimates made on the characteristics of Venus were all based on observations of very tenuous markings on the disk - seen by some observers but not seen by others. But modern estimates made with the precision instruments of our time still show a vast disagreement amongst themselves.

For example, Richardson[1] made spectroscopic measurements at Mt. Wilson in an effort to detect doppler shifts in the spectral lines caused by the differing relative motion of the limbs of Venus. The results were negative, indicating that the effect was too small to overcome the system noise. Richardson concluded that the period must be greater than 14 days, the statement being correct with a probability of 16/17.

On the other hand, Kraus[2], in 1956, analyzed the variations in 11 meter radiation from Venus and found a periodicity that indicated the

day on Venus is 22 hours 17 minutes long.

Speculations about the surface of Venus have been just as divergent. One view[3], supported by temperature measurements made with radio-telescopes, and by the absence of any water vapor lines in the planets optical spectrum, is that Venus is an arid dust bowl, continuously lashed by violent wind storms.

Menzel and Whipple[4] published a completely different view in 1954. Carbon dioxide is known to exist in the atmosphere of Venus because of spectroscopic analysis, and studies of the polarization of scattered light in the Venerian atmosphere indicate that the clouds may be composed of water droplets. Large amounts of carbon dioxide could not exist upon an earth-like planet with continents protruding from oceans of water. The carbon dioxide would be fixed in the rocks in the form of carbonates because of its chemical reaction with silicates in the presence of water. The inference is that continents are absent and that Venus is completely covered by water.

Radar, with its ability to penetrate clouds, seems to be an ideal tool with which to study these problems. The time is especially ripe for this application, since immense steerable parabolic antennas, as well as the ultra-low noise maser amplifier, and digital techniques for complicated data handling are all now available.

Chapter II

The Goldstone Tracking Station

The Goldstone research and tracking facility of Caltech's Jet Propulsion Laboratory is especially well suited for carrying out this type of investigation. Goldstone is located in a low area of the Mojave desert some 50 miles north of Barstow, California. This extremely high degree of isolation guarantees the almost noise free environment which is necessary for planetary radar. Goldstone is divided into two areas. One is the transmitting site. The transmitter operates at 2388 megacycles with a continuous power output of 10 kilowatts. It feeds an 85 foot alt-azimuth mounted paraboloid. This antenna has a gain of over 53 decibels and a beam width of only 0.3°. The receiving site is seven miles away. Both sites are nestled among foothills and mountains and transmitter-receiver isolation is provided by a range of hills directly between the sites. Thus a true continuous wave radar is possible with both transmitter and receiver operating at once. The receiver is equipped with an antenna similar to the transmitter's, except it is equatorially mounted. The two antennas may be locked together electrically so that they both point to the same direction in space.

The antennas may be aimed by two different methods. One is manually, where positions and rates may be set into the drive servos. Both antennas have a television camera mounted at the focus so that aiming can be monitored visually. At inferior conjunction, Venus passed within only seven degrees of the sun, but the glare from the sun did not overpower the optical system and visual monitoring was possible throughout the experiment.

The second method is called the programmed mode, and that is the one that was used for the Venus experiment. In this mode, the angle pointing data, as a function of time, was calculated in advance from the Venus and Earth ephimerides. The data was fed into the antenna servos (which form a sampled data system in this mode) by means of punched computer tape. A new tape was prepared for each day of the experiment. The television monitor was still relied upon to check the accuracy of the tapes and to correct an occasional error.

In addition to the antennas, the receiver local oscillator was programmed. This was necessary because of the doppler shift which the relative Earth-Venus motion produces. This motion can be broken down into two components, the orbital part consisting of the changing distance between the centers of the Earth and Venus, and a diurnal part caused by the Earth's rotation. The orbital component produced a doppler shift changing by several hundred kilocycles during the experiment, while the diurnal component of the shift changed about fourteen kilocycles per day. Figure 2.1 shows how the doppler shift varied as a function of time and demonstrates graphically the magnitude of the task that the local oscillator performed.

The basic frequency standard for the experiment was an Automichron, a cesium beam device. Its stability approached $\pm$ one part per 10^{10} during the few minutes required for the signal to make its sixty million mile round trip. The local oscillator was locked to this base, with the doppler offset added by a single-side-band modulation technique. The doppler offset was derived from a voltage controlled oscillator, the input of which was programmed according to an ephemeris such as that

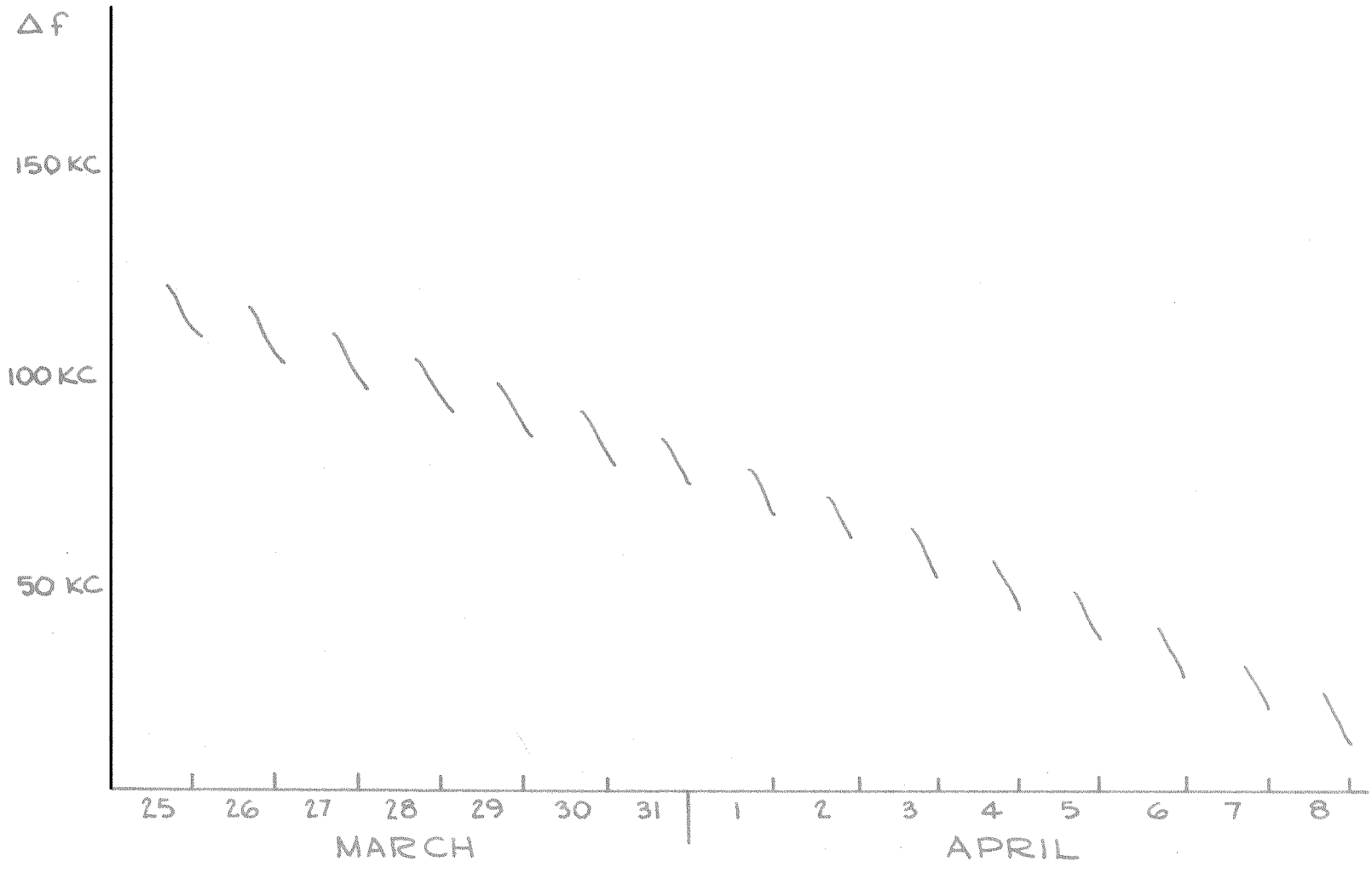

DOPPLER SHIFT AS A FUNCTION OF TIME

FIG. 2.1

portrayed in figure 2.1. A separate punched tape containing the ephemeris was provided for each day of operation, and the crystal in the controlled oscillator was changed every few days. The frequency of the offset oscillator was continuously displayed on a counter, adjacent to a similar display of the desired frequency; hence visual monitoring of this device was possible.

The nature of the Venus experiment required the minimum attainable noise temperature for the receiver. A three level ruby maser was built to satisfy this goal. The operating conditions were: pump frequency = 12,900 mcs., magnetic field = 2,500 gauss, gain = 20 db, and bandwidth = 2 mcs. The noise temperature of the maser, including its circulator, was only 25° K. The noise temperature of the entire system, including the antenna and sky effects was, typically, 65° K.

The balance of the receiving system was that of conventional superheterodyne circuit. Figure 2.2 is a simplified block diagram of the device. The maser, preselector, first mixer, and three stages of 30 mcs. amplification were all housed near the focus of the antenna. The bandwidth of the signal and/or noise at the point where it entered the control building was still over 2 mcs., so a band pass filter was necessary to eliminate the image created in heterodyning down to 455 Kc.

It was found early in the experiment that some form of AGC was necessary to remove the gain variations in the front end. This was accomplished, as shown in figure 2.2, by detecting the thirty kilocycle wide band of signal plus noise at the output of the 455 Kc IF and using this voltage to control the gain of the IF. After this sub-system was installed, the strength of the Venus echos remained remarkably constant.

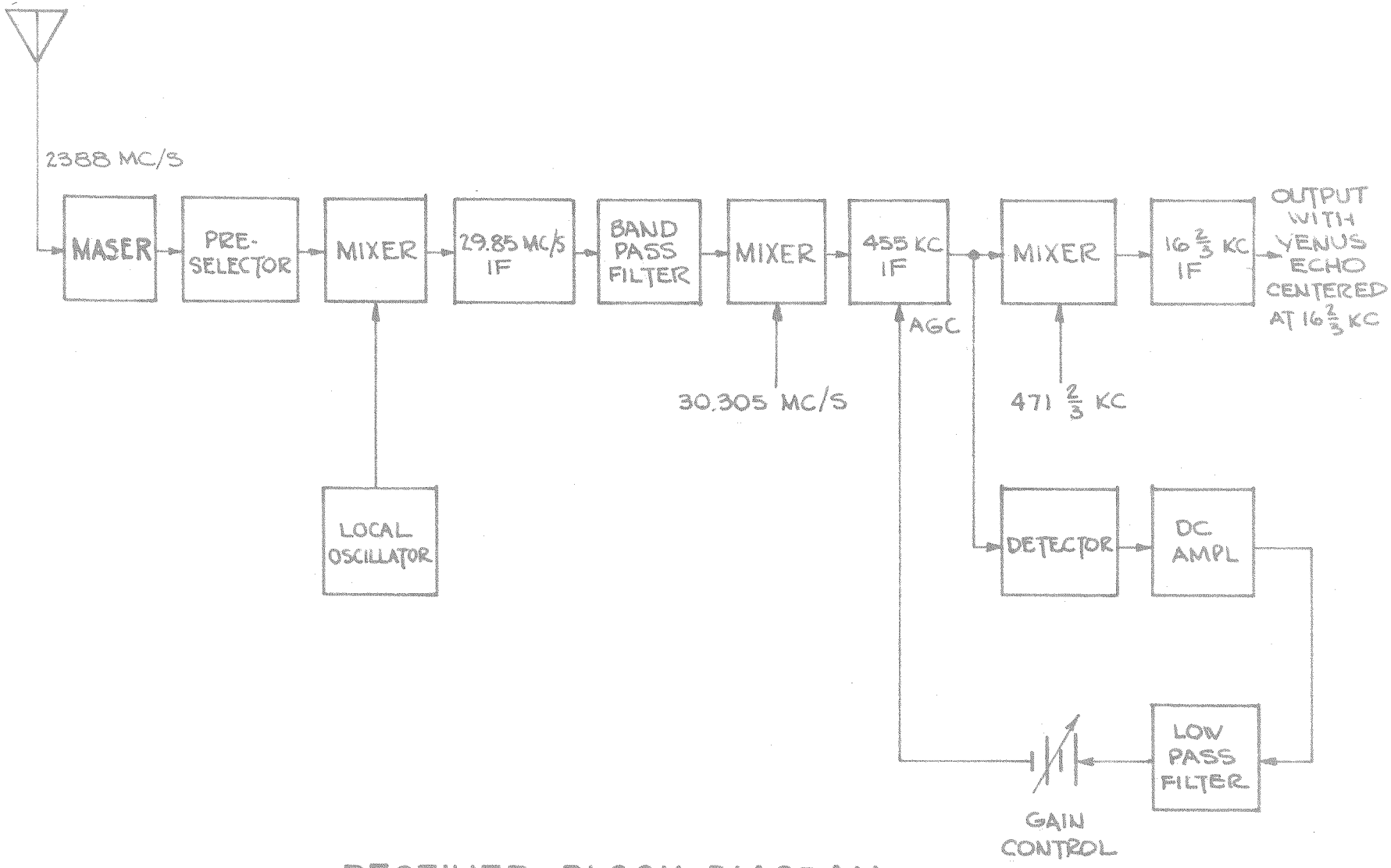

RECEIVER BLOCK DIAGRAM

FIG. 2.2

The 455 Kc IF provided most of the system's gain. It was a wide band amplifier, with its 33-1/3 Kc bandwidth accurately defined by a Collins' mechanical filter. The last IF amplifier, which was at 16-2/3 Kc, was simply an audio stage with a low pass filter in it.

The reference signal at 30.305 megacycles was derived from the primary standard, but the 471-2/3 kilocycle signal was a free-running crystal oscillator. At that low frequency, the instabilities of that oscillator were negligible.

A complete description of the system's capability and of the critical components may be found by consulting the JPL Technical Report (#32-132), Radar Exploration of Venus, pp. 11-36.

The Output shown in figure 2.2 is not the final output but is only the signal prepared for further processing. The signal is centered at 16-2/3 Kc, with a bandwidth of up to 33-1/3 kilocycles. The output level (signal plus noise) was about one volt, R.M.S.

Two distinct types of signal processing were carried out from that point. One was spectral analysis and the other may best be called radiometer analysis. Both modes will be fully described subsequently, but first we shall investigate the spectral properties of the echo; assuming pure CW at the transmitter.

Chapter III

Spectral Broadening and the Backscatter Function

Upon calculating what shape of power spectrum to expect, one finds that it is a function of two things; the rotation rate (and axis orientation) of Venus, and the radar scattering properties of the surface. The pertinent scattering properties may be characterized (at any one wavelength) by a function F called the backscatter function. This is illustrated in figure 3.1. The square represents a unit area of Venerian surface. Radiation arrives at an angle of θ from the normal. Power is scattered in all directions, including backwards along the same line of approach. The intensity in this direction is a function of θ and is called the backscatter function.

Three assumptions are made to calculate the spectrum from the backscatter function. One is a suitably homogeneous surface. This rules out such features as continents and oceans - obviously an unwise thing to do. However, continents and oceans would make themselves known by producing an asymmetry in the power spectrum and variations in the echo's strength, so this assumption can be checked by the experiment. Second, it is assumed that the surface is suitably random so that the phases of the echoes from the various elements of area constitute independent random variables. This allows the individual echoes to be added on a power basis. The third assumption is that there is no modulation effect causing the individual echoes to be broadened in spectrum, but only a shift in frequency caused by the doppler effect. This assumption would not be valid for a very jagged, pathological surface. A verification of this assumption by polarization experiments will be

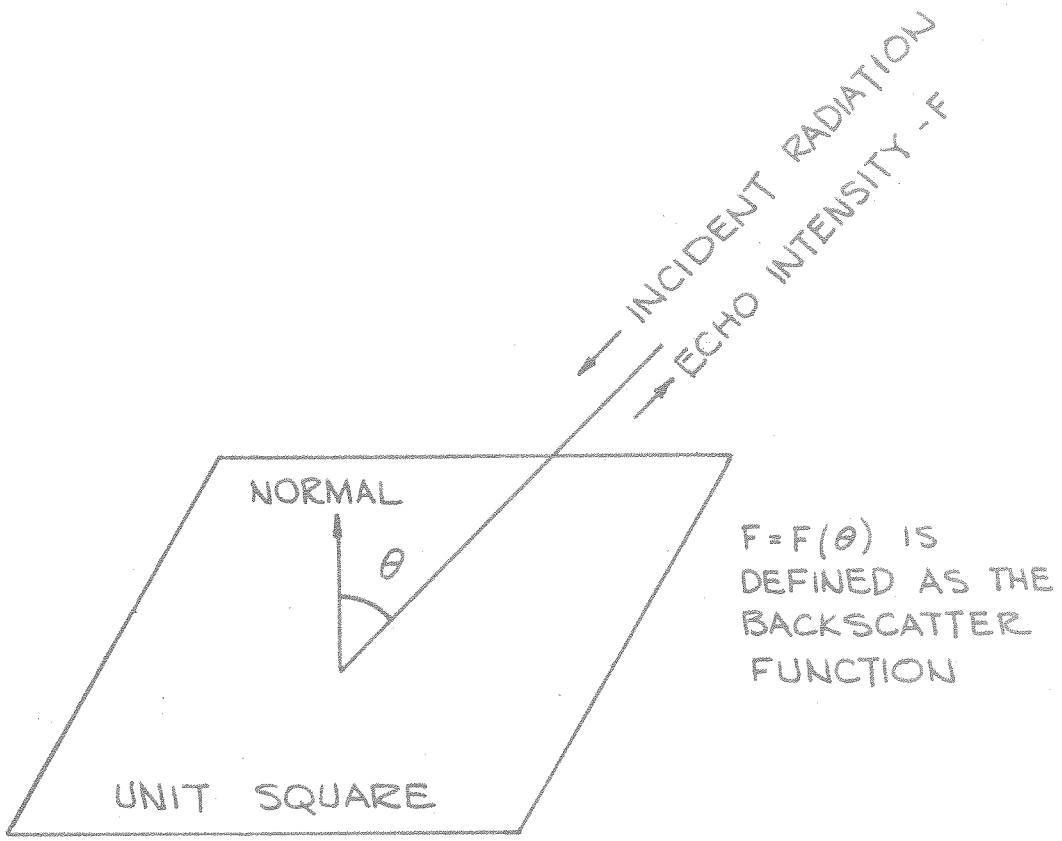

DEFINITION OF BACKSCATTER FUNCTION

FIG. 3.1

mentioned later.

The power spectrum calculation is done as follows. All elements of area that produce a doppler shift between f and f + df cycles per second are considered. Each element contributes an amount of power determined by the backscatter function. These contributions are integrated to give the power density spectrum P(f).

The geometry of the situation is depicted in figure 3.2. A is any point on the surface with spherical coordinates (θ, ϕ). The axis of rotation inclines by an angle of α to the Earth-Venus line. It is convenient to find the z component of the velocity of the point A.

$$z = R \cos \theta, \text{ and}$$

$$dz = -R \sin \theta \, d\theta. \tag{3.1}$$

Using Pierce 625 for any spherical triangle,

$$\cos \theta = \cos\beta \cos\alpha + \sin\beta \sin\alpha \cos\Omega, \text{ and}$$

$$\sin \theta \, d\theta = \sin\beta \sin\alpha \sin\Omega \, d\Omega, \tag{3.2}$$

since β and α are constant for the point in question. From equations 3.2 and 3.1

$$dz = -R \sin\beta \sin\alpha \sin\Omega \, d\Omega, \text{ and}$$

$$\frac{dz}{dt} \equiv v = -R \sin\beta \sin\alpha \sin\Omega \frac{d\Omega}{dt}.$$

From the spherical law of sines:

$$v = -R \sin\alpha \sin\phi \sin\theta \, \omega, \tag{3.3}$$

where $\omega \equiv \frac{d\Omega}{dt}$ = angular velocity of Venus.

Consider, for the moment, that the power is distributed in velocity instead of frequency. Then the power from v to v + dv is:

$$P(v) \, dv = \int F(\theta) \, dA,$$

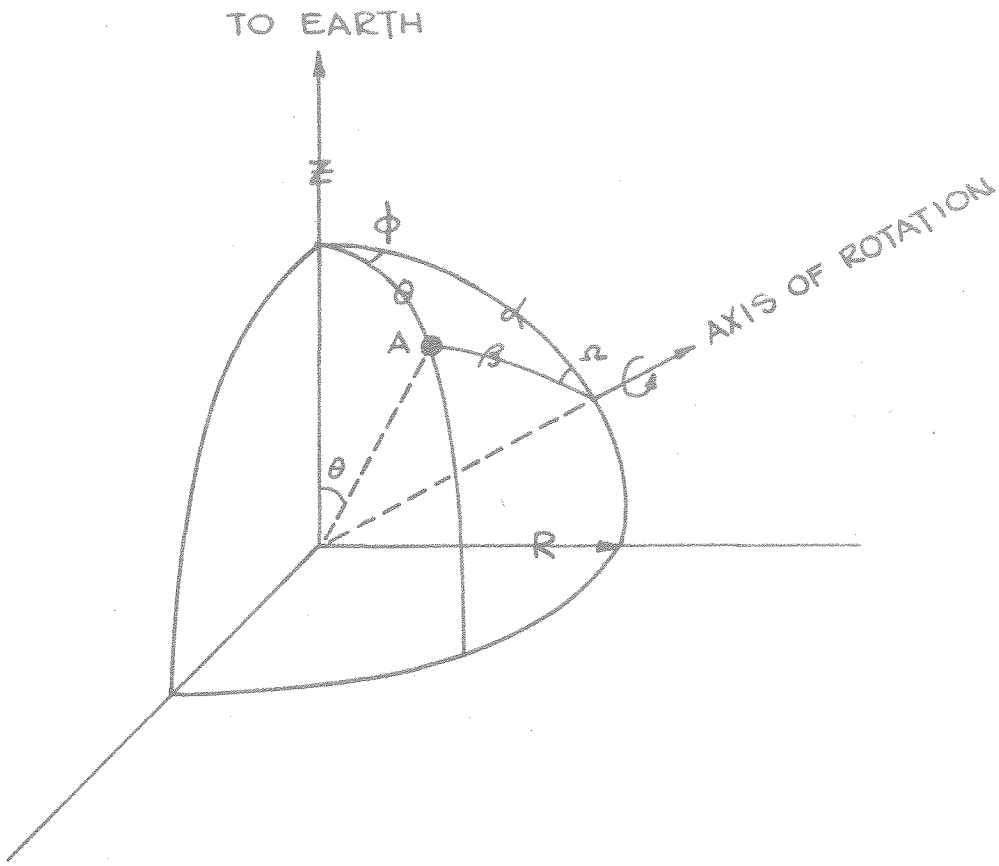

GEOMETRY FOR CALCULATING THE POWER SPECTRUM

FIG. 3.2

where $F(\theta)$ is the backscatter function and dA is the element of area and the integration is over all points having a z component of velocity between v and v + dv. Substituting;

$$P(v) = R^2 \int_0^{\pi/2} F(\theta) \sin\theta \left|\frac{d\phi}{dv}\right| d\theta. \qquad (3.4)$$

$\frac{d\phi}{dv}$ may be found from equation 3.3,

$$dv = -R\,\omega \sin\alpha \sin\theta \cos\phi\, d\phi, \qquad \text{hence}$$

$$\frac{d\phi}{dv} = \frac{-1}{R\,\omega \sin\alpha \sin\theta \cos\phi}, \qquad \text{and}$$

$$\frac{d\phi}{dv} = \frac{-1}{R\,\omega \sin\alpha \sin\theta \sqrt{1 - \frac{v^2}{R^2\,\omega^2 \sin\alpha \sin^2\theta}}}.$$

Equation 3.4 now becomes

$$P(v) = 2R^2 \int_{\theta_1}^{\pi/2} \frac{F(\theta) \sin\theta\, d\theta}{R\,\omega \sin\alpha \sqrt{\sin^2\theta - \frac{v^2}{R^2\,\omega^2 \sin^2\alpha}}}, \qquad (3.5)$$

where θ_1 is the value of θ for which the denominator is zero.

$F(\theta)$ can be written as $F(\cos\theta)$ without any loss of generality. Then, with a proper change of variables, equation 3.5 becomes

$$P(v) = \frac{2R}{\omega \sin\alpha} \int_0^{\pi/2} F\left[\left(1 - \frac{v^2}{R^2\,\omega^2 \sin^2\alpha}\right)^{\frac{1}{2}} \cos\xi\right] d\xi.$$

Let $F(\theta) = \cos^n$, then

$$P(v) = \frac{2R}{\omega \sin\alpha} \left(1 - \frac{v^2}{R^2 \sin^2\alpha\, \omega^2}\right)^{n/2} \int_0^{\pi/2} \cos^n\xi \; d\xi.$$

To find the distribution of power in frequency, f, recall that $P(f)\,df = P(v)\,dv$, and that the doppler equation is $f = \frac{2v}{\lambda}$ where λ = the wavelength.

Therefore,

$$P(f) = \frac{2\lambda R}{2\omega \sin\alpha}\left(1 - \frac{\lambda^2 f^2}{4R^2 \sin^2\alpha \ \omega^2}\right)^{n/2} \int_0^{\pi/2} \cos^n \xi_o \ d\xi_o$$

$$P(f) = \frac{2a_n R^2}{f_o}\left(1 - \frac{f^2}{f_o^2}\right)^{n/2} \qquad (3.6)$$

where $f_o = \frac{2\omega R \sin\alpha}{\lambda}$ and $a_n = \int_0^{\pi/2} \cos^n \xi_o \ d\xi_o$
(see Pierce, 483).

Consider the general case, where any $F(\theta)$ is expanded as a cosine series.

$$F(\theta) = b_1 \cos\theta + b_2 \cos^2\theta + b_3 \cos^3\theta + \ldots \quad 0 < \theta < \pi/2 \qquad (3.7)$$

If only the first term existed, the others being zero, the surface would be known as a Lomel-Seiliger scatterer. If only the second, it would be called a Lambert scatterer.

Because of the linearity of the integral, equation 3.6 becomes:

$$P(f) = \left[\frac{2R^2}{f_o}\right]\left[a_1 b_1\left(1 - \frac{f^2}{f_o^2}\right)^{\frac{1}{2}} + a_2 b_2\left(1 - \frac{f^2}{f_o^2}\right) + a_3 b_3\left(1 - \frac{f^2}{f_o^2}\right)^{3/2} + \ldots\right],$$

$$f^2 \leq f_o^2 \qquad (3.8)$$

Thus the power spectrum for a Lomel-Seiliger scatterer is elliptically shaped, and for a Lambert scatter, it is parabolic.

It is clear from this analysis that given the backscatter function, and the assumptions listed above, the power spectrum follows. The reverse is also true. The terms in equation 3.8 are linearly independent functions, so that any admissible power spectrum may be expanded uniquely into a sum such as equation 3.8. The coefficients of a backscatter function are then determined.

These considerations show the desirability of obtaining as accurate a measurement of the power spectrum of the echo as possible. The problems involved in spectral measurements, and a new technique for solving them are presented in the next chapter.

Chapter IV

A Technique for the Measurement of Power Spectra

A. Introduction

The central problem of measuring the power spectrum of a stochastic process arises from the necessarily finite extent of the sample functions which are available. This forces any measurement of the spectrum to be only an estimate, and our problem is to manipulate the data in such a way as to make the estimate as good as possible.

Given a finite sample function of the process under consideration, an intuitively natural way to proceed is to expand the function in a Fourier series and identify the spectrum with the square of the magnitude of the coefficients. However, analyzing a different sample function of the same process will, in general, yield a different spectrum. This lack of stability in the measurement must be reduced to an acceptable level.

Increasing the length of the data record will not improve the stability of the measurement described above in the important case of a gaussian process. It can be shown[6] that the standard deviation of the measurement is greater than the true value of the spectrum for every frequency.

The difficulty is that too many parameters (the Fourier coefficients) are being estimated for the amount of data available. We should not expect to be able to identify frequencies exactly, using only a finite data record, because neighboring frequencies with random phases will prevent such identification.

Clearly, some type of spectral smoothing, or local averaging, is required. There are several ways of performing such an operation. Perhaps

the first one that would occur to an electrical engineer is the analog process of passing the "signal" through a band pass filter, rectifying, and smoothing. The results of several such filters may be used to form an estimate of the spectrum. This method has the great advantages of simplicity and of producing its results in real time. There are, of course, disadvantages in this approach; among them being an inherent inflexibility where different types of spectra are concerned. Such a device was built for the Venus experiment. In consisted of seven channels, and therefore produced only seven points on the spectrograms. The device is more fully described in chapter VIII of this thesis.

Another approach to spectral smoothing is the process of convolving the estimate with a function, called a window, chosen to produce the desired local averaging. Spectral convolution is, of course, equivalent to multiplying the "signal's" autocorrelation function by the Fourier transform of the window. This makes it convenient to make the Fourier series expansion by way of the time autocorrelation function. Some kind of window must be used simply because the time autocorrelation is not defined for values of the argument greater than the length of the record. It can be shown[7] that the spectral stability of the correlation function method is the same as the analog filtering method provided the spectral window corresponds to the bandpass filter. In either case, good stability inherently requires great quantities of input data.

By far the most convenient method of measuring a spectrum is simply to sample the signal, digitize and record the samples and use a digital computer to find spectrum. For example, the 7090 computer available at

JPL has a standard program (using the correlation approach) that will find the spectrum of 1,000 sample points and will do it in less than a minute. However, for the stability needed to detect a weak echo in the presence of strong noise, a tremendous amount of data must be processed. Original planning for the Venus experiment indicated as much as eight hours of data would be needed. Since a bandwidth of 30 KC was to be provided, approximately 10^9 sample points must be analyzed. The computer group asked for many thousands of hours for each spectrum.

B. The Technique

Figure 4.1 illustrates a scheme to circumvent this problem. The plan is simple. An estimate of the autocorrelation function at y, $\hat{R}_y(\tau)$, is calculated by the correlator. A formula exists relating the autocorrelation function at x to that at y which is valid for gaussian signals[8]. It is:

$$\frac{R_x(\tau)}{R_x(0)} = \sin\left[\frac{\pi}{2} R_y(\tau)\right] . \qquad (4.1)$$

The notation used here designates an estimate of a function by the superscript $\hat{}$.

It is natural to select as an estimator for $R_x(\tau)$ the function:

$$\hat{R}_x(\tau) = \sum_{k=-K}^{K} \delta(\tau - k T_o) \sin\left[\frac{\pi}{2} \hat{R}_y(\tau)\right] , \qquad (4.2)$$

where the train of delta functions is the mathematical characterization of the sampling process, and K is the total number of points measured on the autocorrelation function (called lags), and T_o is the time between samples. The power spectrum estimate $\hat{P}(\omega)$ is then the Fourier transform

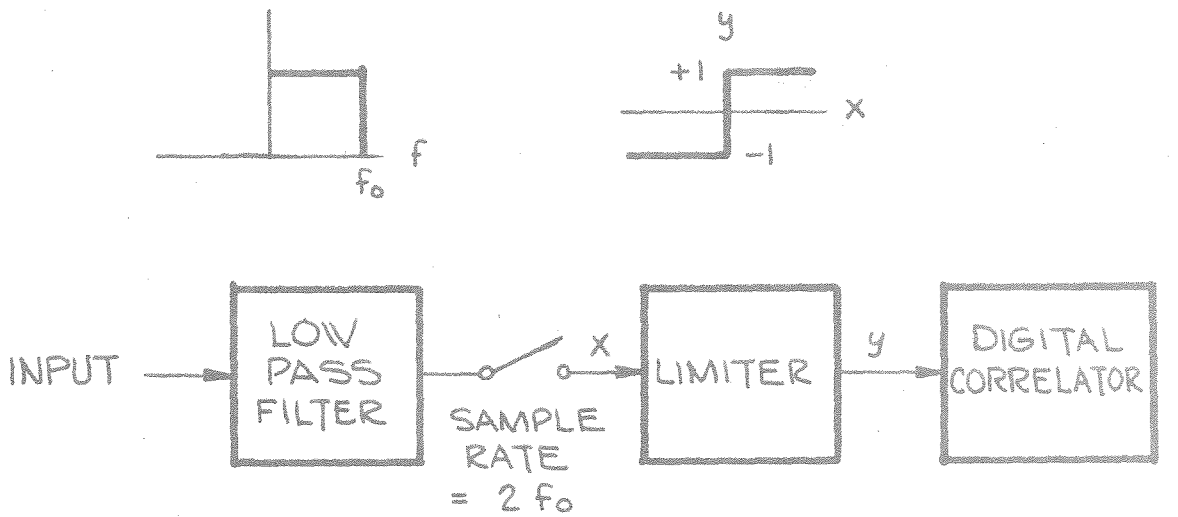

BLOCK DIAGRAM OF DIGITAL SPECTROMETER

FIG. 4.1

of equation 4.2.

$$\hat{P}(\omega) = \int_{-\infty}^{\infty} \sum_{k=-K}^{K} \delta(\tau - k\,T_o) \sin\left[\frac{\pi}{2}\hat{R}_y(\tau)\right] e^{-j\omega\tau}\, d\tau$$

$$\hat{P}(\omega) = \sum_{k=-K}^{K} \sin\left[\frac{\pi}{2}\hat{R}_y(k\,T_o)\right] e^{-j\omega k T_o}$$

$$\hat{P}(\omega) = \sum_{k=1}^{K} 2 \sin\left[\frac{\pi}{2}\hat{R}_y(k\,T_o)\right] \cos \omega\, k\, T_o + 1, \qquad (4.3)$$

where $0 \leq \omega \leq \frac{\pi}{T_o}$, $\hat{R}_y(k\,T_o) = \hat{R}_y(-k\,T_o)$, and $\hat{R}_y(o) = 0$.

The digital correlator estimates $R_y(k\,T_o)$ by the calculation

$$\hat{R}_y(k\,T_o) = \frac{1}{N} \sum_{n=1}^{N} y_n\, t_{n+k}\,, \qquad (4.4)$$

where y_n is the signal at y at the n^{th} sampling instant and $N + 2k$ is the total number of samples in an observation. The values of y_n are always either plus one or minus one. Herein lies the great advantage of this system. The sums and products of equation 4.4 can be realized, with simple gating circuits and binary counters, at over a million operations per second. The wide band correlator constructed for the Venus echo accepted input samples at a 66-2/3 Kc rate and computed $\hat{R}_y(\tau)$ for 45 values of τ. It kept all of the sums up-dated as fast as the samples could come in. It had the capacity to operate for weeks without an overflow. Thus the values of equation 4.4 were ready for use immediately after the end of an observation. $\hat{P}(\omega)$ was computed from this data using a general purpose digital computer, an operation taking less than a minute.

Examining equation 4.4, one can see that this estimator has two very

important properties. First of all, the ensemble average of $R_y(\tau)$,

$$\overline{\hat{R}_y(\tau)} = \frac{1}{N} \sum_{n=1}^{N} \overline{y_n\, y_{n+\tau}} = R_y(\tau) , \qquad (4.4a)$$

and second, in the limit as $N \longrightarrow \infty$

$$\hat{R}_y(\tau) = \lim_{N \to \infty} \frac{1}{N} \sum_{n=1}^{N} y_n\, y_{n+\tau} = R_y(\tau) . \qquad (4.4b)$$

Thus the ensemble average of the estimator equals the true value and, in the limit as N tends to infinity, the estimator also equals the true value. Values of N used in the experiment ranged from 10^6 to 10^7.

It is desirable now to calculate the performance of this system; that is, to find the mean and the standard deviation of $\hat{P}(\omega)$. These quantities depend, of course, on the input spectrum as well as the parameters K and N defined above.

C. Theoretical Performance

We have, upon taking the ensemble average of equation 4.3,

$$\overline{\hat{P}(\omega)} \approx \sum_{k=1}^{K} 2 \sin\left[\frac{\pi}{2} \overline{R_y(k\, T_o)}\right] \cos \omega\, k\, T_o + 1, \qquad (4.5)$$

where the approximation of replacing $\overline{\sin z}$ by $\sin \overline{z}$ is justified as follows. First, since the input spectrum is approximately white and band-limited, $R_y(k\, T_o)$ is nearly zero for all $k \neq 0$. This fact allows one to replace the sine function by its argument. The validity of this step was borne out by the experiment, where $\hat{R}_y(\tau)$ was always less than .25. The second justification arises from the extremely large number of samples (N) that were used. For that case the variance of $\hat{R}_y$ is small, a fact which increases the accuracy of the approximation of equation 4.5.

Equation 4.5 becomes:

$$\overline{\hat{P}(\omega)} \approx \sum_{k=1}^{K} 2 \sin \left[\frac{\pi}{2} R_y(k T_o) \right] \cos \omega k T_o + 1$$

$$= \sum_{k=1}^{K} 2 R_x(k T_o) \cos \omega k T_o + 1, \quad 0 \le \omega \le \frac{\pi}{T_o} . \quad (4.6)$$

Equation 4.6 may be recognized as the Fourier transform of $R_x(\tau)$, after it has been sampled and multiplied by the box-car function $f(\tau)$, where

$$f(\tau) = \begin{cases} 0, & \tau^2 > (K T_o)^2 \\ 1, & \tau^2 \le (K T_o)^2 \end{cases} .$$

Hence the expected value of $\hat{P}(\omega)$ equals $P(\omega)$ convolved with both $F(\omega)$ and with a series of delta functions (because of the sampling), where

$$F(\omega) = \frac{2}{\omega} \sin \omega K T_o . \quad (4.7)$$

This double convolution is the bias created by the use of the estimator of equation 4.3.

It now remains to calculate the RMS error of $P(\omega)$. At this point, the assumption is introduced that the input spectrum is ideal band-limited white Gaussian noise. Replacing the sine function of equation 4.3 by its argument, we have

$$\left[\hat{P}(\omega) - P(\omega) \right]^2 = e^2 = \sum_{k=1}^{K} \sum_{\xi=1}^{K} \pi^2 \hat{R}_y(kT_o) \hat{R}_y(\xi T_o) \cos\omega kT_o \cos\omega \xi T_o .$$

Substitute from equation 4.4:

$$e^2 = \sum_{k=1}^{K} \sum_{\xi=1}^{K} \sum_{m=1}^{N} \sum_{n=1}^{N} \frac{\pi^2}{N^2} y_n y_{n+k} y_m y_{m+\xi} \cos\omega k T_o \cos\omega \xi T_o. \tag{4.8}$$

To find the ensemble average of e^2 one must find $\overline{y_1 y_2 y_3 y_4}$. To this end:

$$\overline{y_1 y_2 y_3 y_4} = \int_{-\infty}^{\infty}\int\int\int y_1 y_2 y_3 y_4 p(y_1 y_2 y_3 y_4)\, dy_1\, dy_2\, dy_3\, dy_4$$

$$\overline{y_1 y_2 y_3 y_4} = \int_{-\infty}^{\infty}\int\int\int y(x_1)\, y(x_2)\, y(x_3)\, y(x_4)\, p(x_1 x_2 x_3 x_4)\, dx_1\, dx_2\, dx_3\, dx_4. \tag{4.9}$$

Because of the assumption, successive samples at x are independent if the sampling period is any non-zero multiple of T_o. If all of the x's are different, (i.e., separated by multiples of T_o), then

$$p(x_1 x_2 x_3 x_4) = \frac{1}{(2\pi)^2} \exp\left\{-\tfrac{1}{2}\left[x_1^2 + x_2^2 + x_3^2 + x_4^2\right]\right\}. \tag{4.10}$$

Equation 4.10 factors so that equation 4.9 becomes

$$\overline{y_1 y_2 y_3 y_4} = \left[\int_{-\infty}^{\infty} \frac{y(x_1)}{\sqrt{2\pi}} \exp\left(-\frac{x_1^2}{2}\right) dx_1\right]^4 = 0,$$

since $y(x_1)$ is an odd function.

The only contribution to e^2 occurs if m = n and k = ξ. Then

$$\overline{y_1 y_2 y_3 y_4} = \overline{y_1^2 y_2^2} = 1. \tag{4.10a}$$

Thus equation 4.8 becomes

$$\overline{(e^2)} = \frac{\pi^2}{N} \sum_{k=1}^{K} \cos^2 \omega k T_o. \tag{4.11}$$

The summation of equation 4.11 is the sum of two parts; a constant equal to K/2, and the first K terms of the Fourier series for an impulse. The impulse part has its greatest magnitude of K/2 at the origin and dies away rapidly with increasing ω, while its average is zero. It is logical, therefore, to average $\overline{(e^2)}$ over frequency, which yields

$$\overline{(e^2)}_{av.} = \frac{\pi^2 K}{2N}. \tag{4.12}$$

Hence the standard deviation, $\sigma = \sqrt{\overline{(e^2)}}$, is

$$\sigma = \pi \sqrt{\frac{K}{2N}} . \qquad (4.13)$$

It is interesting to see what σ would be if there were no limiter, so that the signal at y would equal the signal at x. In that case a very similar parallel argument shows:

$$\sigma = 2 \sqrt{\frac{K}{2N}} .$$

Thus the cost of using this sytem is a factor of $\frac{\pi}{2}$ in RMS error. This seems like a small cost, indeed, if one considers that the experiment may not even be possible without the simplification this system introduces.

D. Spectral Windows

The term spectral window refers to a function such as $F(\omega)$ of equation 4.7. It will be recalled that the expected value of the estimated power spectrum $\overline{\hat{P}(\omega)}$ equals the true spectrum $P(\omega)$ convolved with the window $F(\omega)$,

$$\overline{\hat{P}(\omega)} = P(\omega) * F(\omega) . \qquad (4.14)$$

Convolution in the frequency domain is, of course, equivalent to multiplication of the corresponding auto-correlation functions; so the transform of $F(\omega)$ (designated $C(\tau)$) is also spoken of as a window. The use of a window is unavoidable because only a finite number of points on the autocorrelation function can be measured. From the last point on, the autocorrelation function is presumed zero. Therefore, of necessity, one must multiply the correlation function by at least a box-car function.

The use of a window produces two effects. One is a bias in the measurement, as shown by equation 4.14. The other effect is a control

over the variance of the measurement. This is expressed by equation 4.12 which would read

$$\overline{(e^2)}_{av.} = \frac{\pi^2}{2N} \sum_{k=1}^{\infty} C_k^2 \; ; \; C_k = 0 \text{ for } k > K \qquad (4.15)$$

if an arbitrary window $C_k = C(kT_o)$ were used in the discussion leading up to that equation.

These two effects represent another example of the eternal compromises which arise in engineering. A window chosen to minimize the bias of equation 4.14 only does so at the cost of increasing the variance of equation 4.15; and vice versa. This section is an investigation of the trade-off offered by the use of an arbitrary window.

There are two components of error. Let the figure of merit, I, for the window be the sum of the square of these two components, integrated over the range of ω. Let the true input spectrum be white noise plus a small perturbation $G(\omega)$,

$$P(\omega) = 1 + G(\omega), \quad 0 \leq \omega \leq \frac{\pi}{T_o} \qquad (4.16)$$

Also assume that $G(\omega)$ does not contribute significantly to the variance expressed by equation 4.15. Then

$$I = \int_0^{\pi/T_o} \left[P(\omega) - \overline{\hat{P}}(\omega) \right]^2 d\omega + \int_0^{\pi/T_o} \frac{\pi^2}{2N} \sum_{k=1}^{\infty} C_k^2 \, d\omega. \qquad (4.17)$$

Substitute for $P(\omega)$ from equation 4.16 and for $\overline{\hat{P}}(\omega)$ from equation 4.6, after the term (C_k) for the window has been added. Then:

$$I = \int_0^{\pi/T_o} G^2(\omega) \, d - 2 \int_0^{\pi/T_o} G(\omega) \sum_{k=1}^{\infty} 2R_k C_k \cos \omega kT \, d\omega$$

$$+ \int_0^{\pi/T_o} \left(\sum_{k=1}^{\infty} 2R_k C_k \cos \omega kT \right)^2 d\omega + \frac{\pi^2}{2N} \sum_{k=1}^{\infty} C_k^2 \int_0^{\pi/T_o} d\omega,$$

where $R_k = R_x(kT_o)$, the true autocorrelation function at x, figure 4.1.

Differentiating I with respect to each of the C_i and equating the derivatives to zero will define the best C_i (and therefore the best window) in the sense described above;

$$\frac{\partial I}{\partial C_i} = -4 R_i \int_0^{\pi/T_o} G(\omega) \cos i \omega T_o \, d\omega \qquad (4.18)$$

$$+ \int_0^{\pi/T_o} 2\left(\sum_{k=1}^{\infty} 2R_k C_k \cos \omega kT_o \right) (2R_i \cos \omega iT_o) \, d\omega + \frac{\pi^2}{2N} \frac{\pi}{T_o} 2C_i .$$

The first integral can be recognized as the Fourier series expression for R_i, times a constant. The second integral produces zero for each term of the sum except for k = i. Thus equation 4.18 becomes:

$$\frac{\partial I}{\partial C_i} = -4 R_i^2 \frac{\pi}{T_o} + 4 R_i^2 C_i \frac{\pi}{T_o} + \frac{\pi^2 C_i}{N} \frac{\pi}{T_o} = 0,$$

and therefore,

$$C_i = \frac{R_i^2}{R_i^2 + \frac{\pi^2}{4N}} . \qquad (4.19)$$

Equation 4.19 must be interpreted. Taken literally, it gives the optimum value for the window, C_i. However, one must first know the R_i, which are the quantities that the experiment is designed to measure. Another practical problem arises. Equation 4.19 defines an infinite set of C's, but in practice only a finite number of points on the correlation function can be measured. This number was 63 for the Venus correlator.

These considerations combine to make the following procedure appear reasonable: So long as the square of the estimator for the autocorrelation function at x, $(\hat{R}_x)^2$, is much greater than $\frac{\pi^2}{4N}$, choose the corresponding $C_i = 1$. This condition was satisfied by the Venus measurements for all i.

Thus, we are led back to the "box-car" window originally considered.

E. A Wider Class of Inputs

So far, in the analysis of this spectrometer, the input spectrum $P(\omega)$ has been assumed to be the box-car function:

$$P(\omega) = \begin{cases} 1 & \text{for } \omega^2 \leq \omega_o^2 \\ 0 & \text{otherwise.} \end{cases}$$

Such a function is a convenient mathematical idealization for the characteristic of a low pass filter. However, the box-car function is not physically realizable because of its infinitely sharp cut-off and infinite attenuation outside of the pass band.

One might wonder whether the preceding analysis is in some way dependent upon the non-physical properties of the box-car. This section investigates the result of relaxing some of these restrictions. Consider an input spectrum $W(\omega)$, which is formed by convolving the box-car, $P(\omega)$, with any arbitrary but physically realizable function $H(\omega)$,

$$W(\omega) = P(\omega) * H(\omega). \qquad (4.20)$$

W does not have the infinite cut-off and attenuation characteristics that P has. Now let us consider the action of the sampler by assuming that it multiplies the signal by the customary series of delta functions. Let $R_H(\tau)$ be the transform of $H(\omega)$. Recall that $\frac{\sin \omega_o \tau}{\pi \tau}$ is the transform of the box-car and that $\omega_o = \frac{\pi}{T_o}$. Then the spectrum at the sampler out-put, $W^*(\omega)$, is:

$$W^*(\omega) = \int_{-\infty}^{\infty} \left[R_H(\tau)\right] \left[\frac{1}{\pi \tau} \sin \frac{\pi}{T_o} \tau\right] \left[\sum_{k=-\infty}^{\infty} \delta(\tau - kT_o)\right] e^{j\omega\tau} \, d\tau.$$

$$\left(0 \leq \omega \leq \frac{\pi}{T_o}\right)$$

Interchanging the order of summation and integration yields:

$$W^*(\omega) = \sum_{k=-\infty}^{+\infty} R_H(k T_o) \frac{1}{\pi k T_o} \sin \pi k.$$

All of the terms of the sum are zero, except for k = 0, hence

$$W^*(\omega) = \frac{R_H(0)}{T_o} = \text{constant.} \qquad (4.21)$$

The action of the limiter normalizes the constant to unity for any $R_H(0)$.

Equation 4.21 shows that the spectrum is exactly the same as in the case of the simple box-car input, and so the previous analysis holds for this larger class of inputs. There is, however, a different bias in the estimator because, as can be seen from equation 4.6, $\overline{\hat{P}(\omega)} = 1$ and $W(\omega)$ is not necessarily equal to unity. This bias is not a result of the scheme of this particular spectrometer, but is caused by the sampling process. The inevitable result of sampling a signal which is not band-limited is a folding of the spectrum, sometimes called aliasing[9]. In the class of spectra considered here, the aliasing exactly contrives to produce a flat spectrum.

Chapter V

Hypothesis Testing

It is possible that the signal will be too weak to produce a satisfactory spectrum. In that case it may still be possible to decide if the signal is present or not, or if it was wide or narrow band.

This chapter will present a criterion for such hypothesis testing and will evaluate the reliability of the criterion.

The decisions must be based on the only data available, namely $\hat{R}_y(k\ T_o)$ for $k = 1, 2, \ldots, K$. The plan is to construct a single statistic, I, for each hypothesis to be tested. If I should be greater than a certain threshold, the hypothesis should be accepted; otherwise not.

Following the analogy of linear filtering, let I be a weighted sum of the $\hat{R}_y(k\ T_o)$.

$$I = \sum_{k=1}^{K} a_k \hat{R}_y(k\ T_o). \qquad (5.1)$$

It is proper to point out here that a linear operation on the data is not the only possible one; and that, in fact, a non-linear operation may be better. However, the linear combination has the considerable advantages of simplicity and ease of analysis.

The interested reader can find a good review of this subject in chapter 14 of Random Signals and Noise[6].

The problem is to choose the a_k of equation 5.1 so that I will be as sensitive a criterion as possible. Thus the a_k must be chosen so that the presence of a signal will cause an increase in I (over its value for noise only) by a large amount, ΔI. At the same time, however, it is necessary to keep the second moment of I, $\overline{I^2}$, low so that a given ΔI will "stand out

from the noise". Thus it is clear that the ratio $G^2 = \frac{\overline{\Delta I}^2}{\overline{I^2}}$ is the proper measure for the probability of success in using this criterion, and that the a_k must be chosen to maximize this ratio.

We now evaluate the ensemble average of ΔI, $\overline{\Delta I}$.

$$\Delta I = \sum_{k=1}^{K} a_k \hat{R}_y^{S+N}(k T_o) - \sum_{k=1}^{K} a_k \hat{R}_y^{N}(k T_o) \qquad (5.2)$$

where the superscript S+N refers to signal plus noise and the superscript N to noise only. Equation 4.4a shows that:

$$\overline{\Delta I} = \sum_{k=1}^{K} a_k \left[R_y^{S+N}(k T_o) - R_y^{N}(k T_o) \right].$$

$$\overline{\Delta I} = \frac{2}{\pi} \sum_{k=1}^{K} a_k \left[\frac{R_x^{S+N}(k T_o)}{R_x^{S+N}(0)} - \frac{R_x^{N}(k T_o)}{R_x^{N}(0)} \right]. \qquad (5.3)$$

Since the signal and noise are independent, $R_x^{S+N} = R_x^{S} + R_x^{N}$. Because of the assumption of white, band-limited noise, $R_x^{N}(k T_o) = 0$, and equation 5.3 becomes:

$$\overline{\Delta I} = \frac{2}{\pi} \sum_{k=1}^{K} a_k \frac{R_x^{S}(k T_o)}{R_x^{S}(0) + R_x^{N}(0)} .$$

If the total signal power, $R_x^{S}(0)$, is small compared to the total noise power, $R_x^{N}(0)$, we have:

$$\overline{\Delta I} = \frac{2}{\pi R_x^{N}(0)} \sum_{k=1}^{K} a_k R_x^{S}(k T_o). \qquad (5.4)$$

Next we evaluate $\overline{I^2}$, assuming that the only significant portion of the variance is caused by the noise. From equation 5.1:

$$I^2 = \sum_{k=1}^{K} \sum_{\xi=1}^{K} a_k a_\xi \hat{R}_y(k T_o) \hat{R}_y(\xi T_o).$$

Substitute for $\hat{R}_y$ its value from equation 4.4

$$\overline{I^2} = \sum_{k=1}^{K} \sum_{\xi=1}^{K} \sum_{m=1}^{N} \sum_{n=1}^{N} a_k a_\xi \overline{y_m y_{m+k} y_n y_{n+k}} \frac{1}{N^2}.$$

The argument leading to equation 4.10a shows that four-fold expectation yields zero unless $\xi = k$ and $m = n$, in which case it equals one. Then,

$$\overline{I^2} = \frac{1}{N} \sum_{k=1}^{K} a_k^2. \tag{5.5}$$

From this result and equation 5.5:

$$G^2 = N \left(\frac{2}{\pi R_x^N(0)} \right)^2 \frac{\left(\sum_{k=1}^{K} a_k R_x^S(kT_o) \right)^2}{\sum_{k=1}^{K} a_k^2}, \tag{5.6}$$

and we must now maximize equation 5.6. Multiply the right side of equation 5.6 by unity:

$$G^2 = N \left(\frac{2}{\pi R_x^N(0)} \right)^2 \left\{ \frac{\left(\sum_{k=1}^{K} a_k R_x^S(kT_o) \right)^2}{\sum_{k=1}^{K} a_k^2 \sum_{k=1}^{K} \left[R_x^S(kT_o) \right]^2} \right\} \sum_{k=1}^{K} \left[R_x^S(kT_o) \right]^2.$$

The Schwarz inequality states that the maximum value that the bracketed expression can have is one. It actually attains this value if:

$$a_k = R_x^S(kT_o). \tag{5.7}$$

Then we have for G:

$$G = \frac{2}{\pi R_x^N(0)} \sqrt{N \sum_{k=1}^{K} \left[R_x^S(k T_o)\right]^2} \quad . \qquad (5.8)$$

Equations 5.5 and 5.7 show how the questions at the beginning of this section may be answered. Simply choose the a_k by taking points on the autocorrelation function of the signal which is to be tested (normalize, of course, so that $\sum_{k=1}^{K} a_k^2 = 1$). Construct I according to equation 5.1. If $I \gg \sqrt{\frac{1}{N}}$, then the signal was surely present. To decide between two rival hypotheses, subtract their corresponding I's. If the difference is $\gg \sqrt{\frac{1}{N}}$, a clear choice may be made.

Equation 5.8, which gives the "signal-to-noise" ratio of this process, shows several interesting features. One is the factor $\frac{2}{\pi}$, which does not appear in a parallel analysis in which the system has no limiter. That factor is the cost in detectability which must be paid for the simplicity that is offered. Second, is the fact that signals whose autocorrelation function take a long time to die away (e.g., narrow band signals) are more detectable.

Chapter VI

The First Correlator

The task of the correlator is to compute sums of the form

$$R_\tau = \sum_{n=1}^{N} y_n \, y_{n+\tau}$$

where y_n is the value of y at the n^{th} sample and is always +1 or -1. The logical circuitry available to this project consists of the so-called AND-OR dynamic logic. The basic module is shown in figure 6.1. In this type of circuitry, first introduced as SEAC by the National Bureau of Standards, the state ONE is represented by a pulse on the line in question, and the state ZERO by the absence of a pulse. An AND gate is activated if pulses arrive at all four of its inputs simultaneously. The OR gate is activated if any AND gate "fires". The clock pulse is used to fix precisely the timing of pulses from the OR gate, and the amplifier regenerates the pulse to a standard shape. An output appears one microsecond after the set of inputs that caused it. Two outputs are available from each module. One is the Boolean function F of the inputs, and the other is its compliment $\overline{F}$. This combination of AND-OR and of complimentation allows one module to compute any Boolean function of three variables, and many functions of four variables.

A second basic module is composed of delay lines (1 microsecond duration). An advantage of this dynamic logic is that often a delay line can be used as the equivalent of an active module.

An example, shown in figure 6.2, will demonstrate some of the properties of these devices. Here we have an active module driving 3 delay lines (plus three more for complimentation). The Boolean function generated is

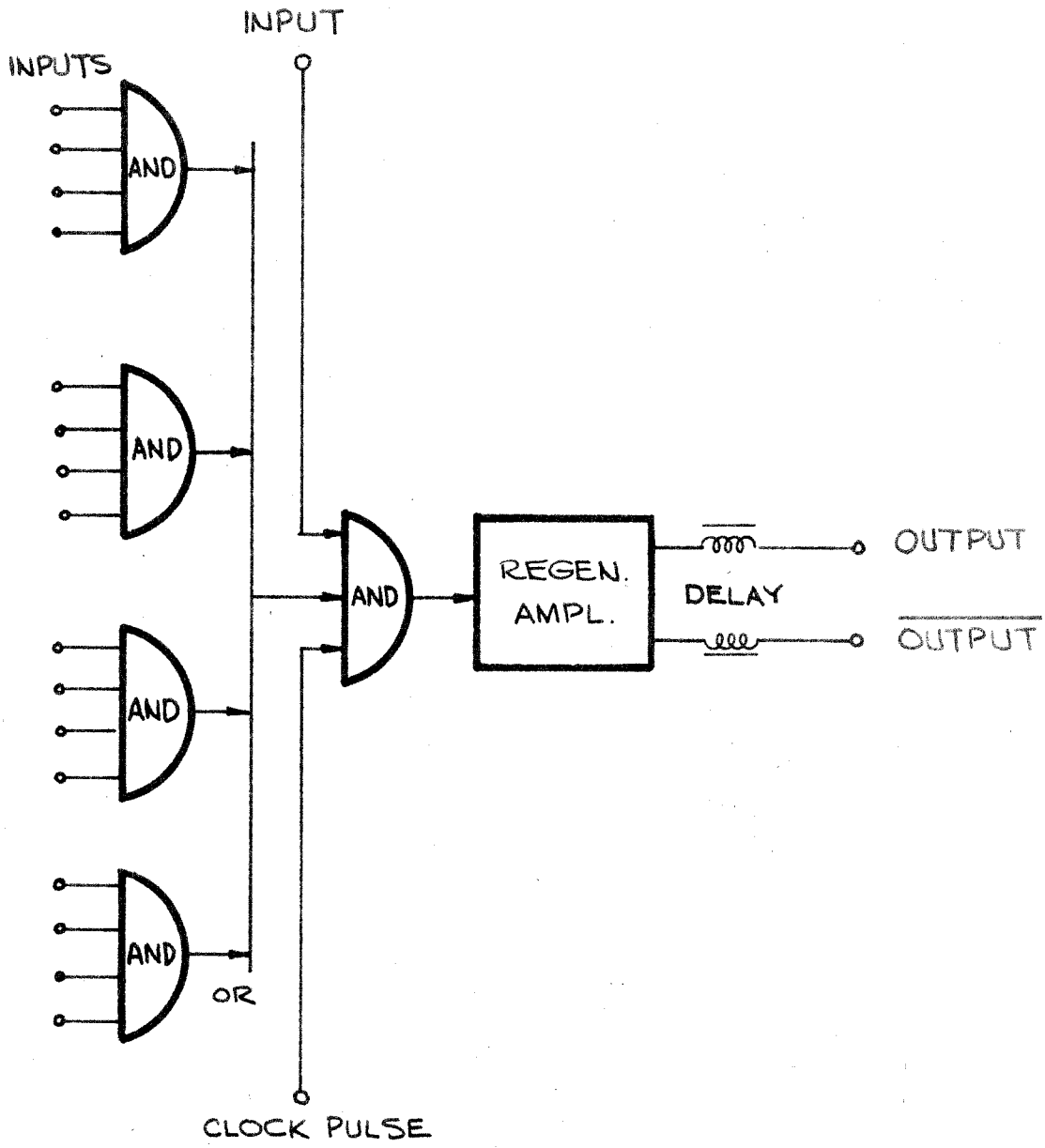

BLOCK DIAGRAM OF DIGITAL MODULE

FIG. G-1

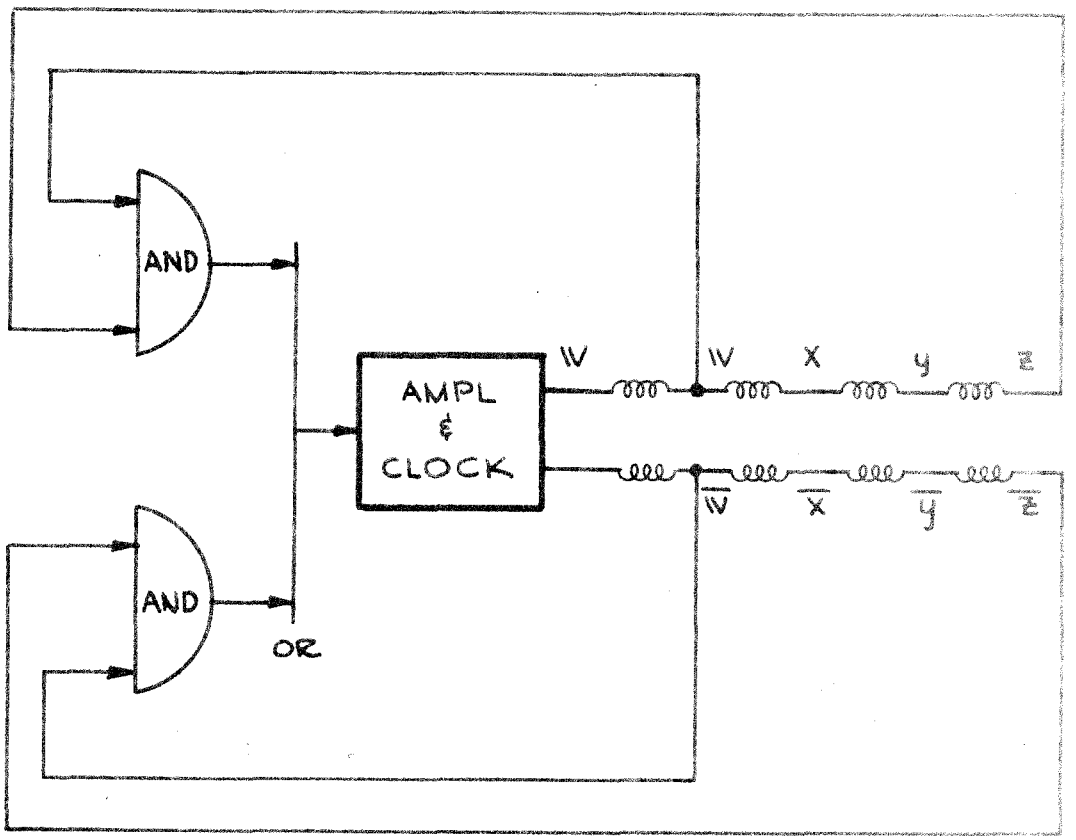

$$W = Wz + \overline{W}\,\overline{z}$$

DIAGRAM OF SEQUENCE GENERATOR

FIG. 6.2

$W = WZ + \overline{W}\,\overline{Z}$. This expression is a standard[5] symbolism for a difference equation relating the output of module W to its inputs one clock period earlier. Literally, this expression means that one clock period hence W will be in the ONE state if W and Z are now in the ONE state, or if W and Z are now in the ZERO state. Otherwise, W will be in the ZERO state. When the circuit is first energized, the delay lines will be empty. That is: W, X, Y, and Z will be in the ZERO state and their complements $\overline{W}$, $\overline{X}$, $\overline{Y}$, and $\overline{Z}$ will be ONE's. The next micro-second W will be ONE (the lower AND-gate will have fired). As the signals propagate down the line, the pattern of table 6.1 is generated.

Table 6.1

	W	X	Y	Z	
	0	0	0	0	1st Bit Time
	1	0	0	0	2nd Bit Time
	0	1	0	0	3rd " "
	1	0	1	0	.
	0	1	0	1	.
	0	0	1	0	.
	1	0	0	1	
	1	1	0	0	
	0	1	1	0	
	1	0	1	1	
	1	1	0	1	
*	1	1	1	0	
	0	1	1	1	
	0	0	1	1	
	0	0	0	1	
	0	0	0	0	

Repeat

This pattern, of 15 μ sec. duration, will keep repeating itself continuously.

If a single pulse once every 15 μ sec. is desired, it may be obtained merely by connecting W, X, and Y to and AND gate (F = WXY). Table 6.1 shows this gate would fire exactly once every cycle (at the time marked with a *).

Figure 6.3 shows a tentative design for a correlator which can be constructed with these modules.

Each multiplier gives an output if both of its inputs are ONE or if both are ZERO, e.g. $F = y_n\, y_{n-\tau} + \bar{y}_n\, \bar{y}_{n-\tau}$. Each accumulator is a chain of flip-flops that adds one to the count every time the corresponding multiplier produces an output. Thus the accumulator for $\tau = \tau_k$ counts the total number of "agreements" between y_n and $y_{n-\tau_k}$. Since $\sum y_n\, y_{n-\tau}$ = number of "agreements" - number of "disagreements" and the total number of agreements + disagreements is stored in the accumulator for $\tau = 0$, then $\sum y_n\, y_{n-\tau_k} = 2$(count in accumulator τ_k) - (count in accumulator 0). This relation obviates the need for accumulators that can count both up and down, and simplifies the circuitry considerably.

The plan described in figure 6.3 is impractical because of the large amount of hardware it demands. Each delay line must be 15 units long (the sampling period = 15 microseconds) and, since 45 points on the auto-correlation function are to be calculated, there must be 45 such delays. This adds up to an extravagant amount of delay. The accumulators represent an impractical amount of hardware also. Since the correlator is to run all day without an overflow, each accumulator must have a capacity of 32 bits. If each bit is realized with a flip-flop; 32 x 45, which equals 1440, flip-flops are necessary. It is clear that simplification must be obtained.

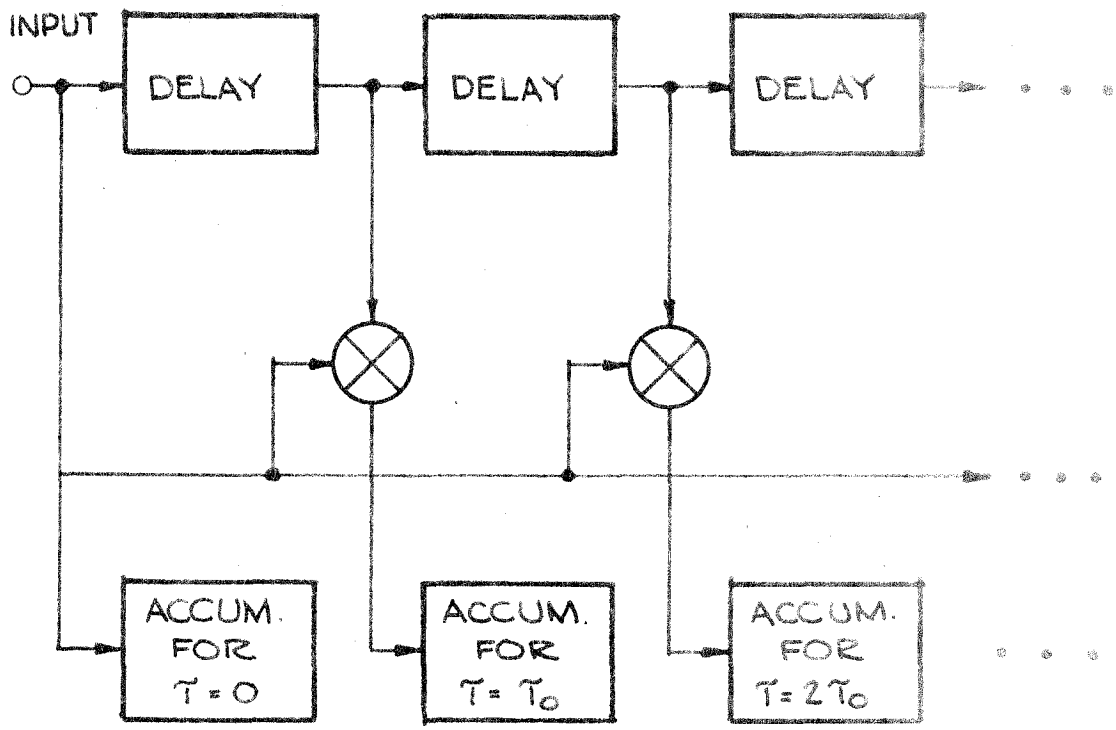

BLOCK DIAGRAM OF CORRELATOR

FIG. 6.3

The amount of delay can be reduced by a factor of 15 by the simple strategy of storing the last 45 samples of the input in a recirculating delay line. Then, whenever the input is to be sampled, the oldest data element is removed from the delay line and lost, while the new sample is inserted into its proper place in the line.

A similar idea can be used to reduce the number of flip-flops in the accumulators. Each accumulator can be realized by a circulating delay line of 32 bits. The disadvantage of this method lies in the timing, i.e. input data can only be assimilated when the circulating line is in the correct alignment, once every 32 bit times. The input rate is much higher than that, although the rate drops one octave for every bit position from the front of the accumulator.

Figure 6.4 illustrates a scheme which allows an accumulator to "fan out" into recirculating delay lines. Assume input pulses arrive no faster than every bit time. Then the minimum period between overflows of the 2^{nd} bit flip-flop is $2^2 = 4$ bit times, the same time that is required between successive alignments of the 4 bit recirculating line. Although the maximum overflow <u>rate</u> is slow enough, an overflow <u>may</u> occur at any time. Hence a buffer stage is necessary to hold the overflow until it can be used by the next stage; at which time the buffer must be reset to zero. This process is repeated in the 4 bit recirculating line, where the 4^{th} bit position is reserved to act as a buffer. The first 3 bits of this line cannot have overflows closer together than $4(2)^3 = 32$ bit times, just right for the 32 bit recirculating line that follows. In this way a 32 bit accumulator (now grown to 37 bits) is realized with 3 flip-flops and 2 recirculating lines.

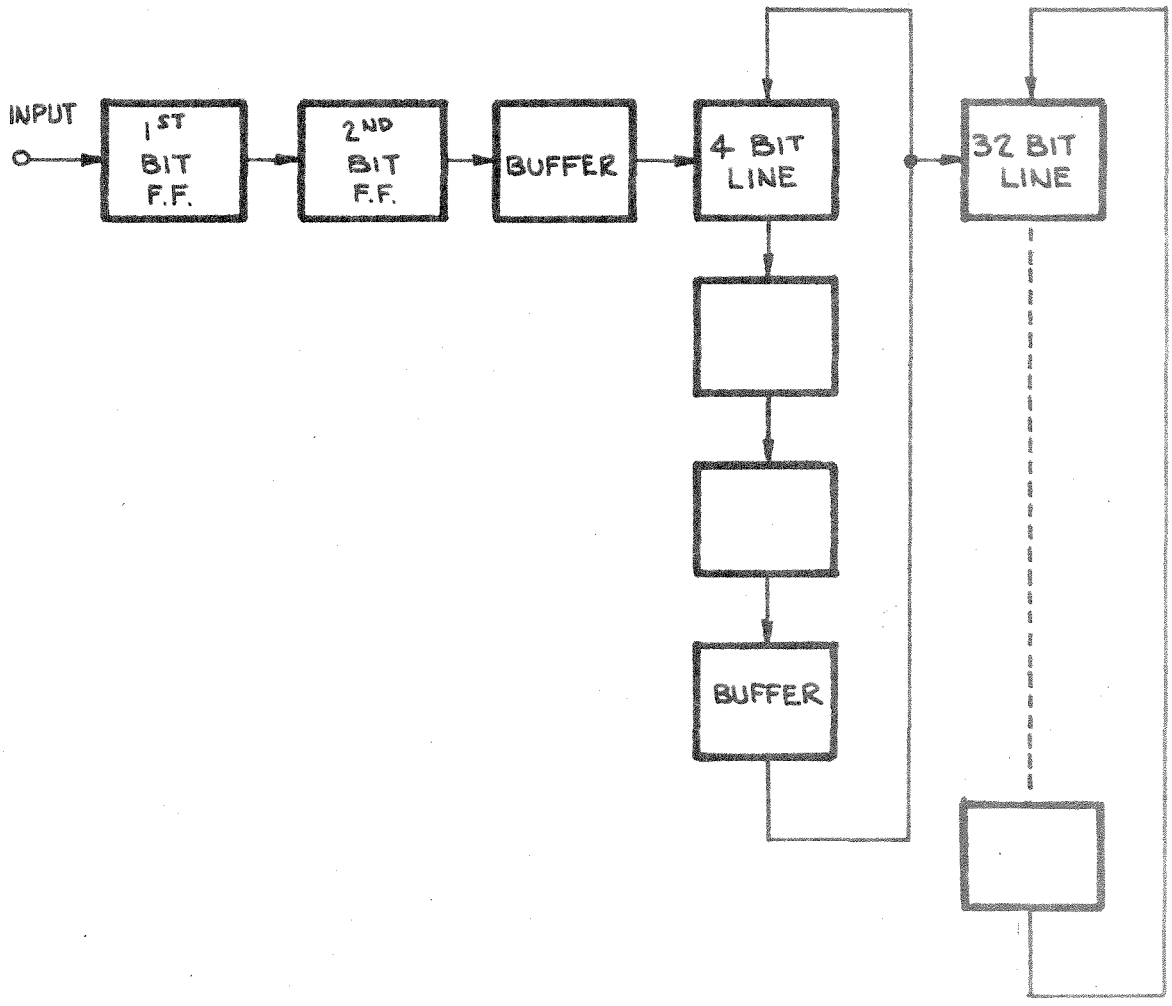

ONE 37-BIT ACCUMULATOR

FIG. 6.4

Next consider what happens if input pulses do not arrive every bit time but only once every 15 times. Then the mechanization of figure 6.4 may be replaced by that of figure 6.5. The timing is still correct since all times have been divided by 15. However, 14/15 of the accumulator's capacity is unused. Now it is possible to make the set of lines of figure 6.5 to perform as 15 independent accumulators, and a great saving of hardware has been achieved. The first bit position in the first line holds the least significant digit for R(0), the second position holds that for $R(T_o)$, the third for $R(2\ T_o)$, and so on. The second line holds the next significant digit for R(0), $R(T_o)$, $R(2\ T_o)$, etc. This interlacing continues through to the last line, where the first 32 positions hold the 32 most significant digits of R(0), the next 32 for $R(T_o)$, the next for $R(2\ T_o)$, etc.

The lines of figure 6.5 were realized with sonic delays employing the principle of magneto-striction to excite sonic waves in nickle wires. Lines were available with delays ranging up to a thousand bit times (microseconds).

Figure 6.6 illustrates how the input storage mentioned earlier may be combined with the 15 accumulators of figure 6.5 to produce the first 15 points on the autocorrelation function. The last 15 samples of the input wave are stored in the recirculating line. In addition, the last sample is stored separately in a flip-flop. The comperator is shown comparing the n^{th} sample with itself. One bit time later, it compares the n^{th} sample with the $(n-14)^{th}$, and the next bit with with (n-13) and then (n-12) and so on. In this way, the successive outputs of the comparator are R(0), $R(14\ T_o)$, $R(13\ T_o)$, ..., $R(T_o)$. At that instant, the input is

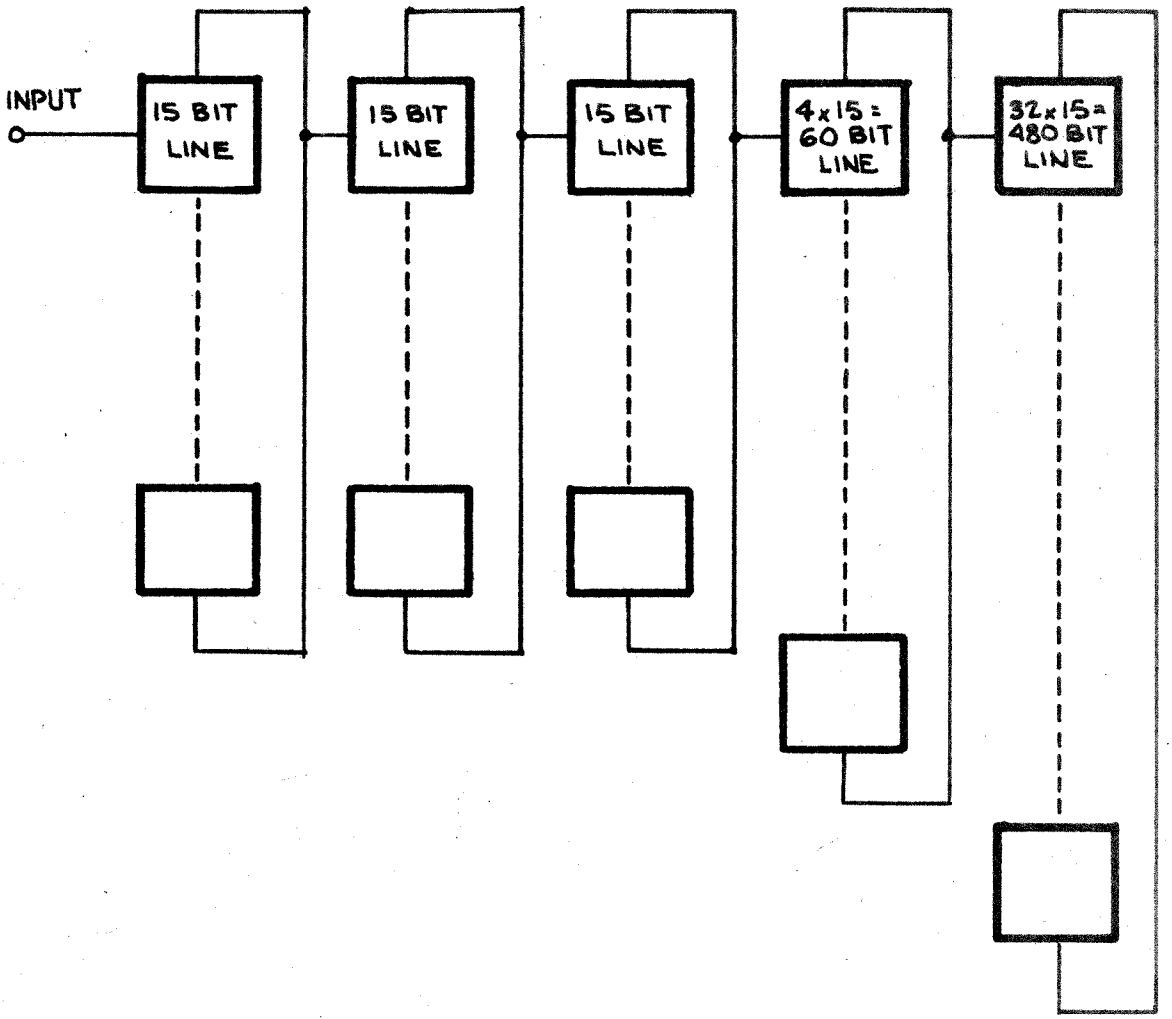

FIFTEEN 37-BIT ACCUMULATORS

FIG. 6.5

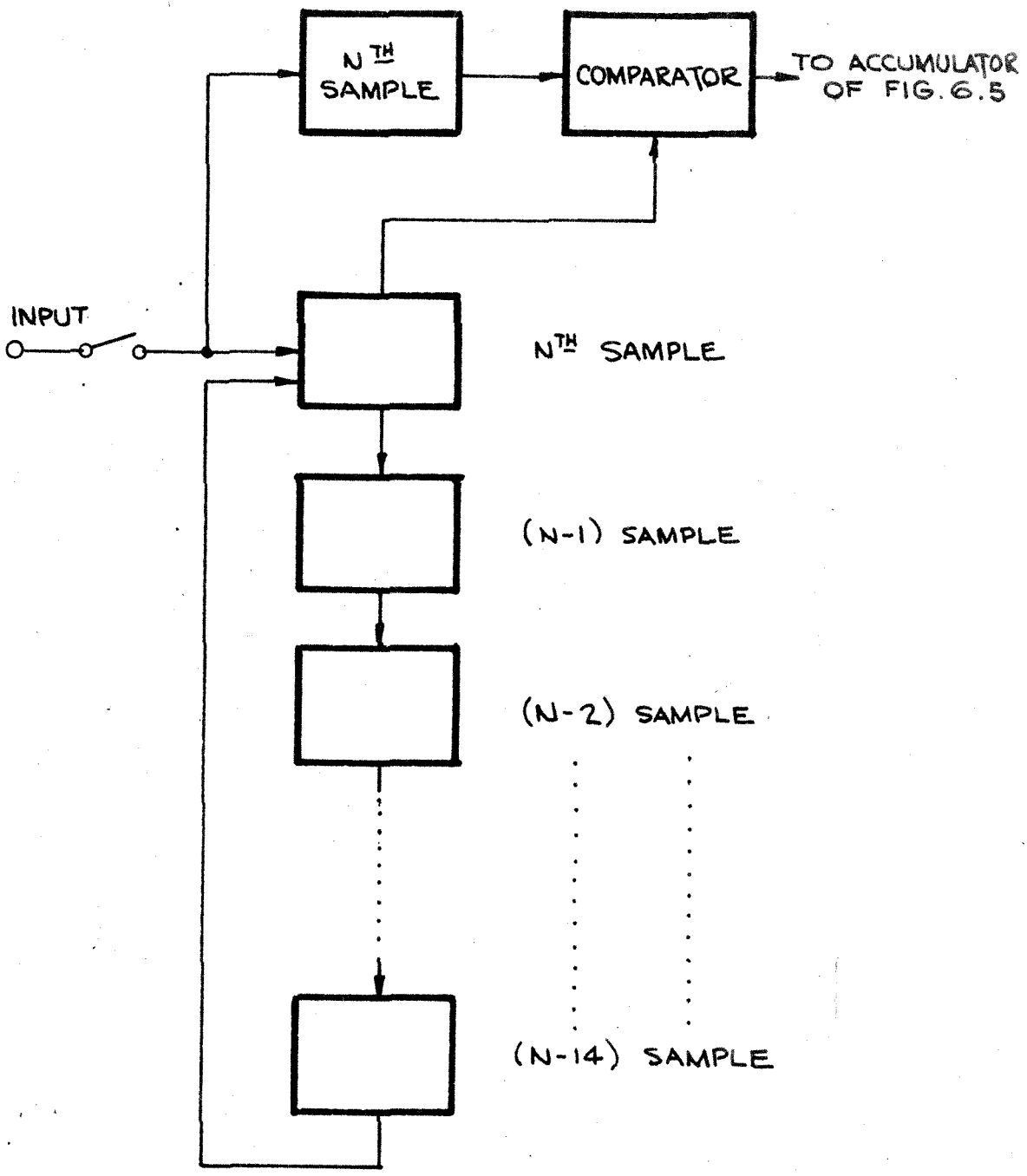

INPUT STORAGE DEVICE

FIG. 6.6

sampled again, the oldest data element (n-14) is removed, each sample is advanced one place in the line, and the new sample is inserted. The comparator output repeats R(0), R(14 T_o), ..., R(T_o); but this time the products are based on the latest piece of input data. These comparator outputs arrive just in time to be accepted by all 15 channels of the composite accumulator.

The Venus project correlator paralleled three sets of devices identical to those illustrated in figures 6.5 and 6.6 in order to compute 3 x 15 = 45 points on the autocorrelation function.

Digital circuitry in addition to that described above is necessary for this scheme. For example, one must have a source of pulses separated by 15 bit times from each other in order to effect the sampling. The realization for this was, of course, the circuit of figure 6.2. Other strings of timing pulses are required to interrogate and reset the buffers of the accumulators of figure 6.5. The first buffer must be tested every four bit times. The circuit to accomplish this is displayed in figure 6.7. The notation has been simplified by reducing the gate-amplifier-delay module to one AND gate, and the subscripts refer to the number of delays. Thus the function generated by the module is

$$X = \overline{X}\,\overline{X}_1\,\overline{X}_2 .$$

Again, the bar denotes complementation. Analysis of this circuit shows that after the module generates a pulse, three bit times must elapse before it can fire again.

The second buffer set must be tested and re-set every 32 bit times. A device similar to that illustrated in figure 6.2 was used to realize that set of pulses. When five stages (one active module and four delay

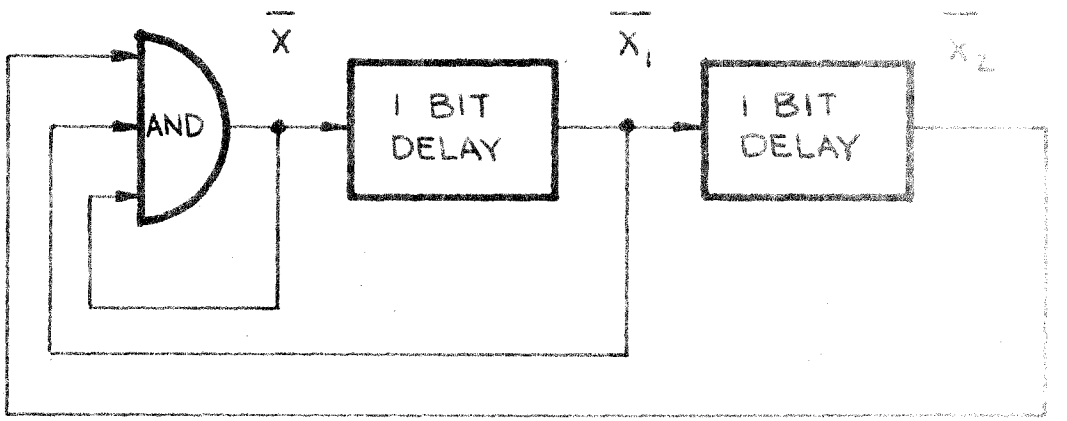

GENERATOR FOR THE SEQUENCE 10001000...

FIG. 6.7

lines) are connected in a suitable feedback circuit a pattern of pulses with a repetition period of $2^5 - 1 = 31$ bit times is produced. One such logic is expressed by the connections.

$$X = X_4 \overline{X}_2 + \overline{X}_4 X_2$$

If the device is started with five consecutive pulses, the following pattern of pulses and no pulses (ones and zeros) will be generated:

1 1 1 1 1 0 0 0 1 1 0 1 1 1 0 1 0 1 0 0 0 0 $\underline{1}$ 0 0 1 0 1 1 0 0 (repeat).

The period of this sequence can be increased to 32 if the pulse at the 23rd position is inhibited. This can be done by a separate module set to fire when it recognizes the combination that comes up one bit time early; i.e. $G = \overline{X}_4 X_3 \overline{X}_2 \overline{X}_1 \overline{X}$. The output of G is used to inhibit F. An additional gate must be used to start the device running again, otherwise it will produce all zeros from then on. The logical equations then become:

$$F = X_4 \overline{X}_2 \overline{G} + \overline{X}_4 X_2 \overline{G} + \overline{X}_4 \overline{X}_3 \overline{X}_2 \overline{X}_1 \overline{X} \qquad \text{and}$$

$$G = \overline{X}_4 X_3 \overline{X}_2 \overline{X}_1 \overline{X}.$$

Figure 6.8 illustrates this device. Note that G produces an output every 32 bit times, as desired.

The correlator described above has, at the end of an observation, 45 binary numbers stored in the recirculating delay lines. For these numbers to be useful, some method of reading them out of the lines must be devised. A Hewlet Packard digital printer was available for this job. The plan for the realization of the print-out is simple. Each bit in the delay lines is loaded into a flip-flop, one at a time, and the printer then records the state of the flip-flop (one or zero). After

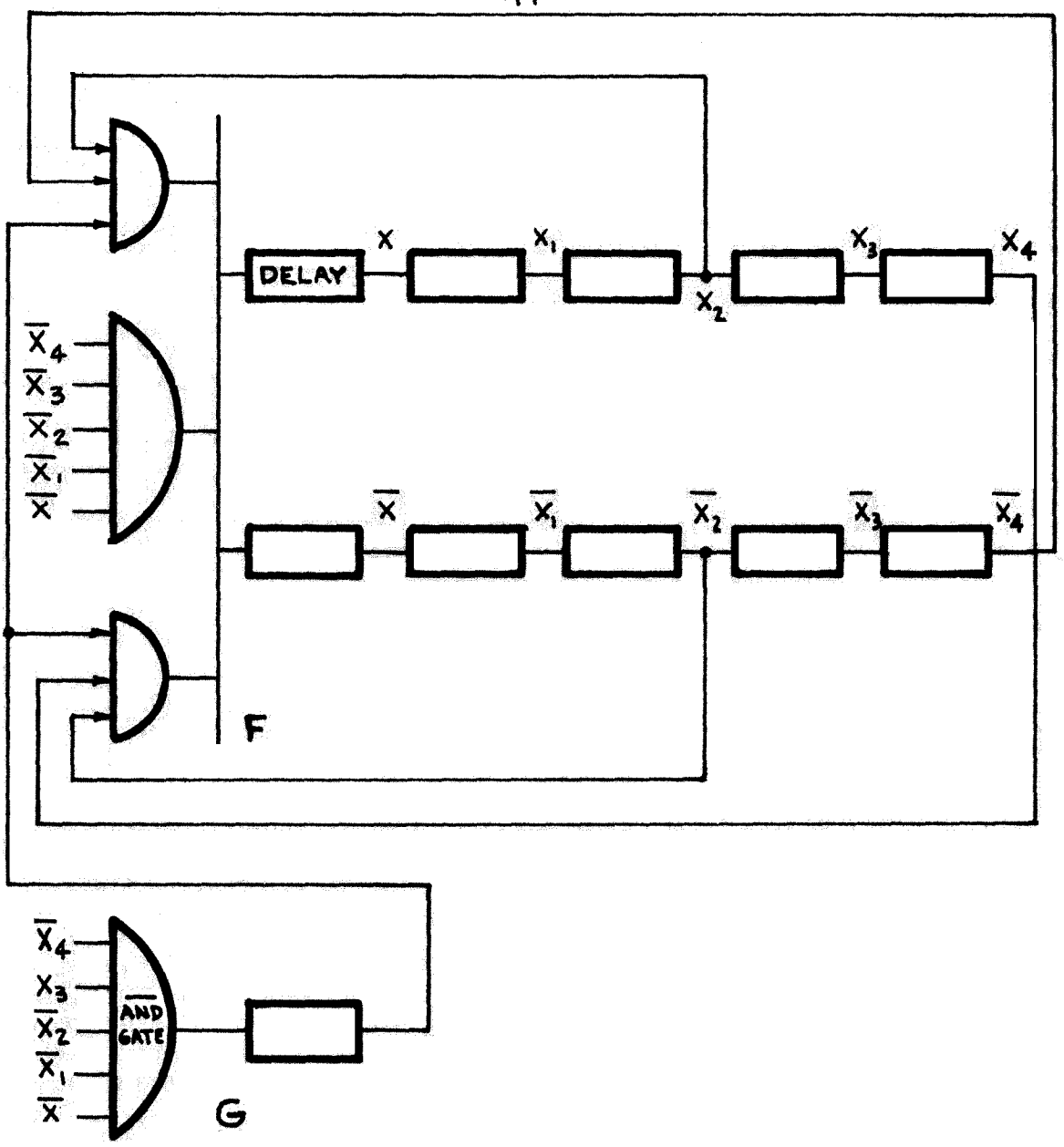

OUTPUT OF F: 1111100011011101010000010010110O (REPEAT)
" " " G: 0000000000000000000010000000000(")

SEQUENCE GENERATOR

FIG. 6.8

allowing sufficient time for the printer to finish (governed by an external oscillator), the next bit is loaded into the flip-flop, and so on until the recording is complete. A marker must be printed after every 32 prints so that the most significant digit of each number may be identified. Finally, the print out routine must stop when every digit has been recorded.

The plan just described is simple in concept, and can be realized easily by having one pulse circulate in a 480 bit delay line identifying the digit to be recorded. After a print out, the delay line is shortened by one bit for a time of 480 bits, allowing the pulse to advance in phase and serve as a marker for the next digit to be printed. Unfortunately, the extra delay line was not available, so a more complicated scheme was necessary. A device similar to the one illustrated in figure 6.8 was built, but containing ten stages instead of five. Appropriate feedback logic was used so that a pulse pattern of period $2^{10} - 1 = 1047$ bit times was generated. An AND gate similar to G of figure 6.8 was set to inhibit the one pulse that reduced the generator's period to 480. Then, whenever the period was to be shortened by one, an additional gate was energized which modified the original logic for just one bit time, producing an output in 479 microseconds instead of 480. The process continued until the pulse was generated back in its original phase, at which time the print-out routine was stopped.

The correlator, including its digital printer, limiter, and a square wave generator to be described subsequently, were all housed in one standard rack.

Chapter VII

Calibration of the Spectrum

The power spectrum of the Venus echo must be calibrated, since the noise spectrum (as modified by the pass band of the receiver) is added to the Venus spectrum. One might measure the spectrum of the noise only (i.e., with the transmitter turned off, but the rest of the system operating) and subtract this from the Venus plus noise spectrum. Of course, the noise-only measurement must be as precise as the signal measurement, which requires as many hours for integrating noise as for signal. A major difficulty arises when one considers that the pass band may change its shape slightly over a period of hours; and slight changes may be important where the signal is weak compared to the noise. The maser amplifier was almost certain to be a source of that kind of drift.

This difficulty was eliminated by interlacing the calibration with the measurement. The transmitter was turned off and on continuously with a two second period. One plan was to measure the autocorrelation function for the time that the transmitter was on (allowing for the time of flight, of course); and then, with a separate correlator, measure the noise only condition. The two autocorrelation functions would then be corrected with formula 4.1, subtracted, and Fourier transformed. This would yield the desired spectrum, free from the influence (to first order) of the band pass of the receiver. Such a plan would double the amount of digital equipment needed, and was therefore out of the question. The following equivalent plan was used. During the time that the transmitter was on (again allowing for the time of flight) the correlator measured R_y, but during the off time $-R_y$ was measured. At the end of an observation, the

correlator's output, ΔR_y, would be

$$\Delta R_y = R_y \text{ for signal plus noise} - R_y \text{ for noise only.} \qquad (7.1)$$

We will now show how the spectrum may be found from ΔR_y.

Let the autocorrelation of the noise only be R_N where $R_N(0) = 1$, and let that of the signal be $\underline{a}R_S$, where $R_S(0) = 1$ and $\underline{a} \ll 1$. The absolute levels are not important because of the action of the limiter. $\underline{a}$ represents the ratio of total signal power to total noise power. From formula 4.1, repeated here for convenience, we have:

$$\frac{\pi}{2} R_y = \sin^{-1} \left(\frac{R_x}{R_x(0)} \right). \qquad (7.2)$$

It then follows that

$$\frac{\pi}{2} \Delta R_y = \sin^{-1} \left(\frac{R_N + aR_S}{1 + a} \right) - \sin^{-1} R_N,$$

$$\frac{\pi}{2} \Delta R_y = \sin^{-1} \left(\frac{a(R_S - R_N)}{1 + a} + R_N \right) - \sin^{-1} R_N,$$

and, since $a \ll 1$,

$$\frac{\pi}{2} \Delta R_y \approx \frac{a(R_S - R_N)}{1 + a} \frac{d}{dR_N} \left[\sin^{-1} R_N \right].$$

or

$$\frac{\pi}{2} \Delta R_y \approx \frac{a(R_S - R_N)}{\sqrt{1 - R_N^2}},$$

$$aR_S - aR_N = \frac{\pi}{2} \sqrt{1 - R_N^2}\, \Delta R_y. \qquad (7.3)$$

Equation 7.3 shows what the proper strategy must be. The right-hand side is the quantity which is measured. It is then Fourier transformed and

the result is the desired spectrogram. The quantity $\underline{a}$ is never measured, but it appears implicitly in the spectrogram. Equation 7.3 shows that in addition to the echo, a diminished and inverted image of the noise (as modified by the pass band of the receiver) appears in the spectrogram. It is diminished by the factor $\underline{a}$ so that the total power as portrayed by the spectrogram is zero. This explains the phenomenon of the negative excursions.

The factor $\sqrt{1 - R_N^2}$ was measured separately, with the receiver picking up noise only. Great precision is not necessary for that measurement, since it does not involve the subtraction of two nearly equal quantities. It is interesting to note that, for the Venus experiment, $R_N(k\ T_o)$ was nearly zero for all values of k except the first four, and that for the worst case, $\sqrt{1 - R_N^2}$ was never less than 0.95.

It is now necessary to describe the procedure by which ΔR_y can be measured by a correlator which has accumulators which can have their contents increased but not decreased. From the definitions:

$$\Delta R_y = \frac{1}{N}\left(\sum_{i=1}^{N} y_i\, y_{i+\tau}\right)_{S+N} - \frac{1}{N}\left(\sum_{i=1}^{N} y_i\, y_{i+\tau}\right)_N , \qquad (7.4)$$

where the subscript S+N refers to the condition of signal plus noise and N refers to noise only. Let:

$A \doteq$ number of times $y_i = y_{i+\tau}$ (agreements)

$D \doteq$ number of times $y_i \neq y_{i+\tau}$ (disagreements).

Then

$$\Delta R_y = \frac{1}{N}\left(A_{S+N} - D_{S+N} - A_N + D_N\right). \qquad (7.5)$$

The two negative quantities in (7.5) can be replaced by positive ones by making use of the facts that:

$$D_{S+N} = N - A_{S+N} \quad \text{and}$$

$$A_N = N - D_N.$$

Hence:

$$\Delta R_y = \frac{1}{N} (A_{S+N} - N + A_{S+N} - N + D_N + D_N)$$

$$\Delta R_y = \frac{2}{N} (A_{S+N} + D_N) - 2. \qquad (7.6)$$

N is, of course, only half of the total number of counts, a number which is stored in one of the accumulators.

Equation (7.6) shows what the proper strategy must be. During the time the signal is being received, accumulate the number of agreements between y_i and $y_{i+\tau}$, and during the noise only period, accumulate the disagreements. This strategy was instrumented easily by switching the logic of one flip-flop in the correlator.

These considerations show the desirability of having two computer modes to calculate the power spectrum from the correlator outputs. In the first, or direct, mode the total number of agreements, A_k, of y_i with y_{i+k} is noted. Then the autocorrelation function at y is calculated as

$$\hat{R}_y(k T_o) = \frac{2A_k - A_o}{A_o} . \qquad (7.7)$$

The autocorrelation function at x is then calculated:

$$\hat{R}_x (k T_o) = \sin \left[\frac{\pi}{2} R_y (k T_o) \right] .$$

Finally, the power spectrum is calculated:

$$\hat{P}(f) = \sum_{k=1}^{K} 2 \hat{R}_x(k T_o) \cos (\pi k \frac{f}{f_o}) . \qquad (7.8)$$

The second mode takes account of the subtraction process described above. The correlator output, B_k, is then the number of agreements during the signal on condition plus the number of disagreements during the noise only period. The following calculations are made:

$$\Delta \hat{R}_y(k\,T_o) = \frac{4B_k}{B_o} - 2, \quad \text{where } B_o = \text{the total number of counts.} \tag{7.9}$$

Then the power spectrum, $\hat{W}(f)$, is calculated as:

$$\hat{W}(f) = \sum_{k=1}^{K} \pi\sqrt{1 - R_N^2}\,\Delta R_y(k\,T_o) \cos\left(\pi k \frac{f}{f_o}\right). \tag{7.10}$$

As discussed above, $\hat{W}(f)$ contains the spectrum of the Venus echo superimposed upon an inverted and diminished noise spectrum. This is not just a result of the particular process described above as the second mode, but is an inherent phenomenon of the subtraction process. This is true because of the action of the limiter, which produces an output of the same total power regardless of what the input level might be. Hence the noise part of the signal plus noise spectrum is somewhat smaller than the spectrum of the noise only.

Chapter VII

Appendix I

There is a question which arises regarding the subtraction process described in Chapter VII which properly belongs in an appendix. That question concerns the results of switching from the signal plus noise condition to noise only (or vice versa). Immediately after switching, the input storage still has data from the previous condition.

Figure 7.1 is a diagram of the situation. Notice that the noise during the noise-only condition is slightly larger than it is during the signal plus noise period. As mentioned before, this is a result of the normalization caused by the limiter.

Consider time broken up into four parts, as indicated in figure 7.1. The correlator produces the following results in each interval:

$$- \tau (bR_{NN} + bR_{NS}) \text{ for the interval } t_1$$

$$+ (P - \tau)(R_{SS} + R_{NN}) \text{ for the interval } t_2$$

$$+ \tau (bR_{NS} + bR_{NN}) \text{ for the interval } t_3 \text{ and}$$

$$- (P - \tau)(b^2 R_{NN}) \text{ for the interval } t_4,$$

where: R_{NN} = noise correlated with noise

R_{SS} = signal correlated with signal and

R_{NS} = signal correlated with noise.

The sum of these, ΔR, equals:

$$\Delta R = R_{SS} (P - \tau) - R_{NN} (P + \tau)(b^2 - 1). \quad (7.9)$$

Two things are made evident by this result. One is the appearance of an inverted and diminished noise spectrum in the final spectrogram.

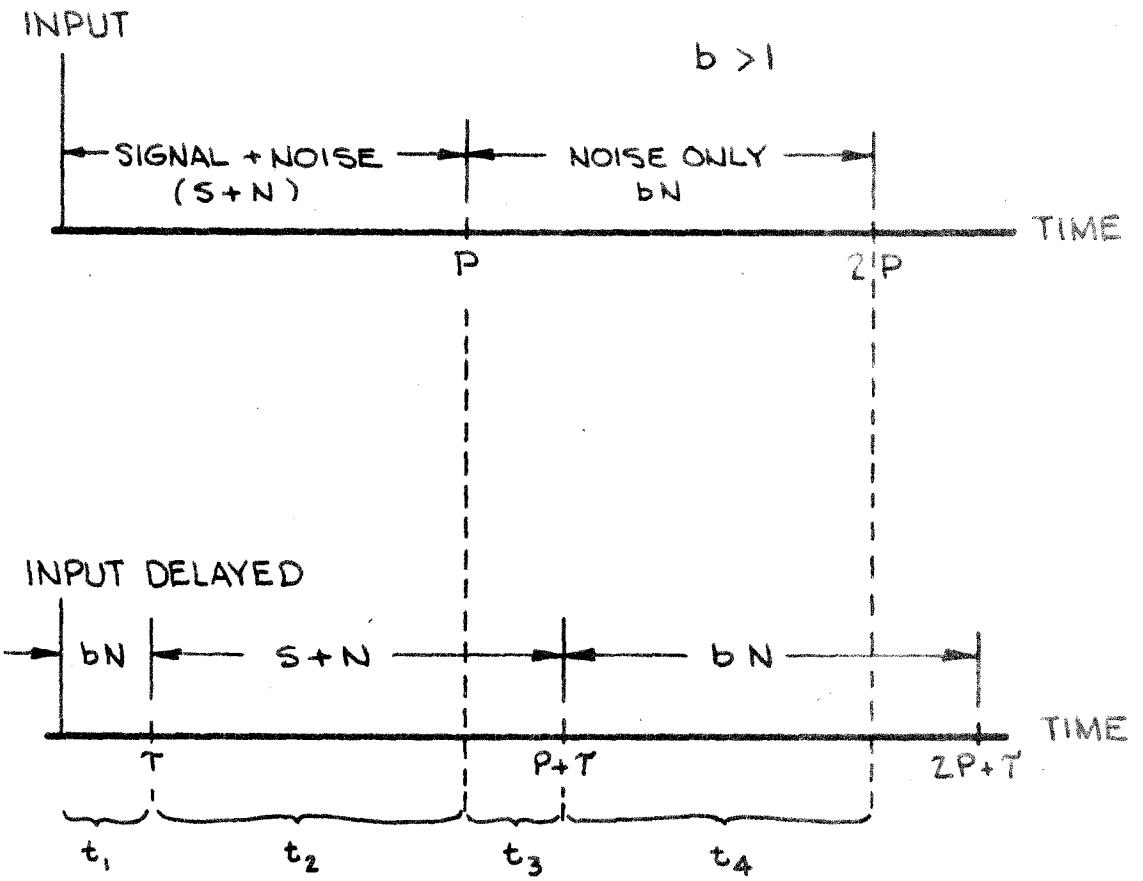

CORRELATION DETAIL

FIG. 7.1

This was explained in chapter VII. The other is the modification of the signal autocorrelation function by the factor $(P - \tau)$. The signal spectrum is then convolved by the transform of this factor.

One can see, from figure 7.1, that this factor is the same which would have resulted if the noise were zero and the transmitter were keyed off and on at the same rate as before. Hence the factor $(P - \tau)$ is the result of the modulation process, and the broadening of the spectrum by convolution may be thought of as broadening by modulation.

For the Venus experiment, the keying rate was $\frac{1}{2}$ CPS. The corresponding broadening was considered quite negligible.

Chapter VIII

Radiometer Analysis

A. Radiometer Description

A method for detecting weak signals masked by receiver noise has long been used by radio astronomers[10]. Called a switched radiometer, the system continuously switches the receiver input off and on detects the small resulting change of signal noise level. This method makes signal detection independent (to first order) of changes or drifts in the gain of the receiver. A serious problem which arises in this type of receiver is the changes of gain which are caused by physical imperfections of the switch. Such changes appear as signals at the receiver's output.

Radar astronomy offers the possibility of avoiding that problem altogether by the simple expedient of switching the transmitter off and on instead of the receiver input. Such a radiometer was constructed for the Venus experiment. Figure 8.1 is a simplified block diagram of the system.

The entire maser, programmed-local-oscillator, receiver complex has been replaced by one block labelled "band pass filter". The signal produces a small square wave at the detector output which is accompanied by relatively strong noise. A multiplier compares this square wave to the locally generated one which has been shifted in phase by just the amount necessary to account for the time of flight. The multiplier leaves the noise essentially unchanged, but converts the signal to DC of a magnitude and polarity which depends upon the relative phases of the two square waves. An RC circuit (a 68 second time constant proved most convenient) allows the DC to pass but removes much of the noise.

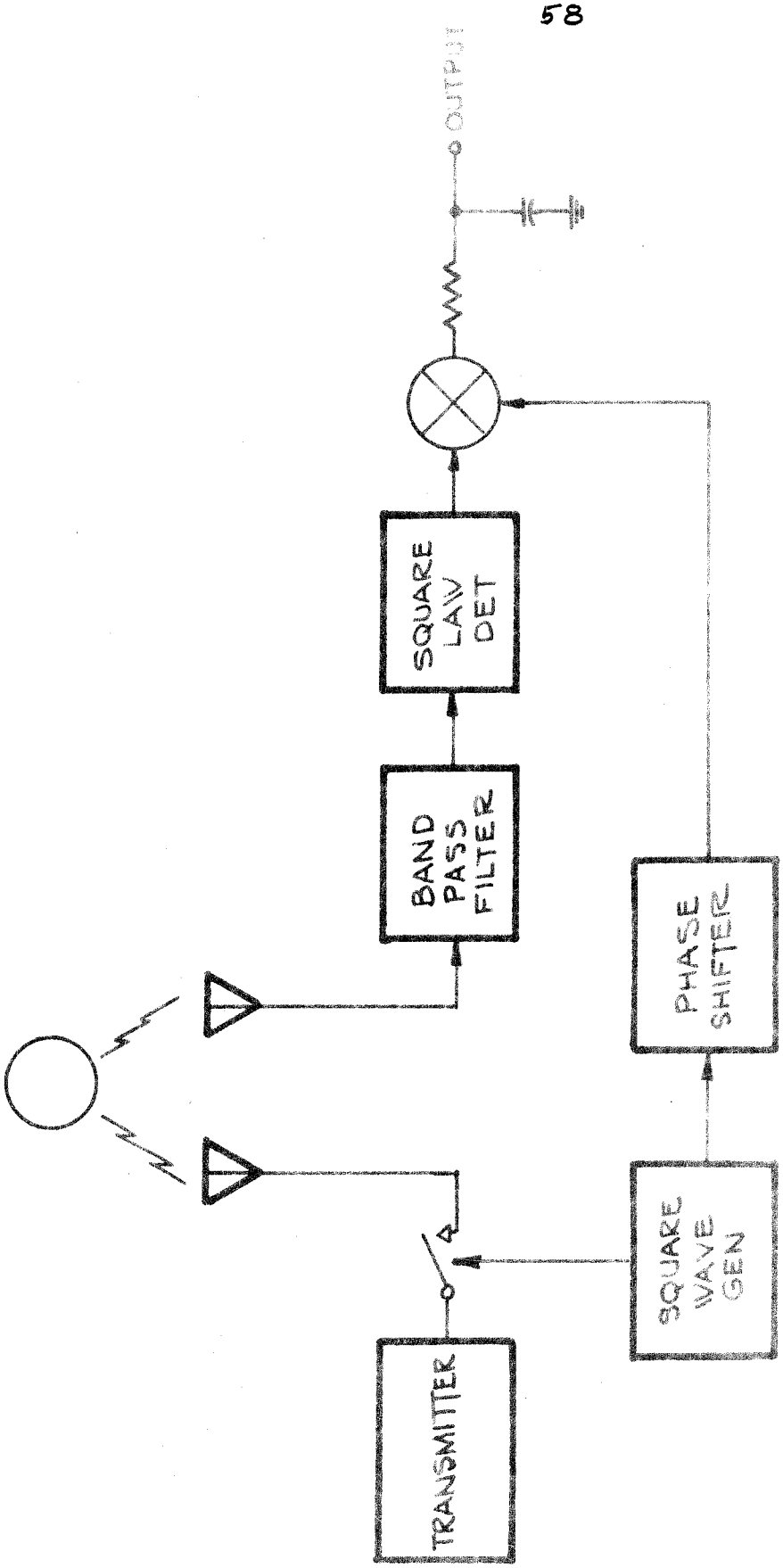

RADIOMETER BLOCK DIAGRAM

Fig. 6.1

A brief description of the blocks of figure 8.1 is in order. The operation of the square wave generator is digital, counting down pulses from a megacycle crystal clock. Output frequencies from $\frac{1}{2}$ to 128 cycles per second are available in octave steps. The phase shifter is also digital. It operates by recognizing any pre-set count in the square wave generator, and controls a flip-flop accordingly. This produces a square wave output with a very accurately known phase relationship to the original one.

The square law detector is simply a diode with a small forward bias. The approximation to square law at the low levels that were used was quite good.

Since one of the inputs to the multiplier is always either plus one or minus one, the multiplier may be realized quite simply with a relay; the coil being one input and a phase inverter supplying the other.

Two modes of operation were used. For the first mode, the phase shifter was programmed in order to keep the two square waves in phase. Programming was necessary because the time delay from the transmitter to Venus to the receiver was continuously changing, due to the relative motion between the Earth and Venus. This time delay can be computed from the astronomical ephemerides, but only to the accuracy of the AU (Astronomical Unit, the yardstick for the solar system) that is used.

In this first mode of operation, the square wave generator was set to $\frac{1}{2}$ cps. This low frequency was chosen to render negligible a possible error in the accepted AU of as much as one part in a thousand.

Several channels were used, each with a different pre-detection filter. Thus it was possible to compare the signal power through filters

of different bandwidths and infer spectral features of the signal. Figure 8.2 shows a sample of such a recording.

At the end of each observation the channels were calibrated by injecting a known amount of excess noise into the system. The calibration applied to the measurement of figure 8.2 showed that the signal power was essentially the same through all of the filters, $1.7\ (10)^{-20}$ watts, referred to the antenna terminals. Similar measurements made throughout the experiment indicate a radar cross-section for Venus of 11% of its geometric cross-section.

B. Signal to Noise Ratio Analysis

The output deflection of the radiometer divided by its standard deviation may be calculated with the aid of an analysis which follows.

Let S be the signal power at the output of the filter, the filter bandwidth being B. Let the noise power density be N_o. Assume that both the signal and the noise are sample functions of a gaussian process. Then the DC at the detector output is[6] $2BN_o$ when there is no signal and $2BN_o + 2S$ when the signal is on. Hence the magnitude of the square wave at the detector output is 2S and the DC out of the multiplier is S.

The noise power density at the detector output is[6] $4N_o^2B$ for low frequencies. This may be assumed flat since the square wave frequency and the RC cut off frequency are both small compared to B. Thus the noise density at the multiplier output is also $4\ N_o^2B$ and at the RC filter output the noise power is

$$4N_o^2B \int_{-\infty}^{\infty} \left| F(\omega) \right|^2 \frac{d\omega}{2\pi} = 4\ N_o^2B \int_{-\infty}^{\infty} \left| \frac{1}{j\omega RC + 1} \right|^2 \frac{d\omega}{2\pi}$$

$$= 4\ N_o^2B\ \frac{1}{2RC}\ .$$

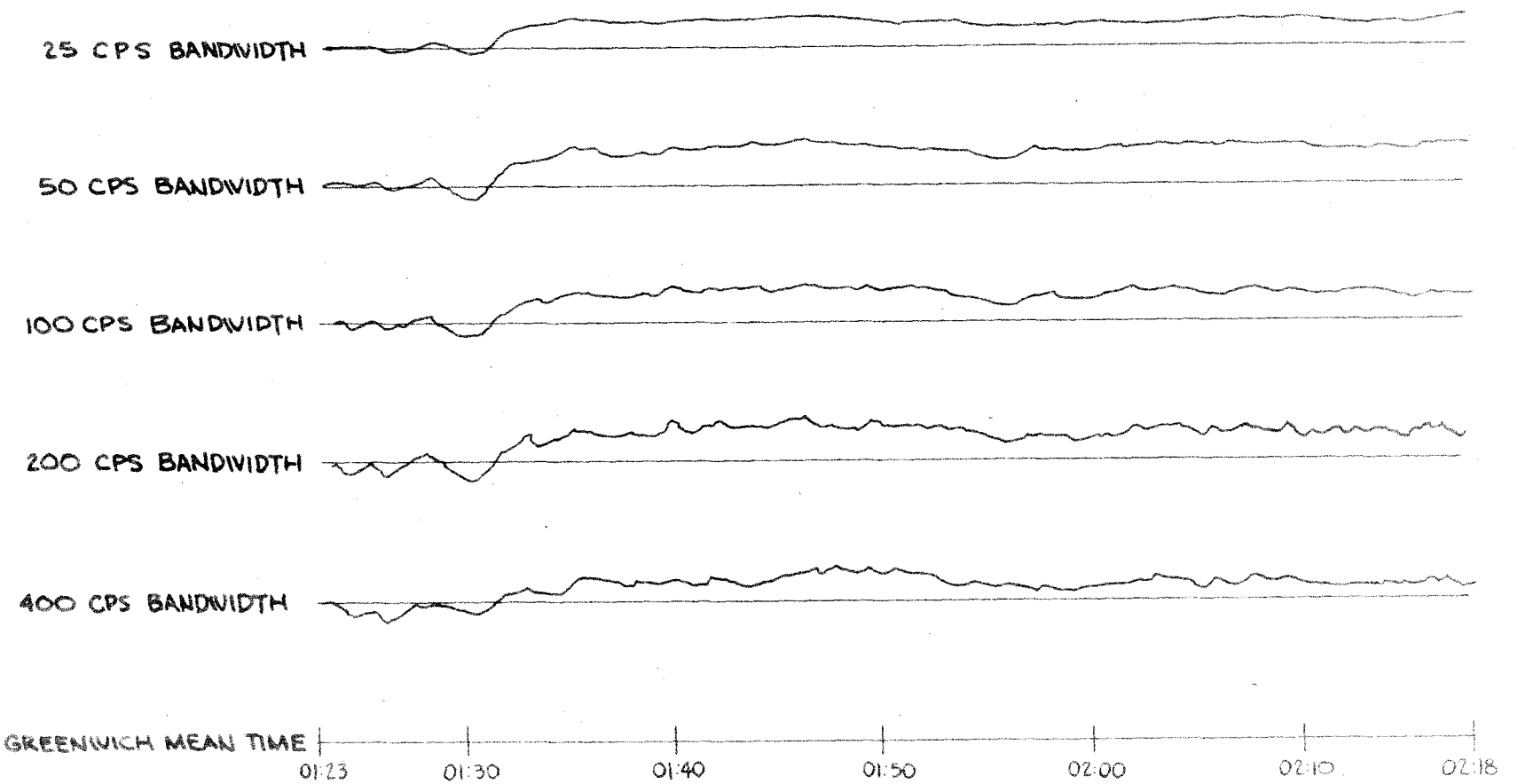

RADIOMETER OUTPUT

DATE - MARCH 29, 1961 PST

FIG. 8.2

The standard deviation is therefore $2N_o\sqrt{\frac{B}{2RC}}$. Combining these two results yields for the device output signal to noise ratio, $\left.\frac{S}{N}\right|_{out}$,

$$\left.\frac{S}{N}\right|_{out} = \frac{S}{2N_o}\sqrt{\frac{2RC}{B}}.$$

Using the following typical numbers in the above formula,

$S = 1.7(10)^{-20}$ watts

$N_o = 8.97(10)^{-22}$ watts/cps (65^o K)

$B = 25$ cps

$RC = 68$ seconds, then

$$\left.\frac{S}{N}\right|_{out} = 22 = 13.4 \text{ db.}$$

This is verified in figure 8.2.

An interesting feature of figure 8.2 is the delay from the start of the record to the beginning of the deflection. This delay was about five minutes and corresponds to the time of flight.

C. Ranging

The second mode of operation utilizes only two channels. One has its reference square wave exactly in phase with the transmitter and the other lags by ninety degrees. Comparing the outputs of the two channels then allows one to determine (to an accuracy limited by the signal to noise ratio) the phase shift of the transmitted square wave caused by the round trip time delay. The DC component of the product of two square waves is a triangular function of the phase difference. Therefore, the output of the first channel, x_1, is a triangular function of the time of flight, T. It is illustrated in figure 8.3 for a square wave of period P. The dotted curve shows the output of the 2nd channel, x_2. Knowing x_1 and x_2, one can find T as follows:

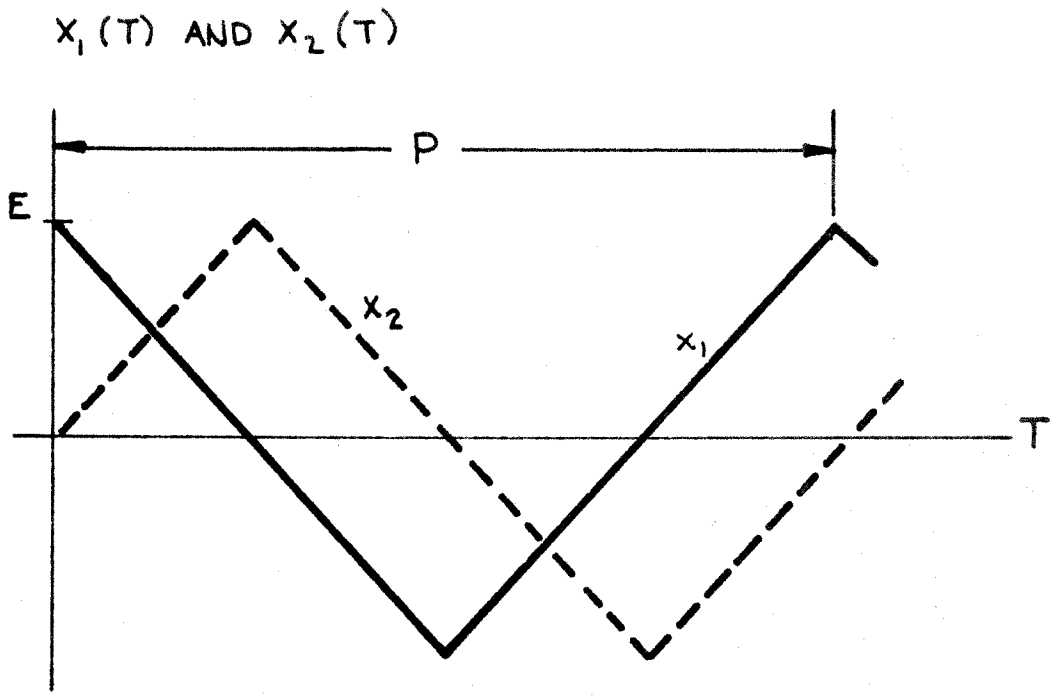

RADIOMETER OUTPUT
VS
TIME DELAY

FIG. 8.3

assume $x_1 > 0$, $x_2 > 0$. Then

$$x_1 = E - \frac{E4}{P} T, \text{ and}$$

$$x_2 = \frac{E4}{P} T,$$

where E is the amplitude of the triangular function. Eliminating E and solving for T yields:

$$T = \frac{P}{4} \frac{x_2}{x_1 + x_2} .$$

Examination of the other three quadrants yields the same formula if it is expressed as:

$$|T| = \frac{P}{4} \frac{|x_2|}{|x_1| + |x_2|}$$

where $|T|$ is the distance from a correlation peak (either a positive or negative peak). Inspection of the algebraic signs of x_1 and x_2 can always resolve the ambiguity.

There exists a different type of ambiguity, however. The time delay is only known to within an arbitrary multiple of P, since x_1 and x_2 are periodic functions. This ambiguity was resolved by making the first measurement with the square wave running at only $\frac{1}{2}$ cps. The old value of the AU was quite accurate enough to place the distance of Venus to the nearest 186,000 miles. Measurements were then made with the square wave generator running at the frequencies 1, 2, 4, 8, 16 and 32 cps; each measurement resolving the ambiguity of the succeeding measurement. 32 cps proved to be the best final frequency, as higher rates required wider band pass filters and degraded the signal to noise ratio.

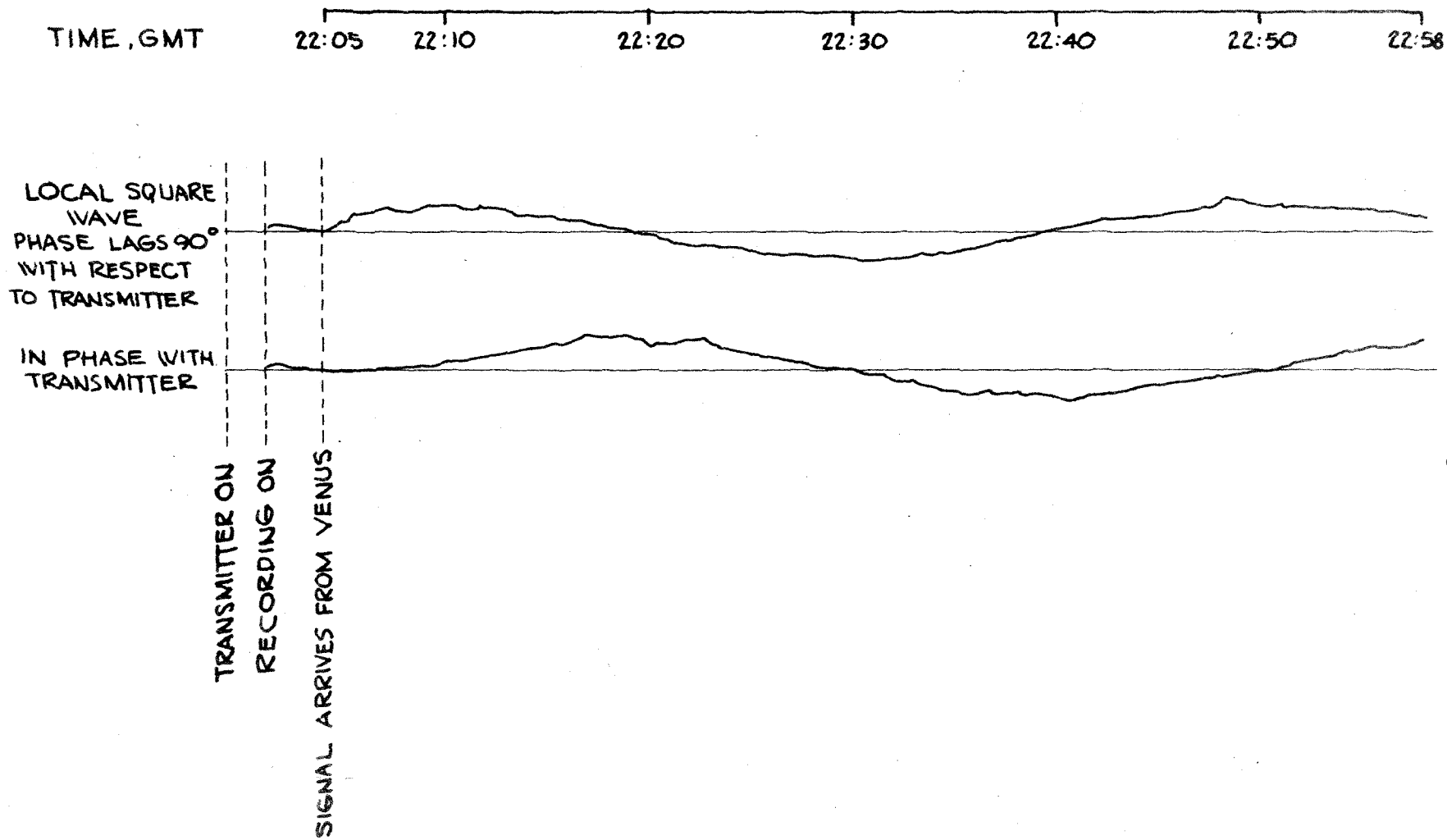

KEYING FREQUENCY 32 CPS
PREDETECTION BANDWIDTH 100 CPS
RECEIVED SIGNAL LEVEL -168 DBM

RADIOMETER OUTPUT, RANGING MODE

FIG. 8.4 DATE - APRIL 6, 1961

Figure 8.4 is a recording taken with a keying frequency of 32 cps. The function illustrated in figure 8.3 has been altered to be sinusoidal because the predetection filter removes the third and higher harmonics of the square wave. Orbital motion of Venus towards the Earth shows up clearly as the channel outputs trace through a sine wave. A precise time of flight measurement can be made by noting the time that channel seven (x_2) has a zero crossing. At that instant, there was an integer number of wavelengths (of 32 cps) filling the space between the transmitter, Venus and the receiver. The entire system was calibrated for incidental phase shifts by aiming the transmitter at the receiver, turning the power down until the Venus level was obtained and adjusting the precision phase shifter until channel seven produced zero output. This one-point calibration did not change through the weeks of the experiment and was independent of signal level.

The time of flight was converted by reference to the orbit of Venus into a new number for the AU: 149,598,820 kilometers. During the one month of closest approach, this number was measured many times, and it never varied by more than ±50 kilometers. This number may have to be revised slightly, pending an up-dating, or improvement, of the ephemeris for Venus.

Chapter IX

Preliminary Results

The first contact with Venus was made on the evening of March tenth, 1961. The signal was detected by the keyed radiometer, which alone of all of the instrumentation produced an output in real time. Experimentation for the next few days was designed to verify the reality of the echoes. This was done by letting Venus drift out of the beam of the transmitting antenna (but with the transmitter continuing to operate). Six and a half minutes later (the round trip time of flight), the radiometer's output fell to zero. The output was observed for over thirty minutes in this condition, verifying that the signal really was zero, and not the result of some chance burst of noise. The transmitter antenna was again correctly aimed at Venus; and after the proper interval of time, an output was registered by the radiometer.

The seven channels of the radiometer were fitted with different filters, each with a bandwidth of 200 C.P.S., but each tuned to a different frequency. The spacing between filters was also 200 C.P.S. A most remarkable fact brought to light by these early contacts is that the bandwidth of the signal was considerably less than 200 cycles. Only one of the channels of the radiometer contained a measurable amount of signal power. The local oscillator was detuned by systematic twenty-cycle steps, and the signal would appear in an adjacent channel only after it started decreasing in the initial channel. Subsequent analysis showed that eighty percent of the signal's power was concentrated into a band of only ten cycles per second.

This fact is all the more remarkable when one considers that

Venerians performing an analogous experiment using the earth for a target might find a spectral spreading (limb-to-limb reflection) of over 14 kilocycles.

Those early results showed that the original wide band (33 kilocycle) design for the experiment was somewhat extravagant.

Two crash programs were initiated. One was to obtain satisfactory filters of narrower bandwidth for the radiometer. A set of filters of 50 cycle and 25 cycle bandwidth were obtained and installed by March 21. These filters provided a five db increase in the signal-to-noise ratio at the radiometer output. They also provided the surprising result that the local oscillator was tuned 80 cycles off of the correct frequency (the computed doppler shift on the twenty-first of March was about 130 kilocycles). This error corresponded to the incorrect value of the AU that was used in the calculation of the ephemeris for the local oscillator.

The second program was the modification of the digital spectrometer. It was clear that the original model did not have enough resolution to give significant information about the detailed shape of a spectrum so concentrated. This may be seen by recalling Chapter Four, where it is shown (eq. 4.7) that the device produces an output which approximates the true spectrum of the signal convolved with an $F(\omega)$, where

$$F(\omega) = \frac{2}{\omega} \sin \omega K T_o \qquad (9.1)$$

Using the value of 44 for the parameter K (the number of points computed on the autocorrelation function) and 15 $(10)^{-6}$ for T_o (the time between successive samples), one sees that the minimum resolution that $F(\omega)$

allows is about 750 cycles per second. Thus it was necessary to revise the correlator so that it could handle samples at a much slower rate.

The emphasis on the design of the first correlator (Mod. I) was high speed and large capacity. Those aims were achieved by the fan-out principle explained in Chapter Six. But a price had to be paid for such speed, and that price was a measure of inflexibility in the timing involved. Each new bit of input data had to be utilized to up-date a given sum at the instant that sum was in the proper position in its recirculating delay line, and at no other time. Slowing down the input rate would upset this timing, so a new design (Mod. II) was needed.

The design of Mod. II was severely constrained by the small amount of time which was left. Venus was almost at conjunction. The constraints were:

1. Mod. II had to be built at Goldstone, a place were construction difficulties appear to be many times larger than at the relatively calm environment of JPL.
2. Mod. II had to be constructed of parts from Mod. I, a requirement which was especially difficult as it pertained to the delay lines. The lines were of the sonic type and could not be shortened or lengthened.
3. Mod. II had to be completed and made to operate correctly before the signal was too weak to be usable.

The design philosophy for Mod. II was easier than Mod. I because high speed was no longer required. Consequently, all of the digits for all of the accumulators were stored in one recirculating delay line of 1449 microsecond length (formed by connecting the lines of Mod. I in series). Each group of 23 successive digits was reserved for one

accumulator, hence there were 1449/23 = 63 points calculated on the autocorrelation function. The sampling rate was chosen to be 600 C.P.S. Thus the accumulators, which could count up to 2^{23}, could operate over 3.7 hours before an overflow would be possible.

Substituting 63 for K and 1/600 for T_o in equation 9.1 produces a much "narrower" $F(\omega)$ which yields a frequency resolution of better than 4.8 C.P.S.

Mod. II differed from its predecessor in that it was asynchronous. That is, its sampling rate was not rationally related to its internal clock. Whenever a new data sample would arrive, it would be stored in the machine until it was time to utilize it (when the delay line was properly aligned). Then each sum would be up-dated as the corresponding accumulator was accessible to the line input. After that operation was completed, the machine would wait quiescently (recirculating) until another input sample would arrive.

The next chapter is devoted to a complete description of the logical design of correlator Mod. II.

Chapter X

Mod. II Correlator

The second correlator was divided into two parts, one which performed the actual calculations required, and one which contrived to print the numbers so calculated on to a paper tape; Figure 10.1 is a block diagram representing the first part.

Two timing generators are needed; one to produce a pulse every 63 bit times (microseconds) and the other every 23 μs. The first one consists of a flip-flop (labelled "A" in Figure 10.1) driving 5 unit delay lines. The logic of A is such that the device produces a sequence of one's and zeros which repeats every 63 μs. The logic is expressed by the Boolean difference equation:

$$A = A_4 A_5 + \bar{A}_4 \bar{A}_5. \qquad (10.1)$$

Equation (10.1) is a difference equation because it expresses the next state A will assume as a function of its present and past states. The symbol A_i indicates the state of A at i μs in the past. As usual, the product notation indicates intersection ("and"), the plus notation indicates union ("inclusive or") and the bar indicates complementation ("not").

C is an and-gate set to recognize a particular state of the generator and produce an output pulse. Since the sequence generated is periodic, C produces a pulse every period (63 μs). The logic for C is:

$$C = \bar{A}\,\bar{A}_1 A_2 \bar{A}_3 A_4 \bar{A}_5. \qquad (10.2)$$

The other generator consists of a flip-flop (D in Figure 10.1) driving 4 delays. Normally, this would produce a pulse pattern of period $2^5-1 = 31$, but the output pulse (from E) is fed back into D and alters the period to

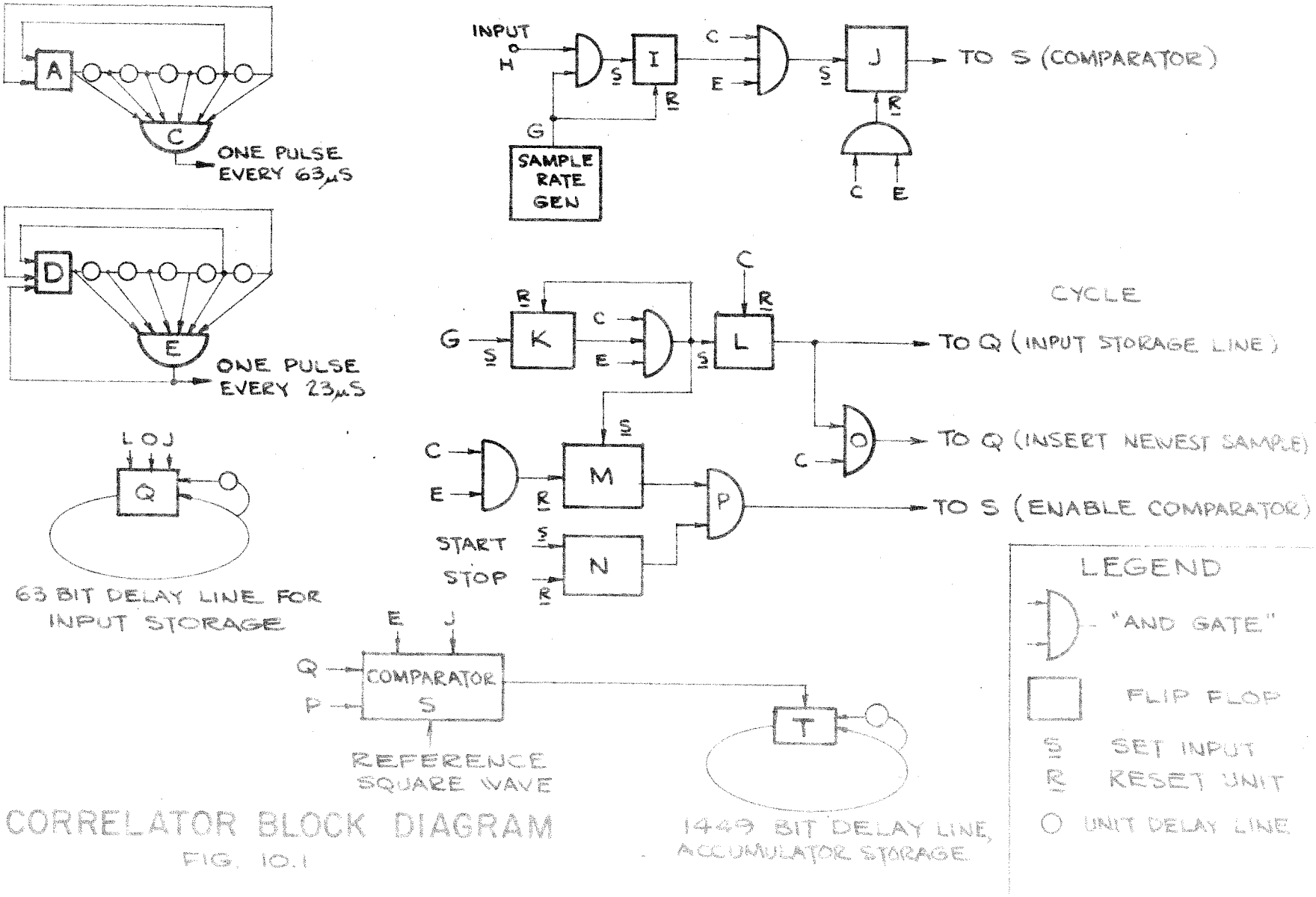

CORRELATOR BLOCK DIAGRAM

FIG. 10.1

23 μs. It is generally possible, by choosing the right logic for the output gate E, to produce any period up to the maximum ($2^m - 1$) where m is the number of stages). The logic for D and E is:

$$D = \bar{D}_2\bar{D}_4 + D_2D_4 + E \tag{10.3}$$

$$E = \bar{D}\, D_1D_2\bar{D}_3\bar{D}_4. \tag{10.4}$$

Now we will proceed with the operation of the correlator itself.

The input is designated H in Figure 10.1. It has been quantized, so that it is either one or zero. G is an external oscillator which produces one pulse whenever the input is to be sampled. This sample is stored in flip-flop I.

$$I = GH + I\bar{G}. \tag{10.5}$$

The output of I is not used directly for computation because a computation may still be in progress from a previous sample. When the two timing generators (C and E) align, the system is ready to utilize the latest sample. It is then transferred to flip-flop J.

$$J = CEI + \bar{C}J + \bar{E}J \tag{10.6}$$

The output of J goes to the comparator S where it is compared with the last 63 samples of the input. To do this, the circulating delay line containing the old samples must be updated. That is done as follows. Immediately after a sample, flip-flop K remembers that a sample has arrived, and allows the next alignment of the timing generators to set flip-flop L.

$$K = G + K\bar{C} + K\bar{E} \tag{10.7}$$

$$L = KCE + L\bar{C}. \tag{10.8}$$

L stays set for exactly 63 μs, at which time C resets it. Thus L produces a burst of 63 pulses. These pulses are used to lengthen the circulating

delay line, which is remembering the 63 previous input samples, by one unit. This operation is equivalent to shifting each data point in the line by exactly one position. At the end of this burst, gate O generates a pulse which inserts the last sample into the line

$$O = LC \tag{10.9}$$

The logic for the driver of the input storage delay line is:

$$Q = \overline{O}LQ_{63} + \overline{LO}Q_{62} + OJ. \tag{10.10}$$

The output of Q is compared with the output of J by the comparator, S. An additional input to the comparator is Z which is derived from the reference square wave. Z commands the comparator to acknowledge either agreements or disagreements, depending upon the phase of the reference. Input E samples the comparator every 23 μs, the time necessary for the next accumulator to reach alignment in the long delay line. After 63 such samples, every bit in the input storage has been utilized to up-date an accumulator exactly once. Input P to the comparator then halts the comparators action until a new input sample is obtained. Thus the machine can handle input samples at any rate up to the maximum of once every 63 x 23 = 1449 μs. The logic for the comparator is:

$$S = PE(ZQJ + Z\overline{QJ} + \overline{Z}\overline{QJ} + \overline{ZQ}J) \tag{10.11}$$

Thus S can have an output only once per 23 μs and then only for 63 such times. After that, the output must be zero until another sample comes in which causes the cycle to repeat. Of course, whether or not S does have an output at those favored times depends upon whether it is responding to an "agreement" or a disagreement".

Flip-flop M is set at the same time that L is (the first instant of alignment of the timing generators after an input sample has been taken).

If, in addition, flip flop N is set (control of N allows the machine to be started and stopped manually), P delivers its enabling signal to the comparator.

$$M = KCE + M\overline{C} + M\overline{E} \qquad (10.12)$$

$$N = \text{Start} + N\,\overline{\text{Stop}} \qquad (10.13)$$

$$P = MN \qquad (10.14)$$

The output of the comparator is fed to the long delay line driver T, which is connected as a standard serial binary adder. That is, the output of T is the modulo two sum of the signal from S and the digit from the end of the delay line. Whenever there is a carry, that fact is remembered by one unit of delay and a "one" is added in at the next μs. The simultaneous arrival of a "one" from S and a carry constitutes an overflow, which can happen only after 2^{23} pulses from S (3.7 hours of observation). The logic for T is:

$$T = S\overline{T}_{1448} + \overline{S}TT_{1448} + \overline{S}T_{1448}\,\overline{T}_{1449} + \overline{ST}_{1448}\overline{T}\,T_{1449}. \qquad (10.15)$$

At the end of an observation, computation is stopped by re-setting N. Then the comparator can produce no more output pulses. The contents of the long delay line are then 63 words, each of 23 digits, and each records the total number of agreements during the signal plus noise condition plus the total number of diagreeements during the noise only periods for one value of the argument of the correlation function. One exception to this is the word for $\tau = o$. That word records only "agreements"; and since there are only agreements at $\tau = o$, that word records the total number of samples. That operation is accomplished by over-riding the reference

square wave with one pulse at the time that the data for $\tau = 0$ is being examined by the comparator.

The words in the delay line re-circulate, and the second part of the machine transfers them to paper tape for further processing. The print-out routine is accomplished by generating a timing pulse every 1449 μs which is in phase with the most significant bit of the first word in the long delay line. The pulse transfers that bit into a flip flop and gives the command to print. The printer then prints out a one or a zero, depending on the state of the flip flop. The timing generator is simultaneously advanced in phase by one μs so that its output pulse is in phase with the second most significant digit. This action occurs far too fast for the print out to follow, so the print commands are gated out until the printer is ready again. An external oscillator supplies this timing. After 23 print-outs have occurred, the timing pulse is in phase with the pulse from E (Figure 10.1). This signals the print out to mark the event with an asterisk, in order to identify the most significant digit of each word. The process continues until all 1449 digits have been printed. Then coincidence is observed between the timing pulses and C and E of Figure 10.1. This coincidence halts the print out routine.

The components that produce this operation are shown in Figure 10.2. Flip flop e controls the print out operation, which starts at the first alignment of C and E (Figure 10.1) after the start button is pushed. The logic for e is:

$$e = CE\ Start + e\bar{x}. \qquad (10.16)$$

x is the gate which resets e and halts the operation.

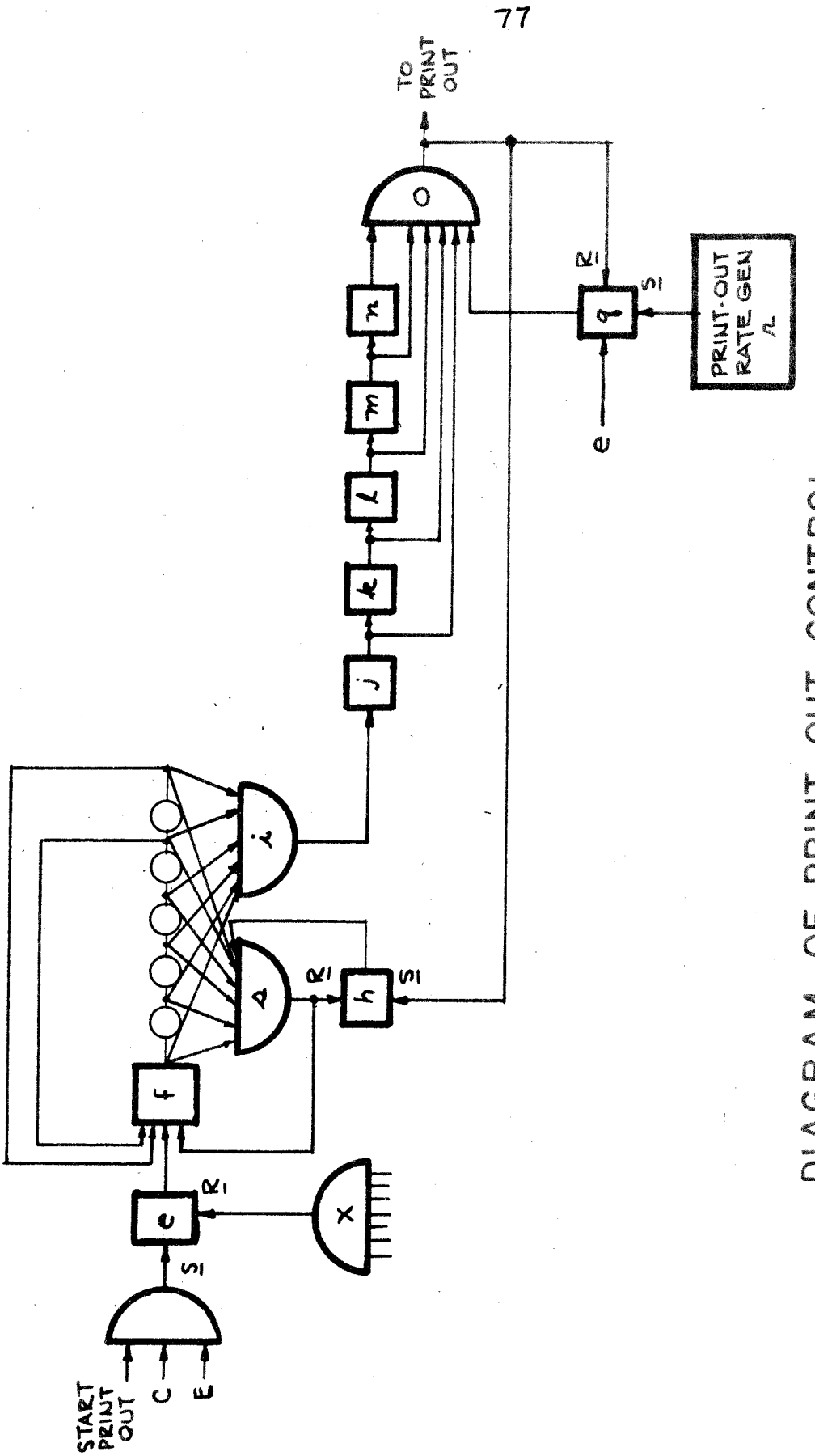

DIAGRAM OF PRINT-OUT CONTROL

FIG. 10.2

In the notation utilized here, capital letters are used to indicate amplifiers and flip flops in Figure 10.1, while lower case letters are used for those in Figure 10.2.

The timing generator is divided into two parts. The first part is similar to A of Figure 10.1. Flip flop f drives five unit delays and the logic is such that the pattern generated has a period of 63 μs. Gate i produces an output pulse at that rate. However, when flip flop h is set, the gate s allows an additional pulse to enter into the logic of f. This pulse reduces the period between outputs of i by exactly one μs, and resets h, so that successive outputs of i are again 63 μs apart. The logic which accomplishes this is:

$$f = (f_4 f_5 + \bar{f}_4 \bar{f}_5 + s)e \qquad (10.17)$$

$$i = \bar{f}_5 f_4 \bar{f}_3 f_2 f_1 \bar{f} \qquad (10.18)$$

$$s = h\bar{f}_5 f_4 \bar{f}_3 \bar{f}_2 \bar{f}_1 \bar{f} \qquad (10.19)$$

$$h = o + h\bar{s} \qquad (10.20)$$

where o is the pulse which commands the printer to print. Equation 10.17 shows that there will be no output at all from f until that amplifier is "enabled" by e.

The second part of the timing generator is a device which counts pulses from i and produces an output after every 23 such pulses. The device is essentially a shift register, where pulses from i do the shifting, which generates a sequence of period 23. The equations are:

$$j = (\bar{i}j + ilm + i\overline{lm} + \overline{mk}j)e \qquad (10.21)$$

$$k = \bar{i}k + ij + \bar{e} \qquad (10.22)$$

$$l = \bar{i}l + ik + \bar{e} \tag{10.23}$$

$$m = \bar{i}m + il + \bar{e} \tag{10.24}$$

$$n = \bar{i}n + im + \bar{e} \tag{10.25}$$

The presence of the variable e in these equations ensures that the shift register will start out at the proper phase.

Gate o produces an output whenever i, j, k, l, m and n cycle around to the proper phase and if flip flop q is set.

$$o = inmlk\bar{j}q. \tag{10.26}$$

The pulse from o then loads the proper bit from the delay line into a flip flop, signals the printer to print that bit, resets q so no further print commands will be given, and sets flip flop h so that the phase of i may be advanced by one μs.

A print-out rate generator then sets q so that the cycle may continue, but only after enough time has elapsed to ensure that the printer is ready. The equation for q is

$$q = re + \bar{q}oe \tag{10.27}$$

Again, e is used to ensure the correct starting phase for q.

Gate x senses the phase of o compared to the two timing generators of Figure 10.1 and is thus able to halt the print-out routine after all digits have been recorded.

$$x = \bar{A}A_1\bar{A}_2\bar{A}_3\bar{A}_4\bar{A}_5\bar{D}D_1\bar{D}_2\bar{D}_3D_4o. \tag{10.28}$$

The digital equipment just described used up 15 inches of standard rack space to a depth of 7 inches. The necessary power supply, printing mechanism and external oscillator is not included in those dimensions.

Chapter XI

Data

This chapter is devoted to the results of power spectra measurements made by the correlator described in Chapter X.

The first measurement was a calibration, made in the laboratory, to establish the validity of the formulas derived in Chapter IV and the assumptions on which they depend. The experimental configuration was that presented in figure 4.1 of Chapter IV, but with a noise generator connected to the input. The correlator was operated in the first mode, as described in Chapter VII. The result of this measurement is displayed in figure 11.1, which shows the shape of the pass-band of the filter. The sampling rate of 600 cps suits a spectrum which covers a 300 cps range. Figure 11.1 shows that the pass band is 200 cps wide at the half power points. The same filter was used for all subsequent measurements. The integration time for figure 11.1 was .8 hours.

The second laboratory measurement was the same as above, except the correlator was operated in mode II. The effect of this was to produce the difference between two independent measurements of the spectrum of figure 11.1. The resulting spectrum is shown in figure 11.2. The shape of the bandpass is obliterated because of the subtraction process, but the variation between measurements remains. It is important to calculate the standard deviation from the formulas derived in Chapter IV and to compare it with the value measured from figure 11.2. Equation 4.13 of that chapter is the one which applies. It is repeated here for convenience.

$$\sigma = \eta\sqrt{\frac{K}{2N}} . \qquad (11.1)$$

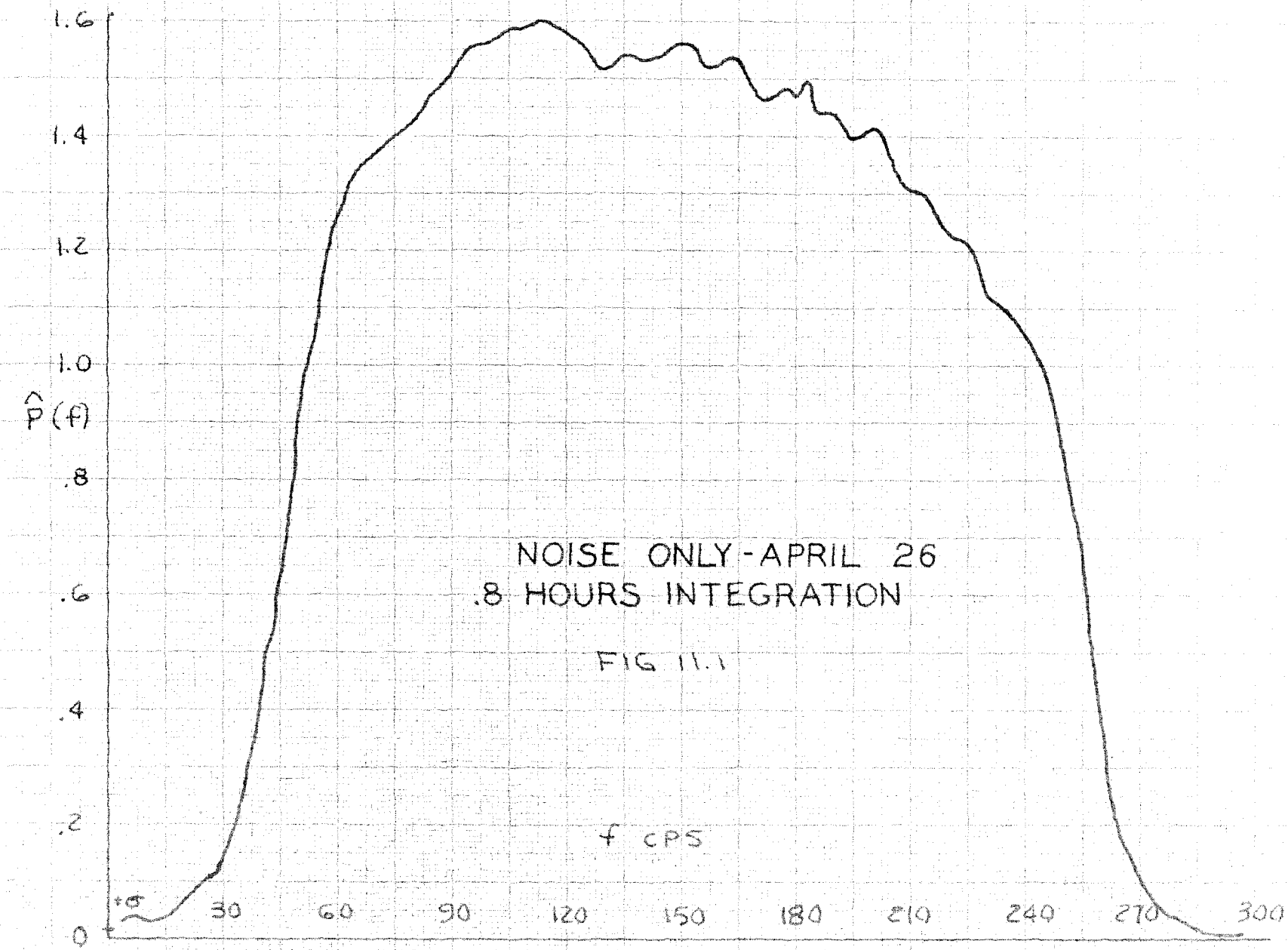

NOISE ONLY - APRIL 26
.8 HOURS INTEGRATION

FIG 11.1

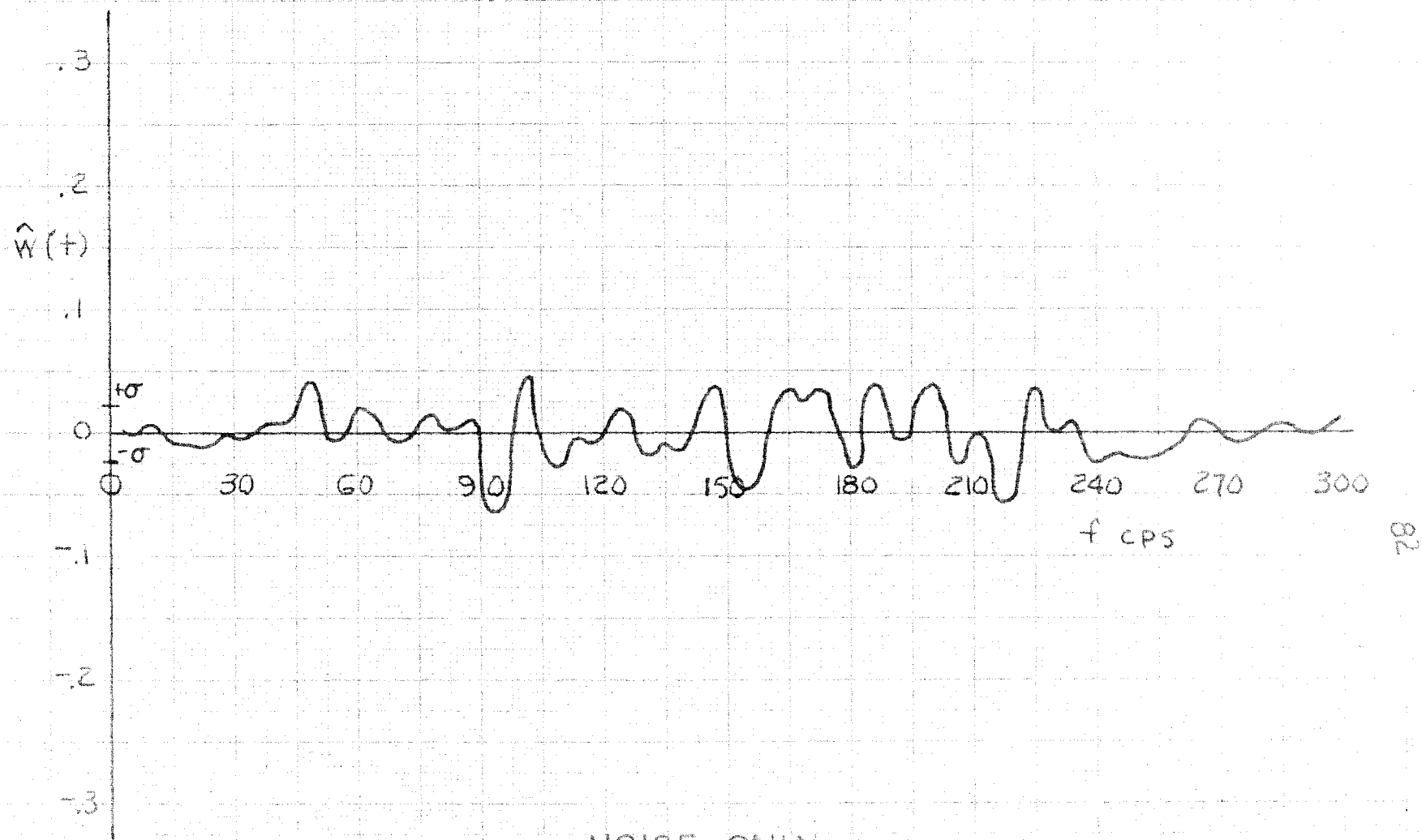

NOISE ONLY

FIG II.2

Each of the two component spectra of figure 11.2 was produced with one half of the total number N of signal samples. Also, upon subtracting two independent measurements, σ must be multiplied by $\sqrt{2}$. Taking account of these two factors, the correct formula for σ for operation of the correlator in the second mode is:

$$\sigma = 2\pi\sqrt{\frac{K}{2N}} . \qquad (11.2)$$

K, for the correlator under discussion, is 62. N, for the experiment of figure 11.2, is 2,367,684 (the result of integrating for 1.1 hours). Thus the theoretical value for σ is:

$$\sigma = .0227$$

The value of σ found by squaring each of the one hundred numbers from the computer print out, averaging, and extracting the square root is:

$$\sigma = .0220.$$

These two numbers are in splendid agreement.

The next laboratory test of the spectrometer is portrayed in figure 11.3. A sine wave generator simulates a signal which is keyed on and off by the square wave generator. Noise, from a separate generator, is added, and the relative amounts of signal and noise power are monitored by an RMS meter. Figure 11.4 is the resulting spectrogram, the integration time being one hour. The sin x/x form predicted in Chapter IV (equation 4.7) shows up clearly in this figure.

Both the bandwidth and the amplitude of figure 11.4 will be compared with their values as calculated from the analysis of Chapter IV, so that the accuracy of the latter may be tested. From equation 4.7, the

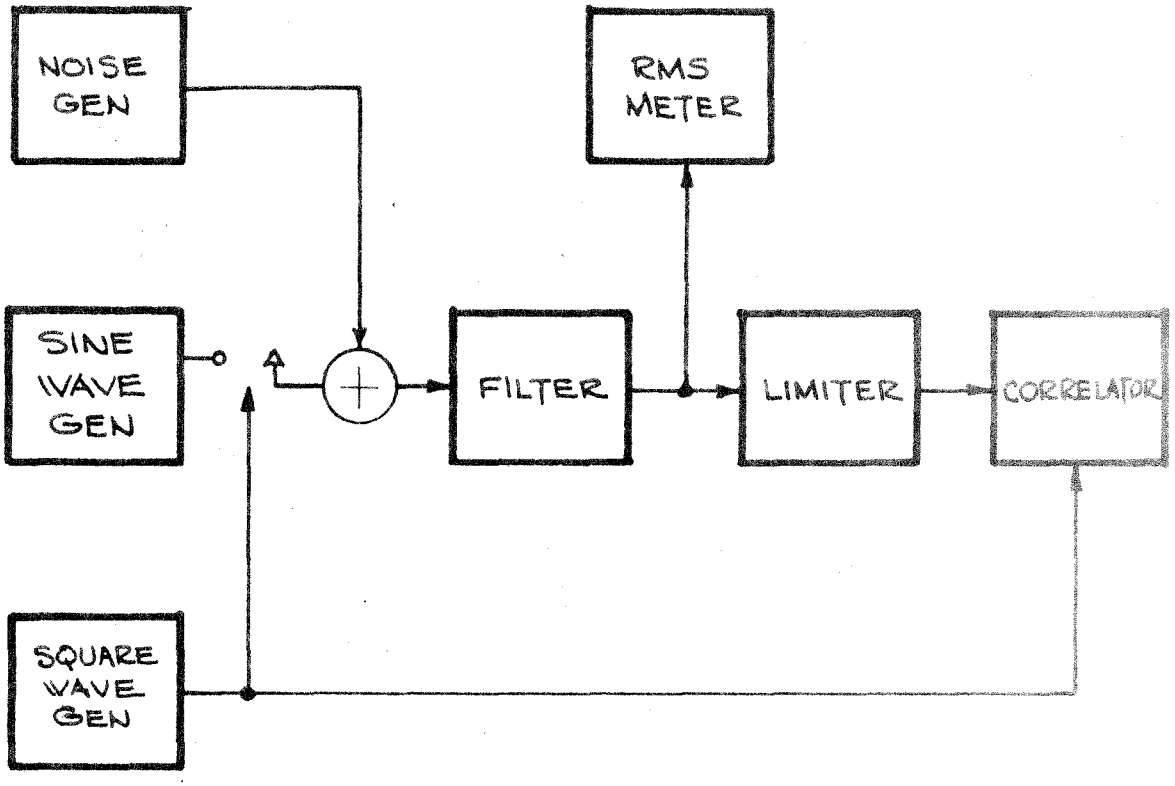

EXPERIMENTAL CONFIGURATION

FIG. 11.3

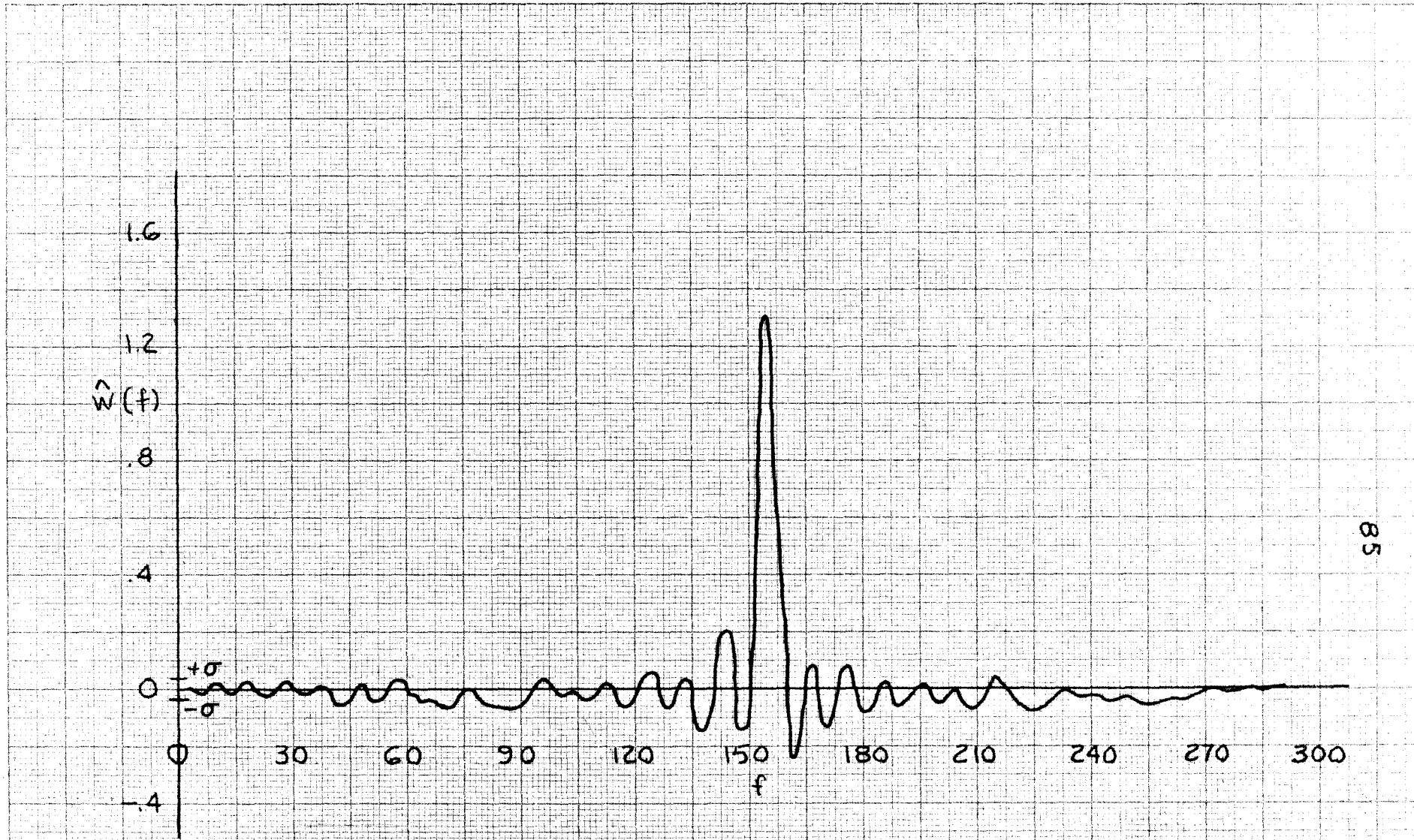

SIMULATED SIGNAL PLUS NOISE

FIG 11.4

bandwidth, B, between zero crossings is:

$$B = \frac{1}{KT_0} \text{ cps.}$$

Substituting K = 62 and $T_0 = 1/600$ yields:

$$B = 9.68 \text{ cps.}$$

The value scaled from figure 11.4 is: B = 9.3 cps.

The next step is to calculate the amplitude as predicted by Chapter IV. Let $\hat{P}_S$ be the estimate of the total signal power, and $\hat{P}_{S+N}$ that of signal plus noise. Let P_S and P_{S+N} be the true values as measured with the RMS meter. Since the spectrograms produced by this device are normalized to unit power density, the total integrated power equals the bandwidth, $1/2\ T_0$. Thus

$$\hat{P}_{S+N} = \frac{1}{2T_0} \text{ , and}$$

$$\hat{P}_S = \frac{\hat{P}_S}{\hat{P}_{S+N}} \frac{1}{2T_0} = \frac{P_S}{P_{S+N}} \frac{1}{2T_0} .$$

Since the true signal spectrum for this measurement is an impulse, the estimated spectrum is an impulse of magnitude $\hat{P}_S$ convolved with the function of equation 4.7,

$$\frac{2}{\omega} \sin \omega KT_0 .$$

Hence the peak power density, P_{max}, is:

$$P_{max} = \frac{P_S}{P_{S+N}} \frac{1}{2T_0} 2KT_0 = \frac{P_S}{P_{S+N}} K.$$

The RMS meter, for signal only, read .165 volts and for signal plus noise 1.09 volts. Hence

$$P_{max} = \left(\frac{0.165}{1.09} \right)^2 62 = 1.42.$$

P_{max} scaled from figure 11.4 is

$$P_{max} = 1.34.$$

The agreement between these three pairs of numbers is quite gratifying.

The nine figures that follow are all spectrograms of the Venus echo, made in the field with the second model of the correlator. Except for figure 11.13 they were taken in the second mode; that is, the subtraction process described in chapter VII was used. Figure 11.13 was taken in the first mode, and that spectrogram shows the entire signal plus noise spectrum. The bandwidth marked on the figures indicates the maximum doppler spread possible under the assumption that Venus keeps one face turned toward the sun. σ indicates the calculated RMS error. For neatness, only the data points on the first curve are shown.

The most striking fact observable from these spectrograms, aside from a truly remarkable signal-to-noise ratio, is the very narrow bandwidth of the echoes. One is forced to conclude from this data that either Venus is very shiny or else she must rotate very slowly.

In order to investigate the roughness of Venus, a polarization experiment was performed. Circular polarization was transmitted, and the receiver was set up for circular polarization of the same sense. If the target were a perfect reflector, the signal would drop 28 db (not the theoretical infinite drop because of the measured ellipticity of the polarization). The signal actually dropped only 12 db. A similar experiment using the moon for a target produced a change of 12 db also, hence Venus is as rough (in this sense) as the moon. Since reflections are detected from the limbs of the moon, it is possible that reflections

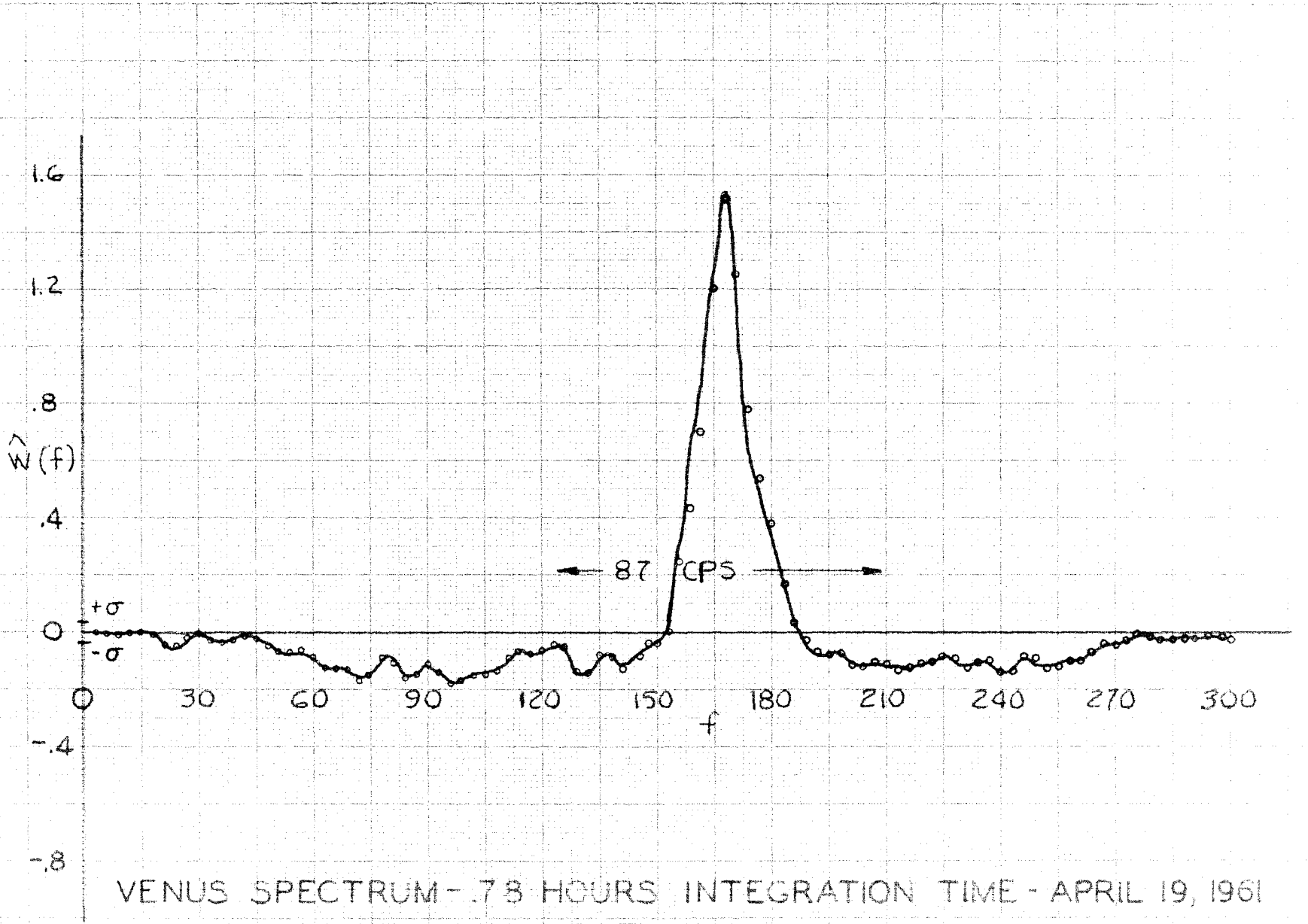

VENUS SPECTRUM - .78 HOURS INTEGRATION TIME - APRIL 19, 1961

FIG 11.5

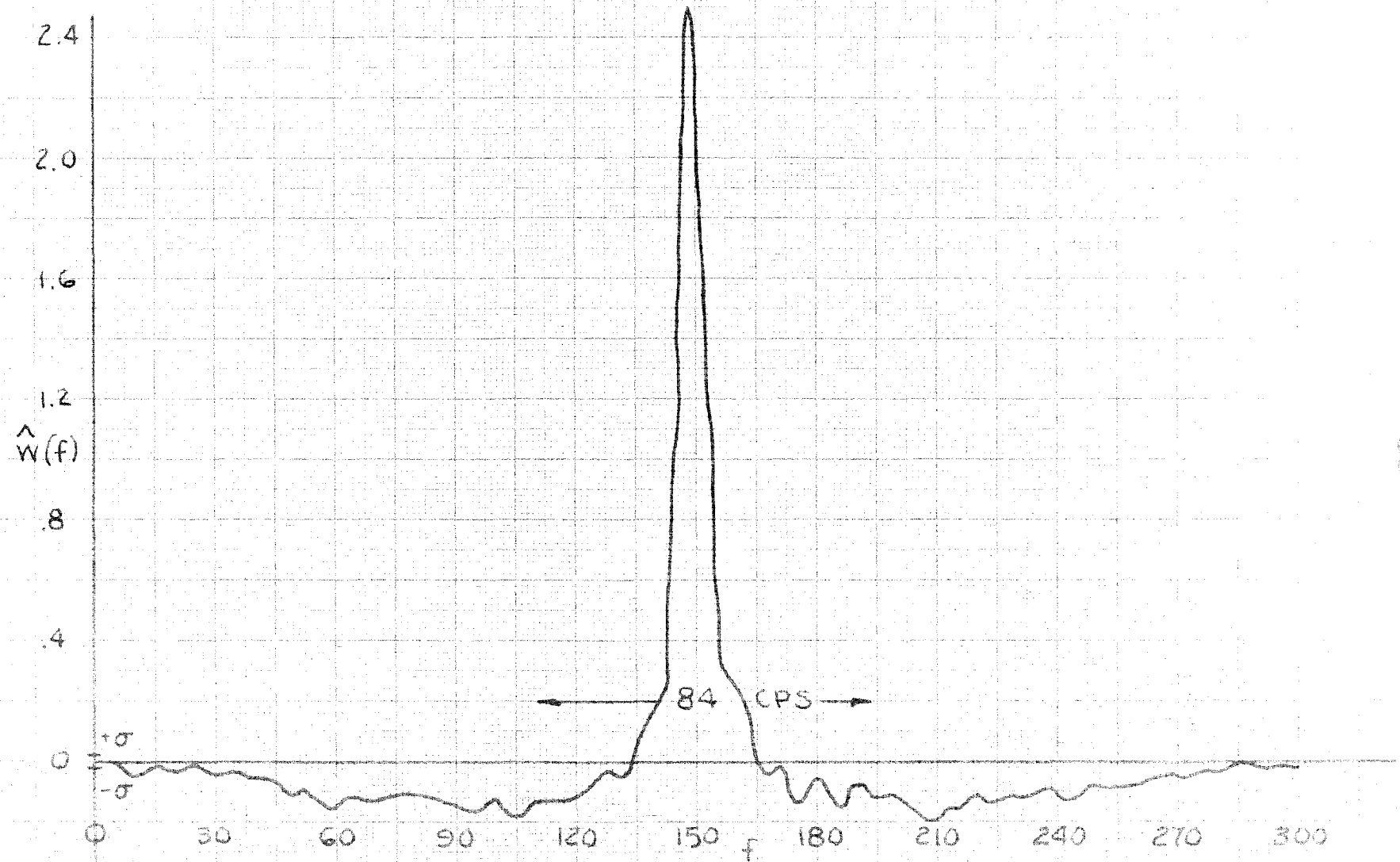

VENUS SPECTRUM - 1.4 HRS INTEGRATION TIME - APRIL 21, 1961

FIG II-6

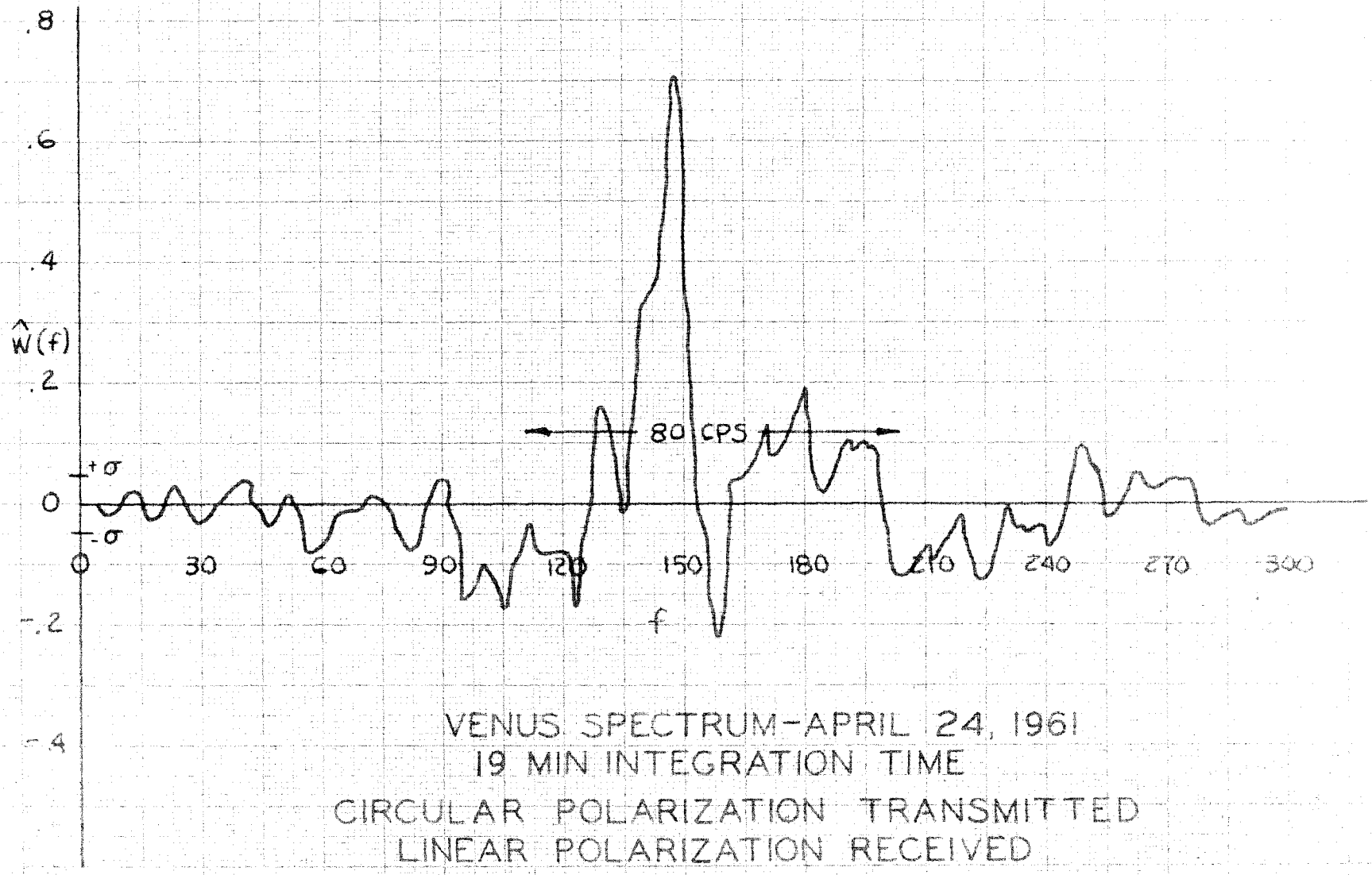

VENUS SPECTRUM–APRIL 24, 1961
19 MIN INTEGRATION TIME
CIRCULAR POLARIZATION TRANSMITTED
LINEAR POLARIZATION RECEIVED

FIG 11.7

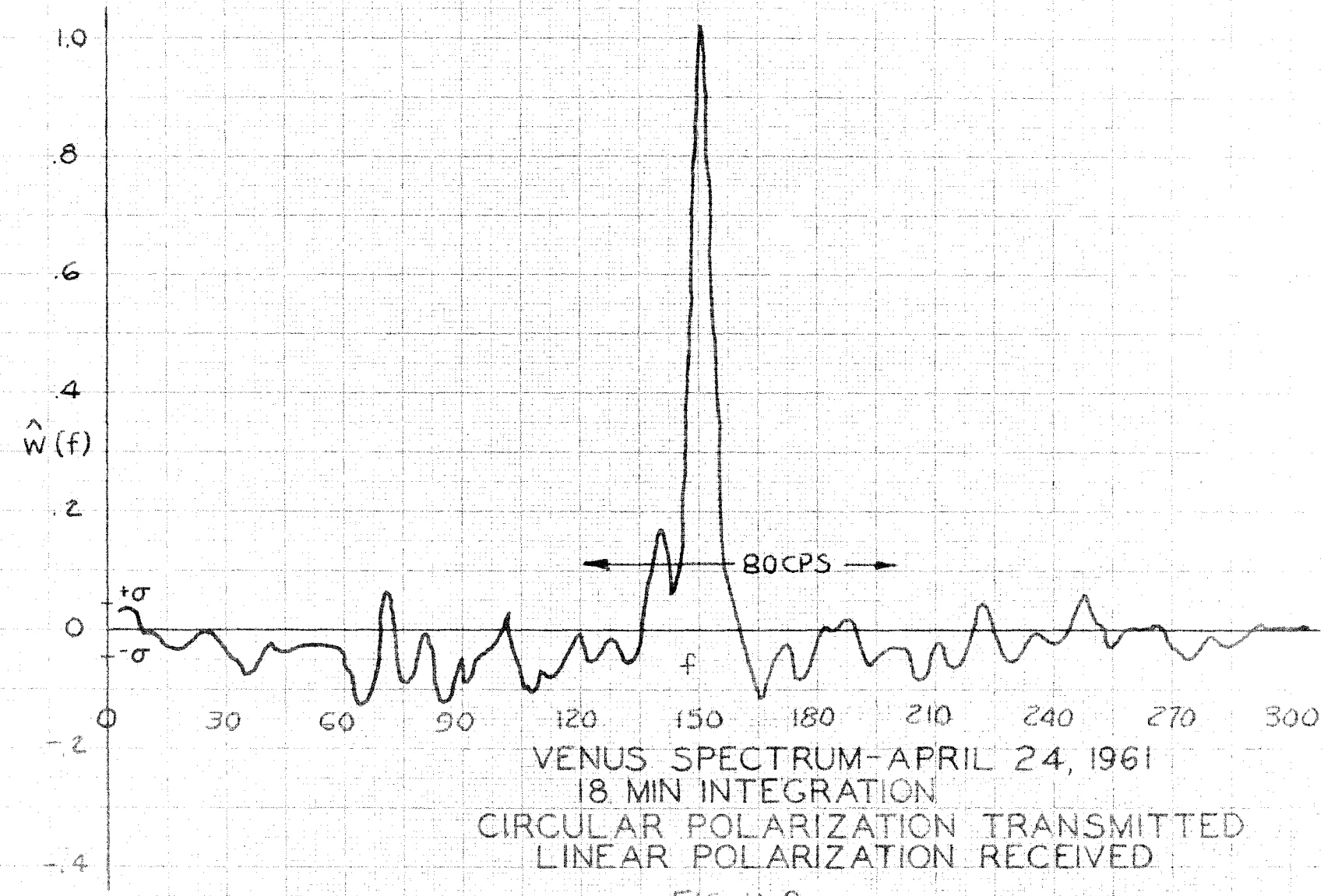

VENUS SPECTRUM-APRIL 24, 1961
18 MIN INTEGRATION
CIRCULAR POLARIZATION TRANSMITTED
LINEAR POLARIZATION RECEIVED

FIG II.8

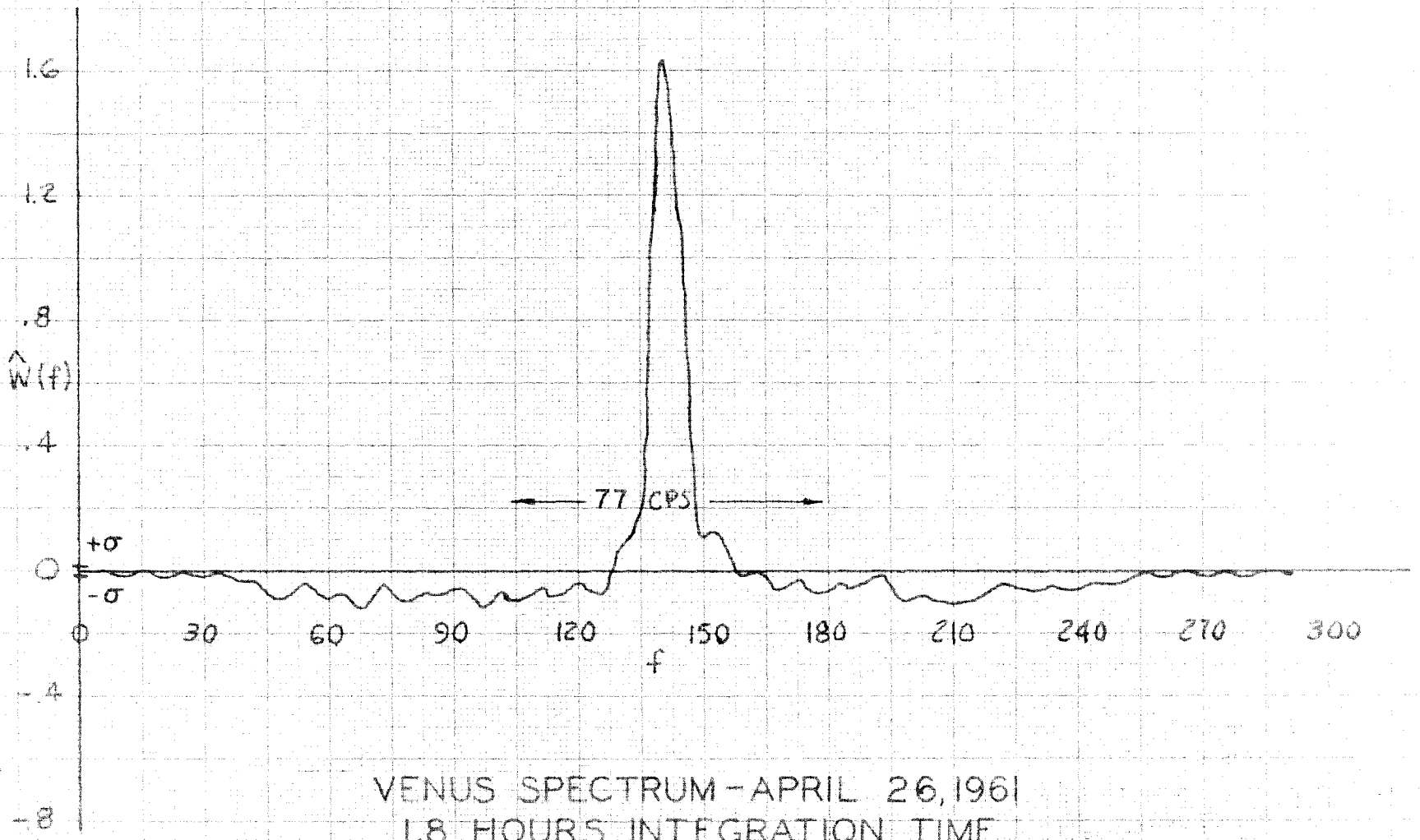

VENUS SPECTRUM - APRIL 26, 1961
1.8 HOURS INTEGRATION TIME

FIG 11.9

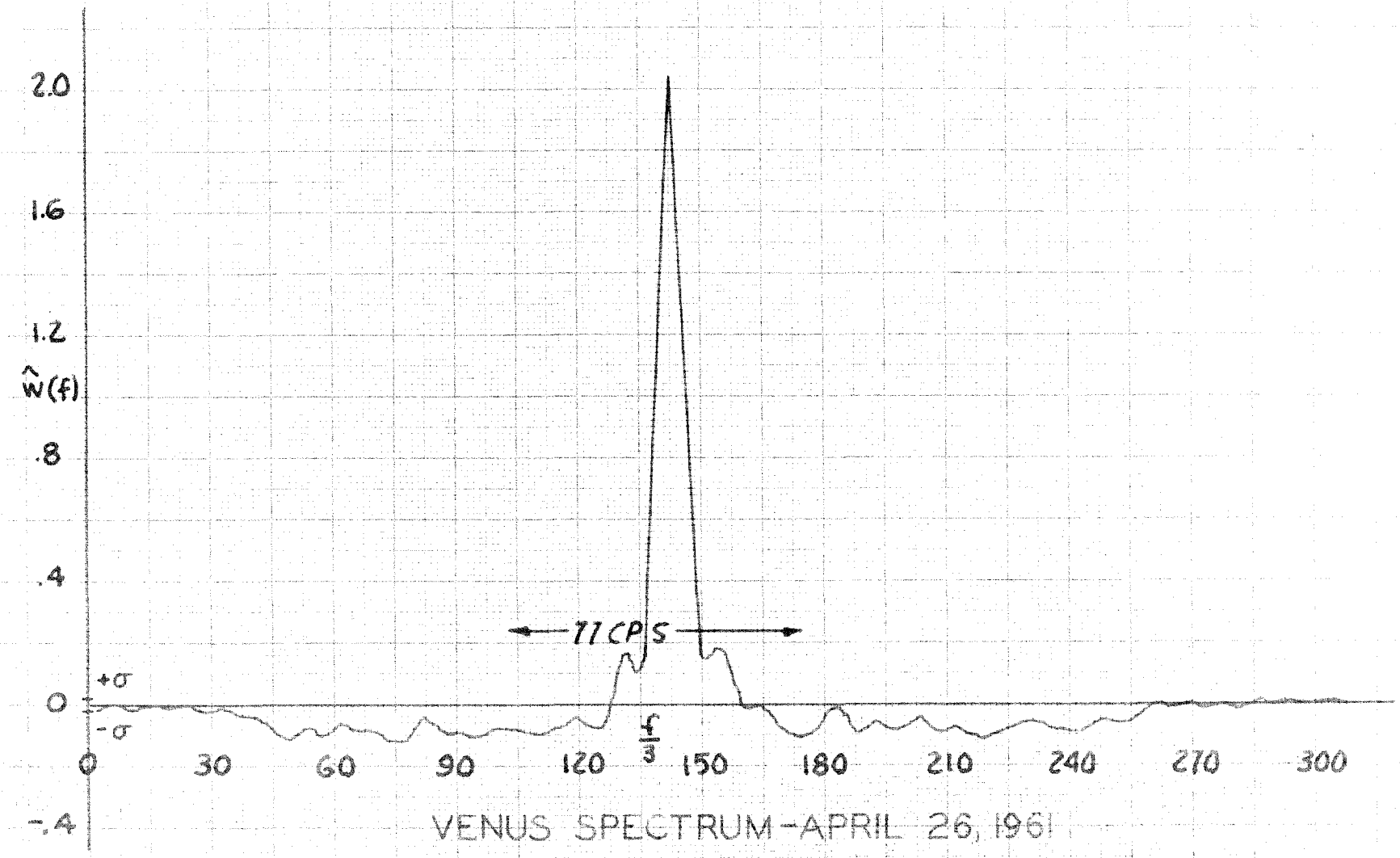

VENUS SPECTRUM - APRIL 26, 1961
1.6 HOURS INTEGRATION TIME

FIG. II.10

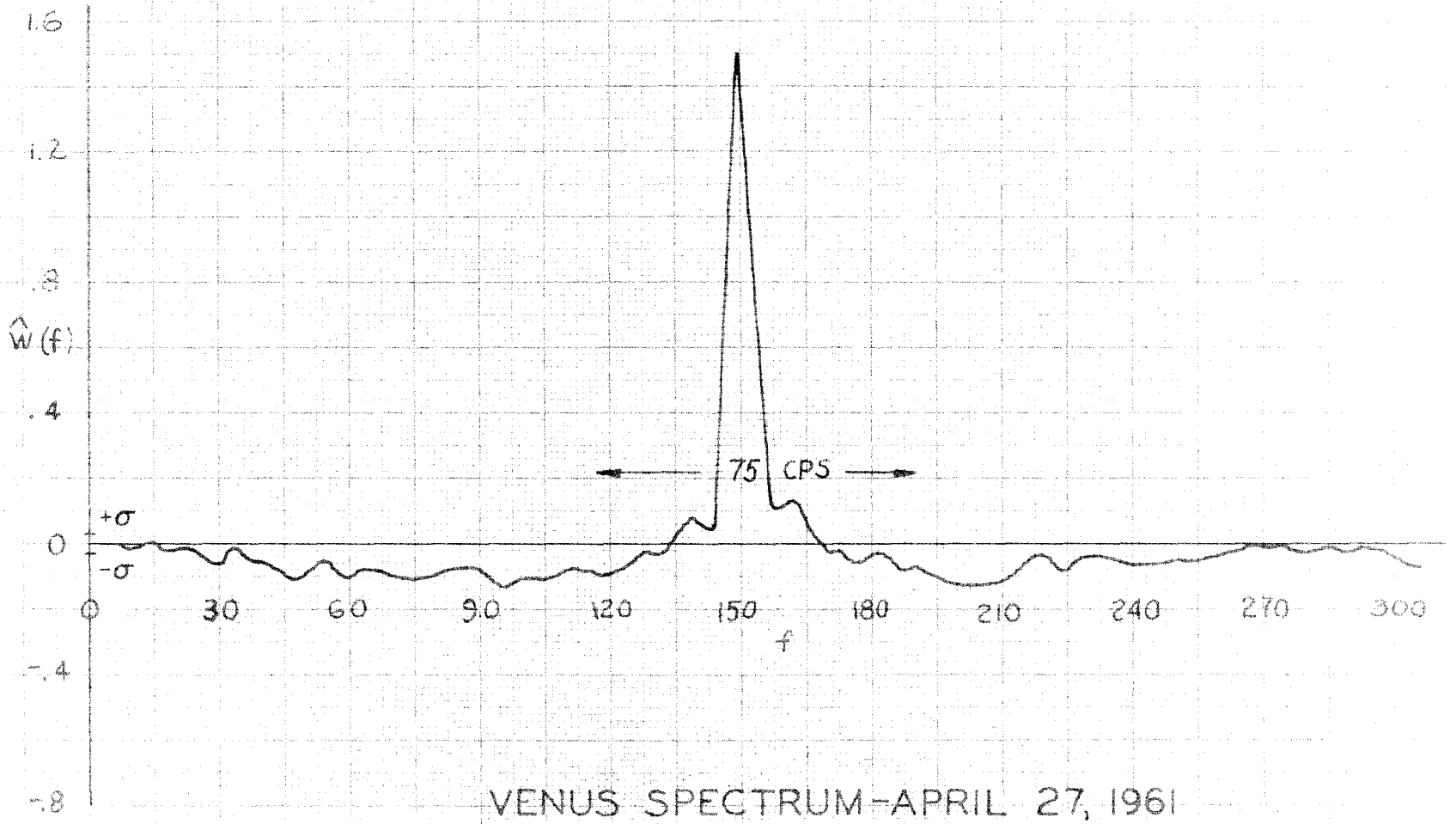

VENUS SPECTRUM-APRIL 27, 1961
1.1 HOURS INTEGRATION TIME

FIG. II.11

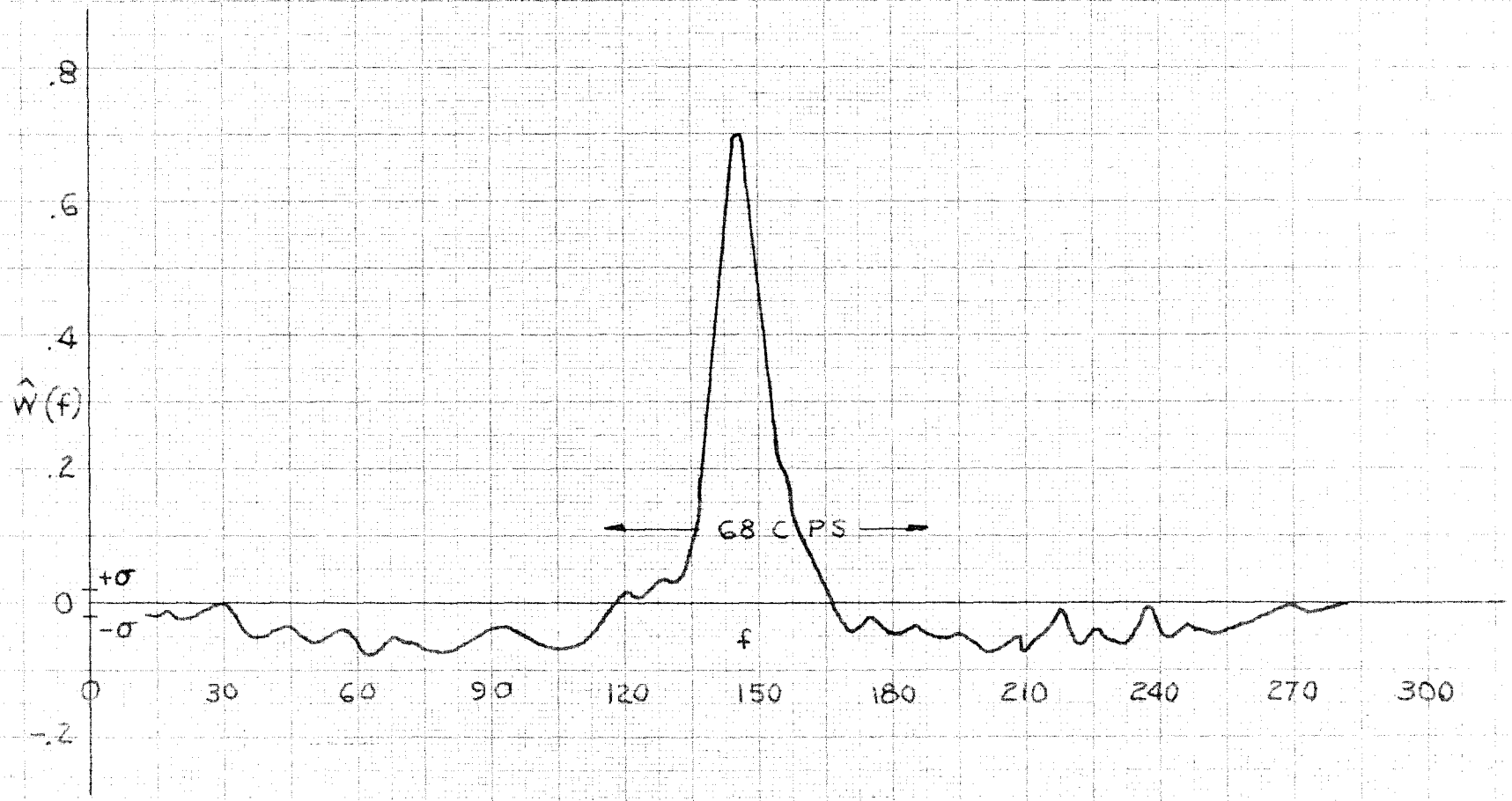

VENUS SPECTRUM - MAY 1, 1961
1.5 HOURS INTEGRATION TIME

FIG 11.12

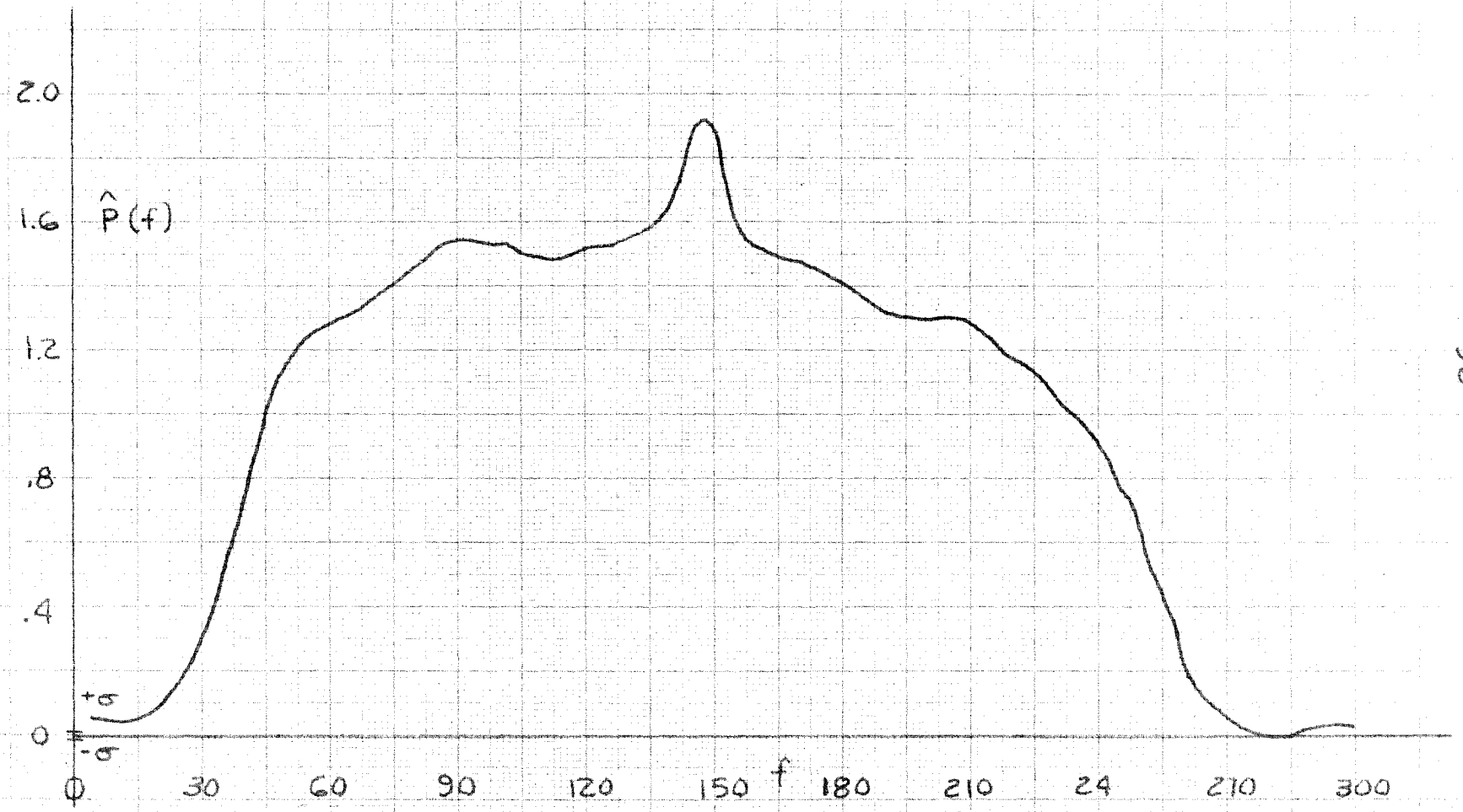

VENUS SPECTRUM PLUS NOISE - MAY 3, 1961
2.9 HOURS INTEGRATION TIME
SIGNAL PLUS NOISE (MODE I)
FIG II.13

were also obtained from the limbs of Venus.

These considerations suggest the possibility that Venus spins in "trapped rotation," where one hemisphere continuously faces the sun. Trapped rotation is not a rare phenomenon in our solar system, as Mercury always keeps one face turned toward the sun, and the moon exhibits trapped rotation with respect to the earth.

It is interesting to calculate the spectral broadening that would occur in this mode of rotation. The bandwidth would change from day to day as a consequence of the orbital motion of both Venus and Earth. Figure 11.14 shows the situation. The orbits of Earth and Venus are assumed co-planar. Actually, their orbital planes intersect at an angle of only 3 degrees. The orbits are also assumed circular, which is a good approximation for Earth, and an even better one for Venus whose eccentricity is only .0068.

Under these assumptions the apparent rotation of Venus as seen from Earth is simply $d\phi / dt$.

Using the law of sines on the triangle of figure 11.14, one sees that:

$$\frac{\sin \phi}{x} = \frac{\sin (\omega + \phi)}{z} \qquad (11.1)$$

$$\frac{\cos \phi}{x} = \frac{\cos (\omega + \phi)}{z} \left[d\omega + d\phi \right]$$

$$d\phi = \frac{d\omega \quad \frac{\cos(\omega + \phi)}{z}}{\frac{\cos \phi}{x} - \frac{\cos (\omega + \phi)}{z}} \qquad (11.2)$$

Eliminating ϕ reduces equation 11.2 to:

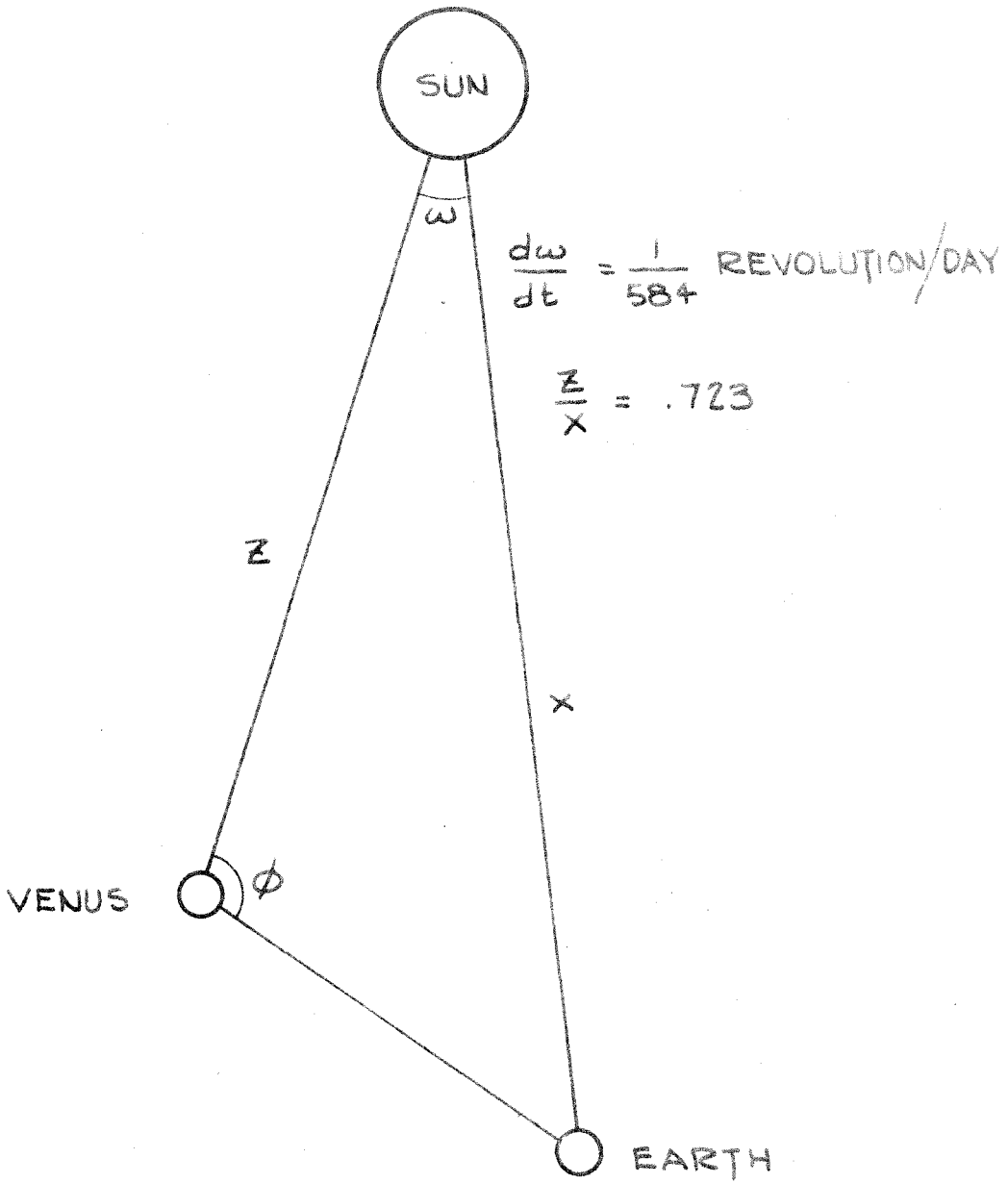

SUN-VENUS-EARTH GEOMETRY

FIG. 11.14

$$d\phi = - \frac{d\omega}{\frac{z}{x}\left(\frac{\frac{z}{x} - \cos\omega}{1 - \frac{z}{x}\cos\omega}\right) + 1} \qquad (11.3)$$

The frequency separation between echoes from opposite limbs is found from the formula

$$\Delta f = \frac{4v}{\lambda} = 195\ (10)^6 \ \frac{d\phi}{dt} \text{ cps} \qquad (11.4)$$

where v is the rotational velocity of the limb and λ is the wavelength.

Values of Δf are listed in Table 1 for various days after conjunction. Recall that Δf is the maximum spectral broadening possible, under the assumptions made above, and corresponds to echoes all the way to the limbs.

The value of Δf is indicated on each spectrogram of figures 11.5 through 11.13. As can be seen, trapped rotation is not inconsistent with the data.

TABLE I

Date	No. of Days from Conjunction	Δf cps
4/11	0	92.3
4/16	5	90.0
4/21	10	84.4
4/26	15	76.7
5/1	20	68.1
5/6	25	60.1
5/11	30	53.1
5/16	35	47.0

Chapter XII

Summary and Conclusions

A technique has been presented which makes it practical to analyze many hours of a signal and hence to produce a very accurate measurement of the power spectrum of the signal. The basis of the technique is the quantization of the signal into only two levels, thereby enabling the autocorrelation function of the signal to be measured with relatively simple digital equipment. The autocorrelation function is then corrected for the effect of the quantization and Fourier transformed to yield the power spectrum.

A mathematical analysis of this technique has also been presented which predicts the quality of the spectrograms which are obtained in the special, but interesting, case of a weak signal immersed in strong noise. The accuracy of the predictions was confirmed by direct measurement in the laboratory on the completed system.

A realization of the special purpose computer to calculate the autocorrelation function of the signal was presented. This realization utilizes the standard digital components of AND gates, OR gates, flip-flops and delay lines in a novel and economical configuration. The design considerations and the complete logical equations were also presented.

This realization was constructed and used to measure the spectrum of echoes from Venus. Since the transmitter illuminated Venus with pure CW, the spectral broadening of the echo may be attributed to doppler shifts caused by the Venerian rotation. The spectrograms are presented in Chapter XI.

One can notice many things in these curves, but the high resultant signal-to-noise ratio is the most outstanding. This points out the advantage of using a long integration time.

The next most salient feature is the small amount of spectral broadening which occurred, the maximum bandwidth observed being less than 100 cps. If Venus rotated as the Earth, once in 24 hours, and if echoes were detected from the limbs, then the bandwidth would be about 14,000 cps. One is forced to conclude from this data that either Venus is very shiny or else rotates very slowly. The polarization experiments mentioned on page 87 indicate strongly that Venus is not shinier than the moon. Since reflections are detected from the limbs of the moon, the evidence is that the maximum spread on the spectrograms corresponds to echoes from the limbs of Venus.

Thus we are led to suspect slow rotation. Slow rotation suggests the possibility of trapped rotation since there are tidal forces which favor that mode. The bandwidths marked on the spectrograms by arrows are the maximum observable bandwidths, assuming trapped rotation. There is a remarkable agreement between these and the maximum bandwidths actually observed.

We conclude from this evidence that Venus does exhibit trapped rotation.

The spectra shown in chapter XI seem to be comprised of two parts, indicating that there are only two dominant terms in the backscatter function of equation 3.7 (page 14). The first part, which contains most of the power, gives rise to the high central peak of the spectrograms and may be called the glare, or narrow-band, component. Its bandwidth at the half power points is, typically, 8 cps. However, because of the limited resolution of these spectrograms, a pure sine wave produces a bandwidth of 6 cps (see figure 11.4). The local oscillator was held to within one cps, so there is about one cps left for doppler broadening.

This corresponds to a term in the backscatter function of a very high power of the cosine. For the glare component,

$$F(\theta) = \cos^{n}\theta; \quad n > 1000.$$

The second part of the spectrograms is the distributed power in the shoulders of the curve. This is called the background component and results from reflections over all of the Venerian hemisphere that is nearest Earth. The corresponding exponent of the backscatter function is much lower;

$$F(\theta) = \cos^{7}\theta.$$

It must be remarked that the exponent 7 is only approximate, with 6 or 8 fitting the data almost as well.

One can see from the curves of Chapter XI that (at least from the curves made with long integration time) the spectra are all quite similar, indicating a high degree of homogeneity for the surface of Venus. Asymmetry in the spectra might indicate mountainous terrain towards one limb and plains towards the other; or perhaps continents and oceans. However, within the probable error, no asymmetry can be found.

These spectra cover a time period of only two weeks. Because of Venus' slow rotation, such interesting features, if any, may not have been brought into view. It would be very interesting to have spectra spaced uniformly over a much longer interval.

PARTIAL LIST OF SYMBOLS

θ = co-latitude angle

ϕ = longitude angle

B = filter bandwidth

$C(\tau)$ = correlation window

$F(\omega)$ = spectral window

G = ratio of mean to standard deviation

K = number of lags

N = number of samples taken for a given observation

N_o = noise power density

$P(\omega)$ = true spectral density

$\hat{P}(\omega)$ = estimated spectral density

$R_y(\tau)$ = true autocorrelation function at limiter output

$\hat{R}_y(\tau)$ = estimated autocorrelation function at limiter output

$R_x(\tau)$ = true autocorrelation function at limiter input

$\hat{R}_x(\tau)$ = estimated autocorrelation function at limiter input

S = signal power at filter output

T_o = time between successive samples

$\hat{W}(f)$ = estimate of signal plus noise spectrum minus noise only spectrum. $\hat{W}(f)$ is calculated by the "second mode" of chapter VII

σ = RMS error (calculated)

REFERENCES

(1) R. S. Richardson: Publications of the Astronomical Society of the Pacific, p. 259, 1958.

(2) J. D. Kraus: Nature, p. 687, 1956.

(3) H. Spencer Jones: Life on Other Worlds, p. 170, London, 1952.

(4) D. H. Menzel and F. L. Whipple: Publications of the Astronomical Society of the Pacific, p. 161, 1955.

(5) M. Phister, Jr.: Logical Design of Digital Computers, p. 116, Wiley, 1960.

(6) Davenport and Root: Random Signals and Noise, p. 107, McGraw-Hill, 1958.

(7) Blackman and Tukey: The Measurement of Power Spectra, p. 265, Dover, 1959.

(8) Davenport and Root: Op. cit., p. 276, problem 10.

(9) Blackman and Tukey: Op. cit., p. 31.

(10) Hanbury Brown and Lovell: The Exploration of Space by Radio, p. 29, Wiley, 1958.